

**Petrography of the Doña Juana Volcanic Complex (DJVC) basement: implications in the
Quaternary magmatism**

María Paula Rodríguez Navarrete

Advisor: Natalia Pardo Villaveces, PhD

Co-Advisor: Ana Ibis Despaigne, PhD

Undergraduate thesis

Universidad de Los Andes

Faculty of Sciences – Department of Geosciences

Bogotá, Colombia

August 2018

Table of contents

Agradecimientos	4
Abstract	5
1. Introduction	6
2. Conceptual Framework.....	8
2.1. Petrogenesis of continental arc magmas.....	8
2.2. Open magmatic systems	9
2.2.1. Magma mingling and mixing	9
2.2.2. Assimilation.....	10
3. Geological Framework	11
3.1. Mesozoic Units	12
3.1.1. Pompeya Metamorphites (PZpom).....	12
3.1.2. Buesaco Schists (PZBue).....	12
3.1.3. Quebradagrande Complex (K1cqq)	13
3.2. Cenozoic Units.....	13
3.2.1. Esmita Formation (Nesm).....	13
3.2.2. Dacite-Andesite Porphyritic Bodies (Npda).....	13
3.2.3. Granatífera Tuff (tgr).....	14
4. Methodology and Analytical techniques	15
4.1. Petrography.....	15
5. Results	16
5.1. Buesaco Schists (PZBue).....	16
5.1.1. Sample B15-1.....	16
5.2. Quebradagrande Complex (K1cqq)	18
5.2.1. Sample B10-1.....	18
5.2.2. Sample B13-1.....	22
5.2.3. Sample B19-2.....	26
5.2.4. Sample B31-1.....	29
5.3. Esmita Formation (Nesm).....	33
5.3.1. Sample B24-1.....	33
5.3.2. Sample B29-1.....	39
5.3.3. Sample B32-1.....	45

5.4.	Dacite-Andesite Porphyritic Bodies (Npda).....	47
5.4.1.	Sample B26-1.....	47
5.5.	Granatífera Tuff (tgr).....	52
5.5.1.	Sample B27-1.....	52
5.6.	Doña Juana Volcanic Complex (DJVC)	57
5.6.1.	Sample B22-1.....	57
5.6.2.	Sample B22-2.....	61
6.	Discussion.....	66
6.1.	Buesaco Schists (PZBue)	66
6.1.1.	Interpretation Sample B15-1.....	66
6.2.	Quebradagrande Complex (K1cqq)	66
6.2.1.	Interpretations Samples B10-1, B13-1, B19-2 and B31-1.....	66
6.3.	Esmita Formation (Nesm).....	66
6.3.1.	Interpretations Samples B24-1, B29-1 and B32-1.....	66
6.4.	Dacite-Andsite Porphiritic Bodies (Npda)	67
6.4.1.	Interpretation Sample B26-1.....	67
6.5.	Granatífera Tuff (tgr).....	69
6.5.1.	Interpretation Sample B27-1.....	69
6.6.	Lavas from the Doña Juana Volcanic Complex (DJVC)	71
6.6.1.	Interpretation Sample B22-1.....	71
6.6.2.	Interpretation Sample B22-2.....	73
6.7.	General interpretation	75
6.8.	Implications on the DJVC chemistry.....	76
7.	Conclusions	76
	References.....	78

Agradecimientos

Comienzo agradeciendo a mis padres y a mi hermano por su apoyo incondicional, por brindarme todas las herramientas posibles para llevar a cabo mis proyectos, por darme los mejores consejos y enseñanzas, por tenerme paciencia en los momentos estresantes y por siempre ayudarme a salir adelante. Agradezco también a la profesora Natalia Pardo, quien me dio su confianza para trabajar en este proyecto, por guiarme y transmitirme su pasión por la Vulcanología a través de las clases, del campo y de las horas compartidas en el laboratorio. Asimismo, le agradezco a mi co-directora Ana Ibis Despaigne por su gran ayuda en el desarrollo de este trabajo y por abrir mi mente en el mundo de la petrografía, que va más allá de identificar los minerales de la muestra. Le agradezco también al profesor Andrés Rodríguez, quién me impulsó a empezar a investigar sobre los temas que me cuestionaban en Geociencias. Quiero dar un especial agradecimiento a mi mejor amiga Valentina Carmona, quien con su talento y amor por la ciencia me ayudó a llevar a cabo este trabajo, observando durante varias horas láminas en el laboratorio, pensando e investigando sobre posibles explicaciones a lo que veíamos. Además, me brindó su gran amistad en estos últimos cuatro años, haciendo de esta etapa una experiencia increíble. A todos mis compañeros, gracias por su apoyo.

Abstract

The Doña Juana Volcanic Complex (DJVC) is a composite volcano with a calc-alkaline dacitic composition, which activity began about 1125.4 ± 4.4 ka ago. It is located in the region of Nariño (southwest Colombia), at the Central Cordillera of the Northern Andean Block. The lithological units that conform the volcanic complex basement consist of the Pompeya Metamorphites (Triassic), the Buesaco Schists (Cretaceous), the metamorphic and volcanic rocks of the Quebradagrande Complex (Cretaceous), the sedimentary rocks of the Esmita Formation (Neogene) and the Neogene Porphyritic Bodies. A petrographic description of representative samples of these units and from the Granatífera Tuff (Quaternary), that contain xenoliths of the continental crust, was done in order to understand the influence of the basement in the magmatism and whole-rock geochemistry of the dacitic effusive rocks from the DJVC. Based on the different textures identified in the mineral assemblage of the samples, a simplified magma plumbing model for the rocks of the DJVC was proposed. It consists of five (5) possible stages that evidence the open-system magmatic behavior of the DJVC in which hotter pulses of melt entered and there was assimilation of xenoliths from the basement. The latter has important consequences for the analysis of the chemistry of the dacitic rocks. It is expected data dispersion in the Harker diagrams of CaO, Na₂O, K₂O and Al₂O₃ against silica, an inconstant ratio in bivariable plots of two incompatible elements with similar bulk partition coefficients and decoupling patterns in bivariable plots of an incompatible element in the melt vs. the proportion of this element with a similar incompatible element.

Key words: *basement, volcanic complex, magmatism, geochemistry, open system, AFC, mixing*

1. Introduction

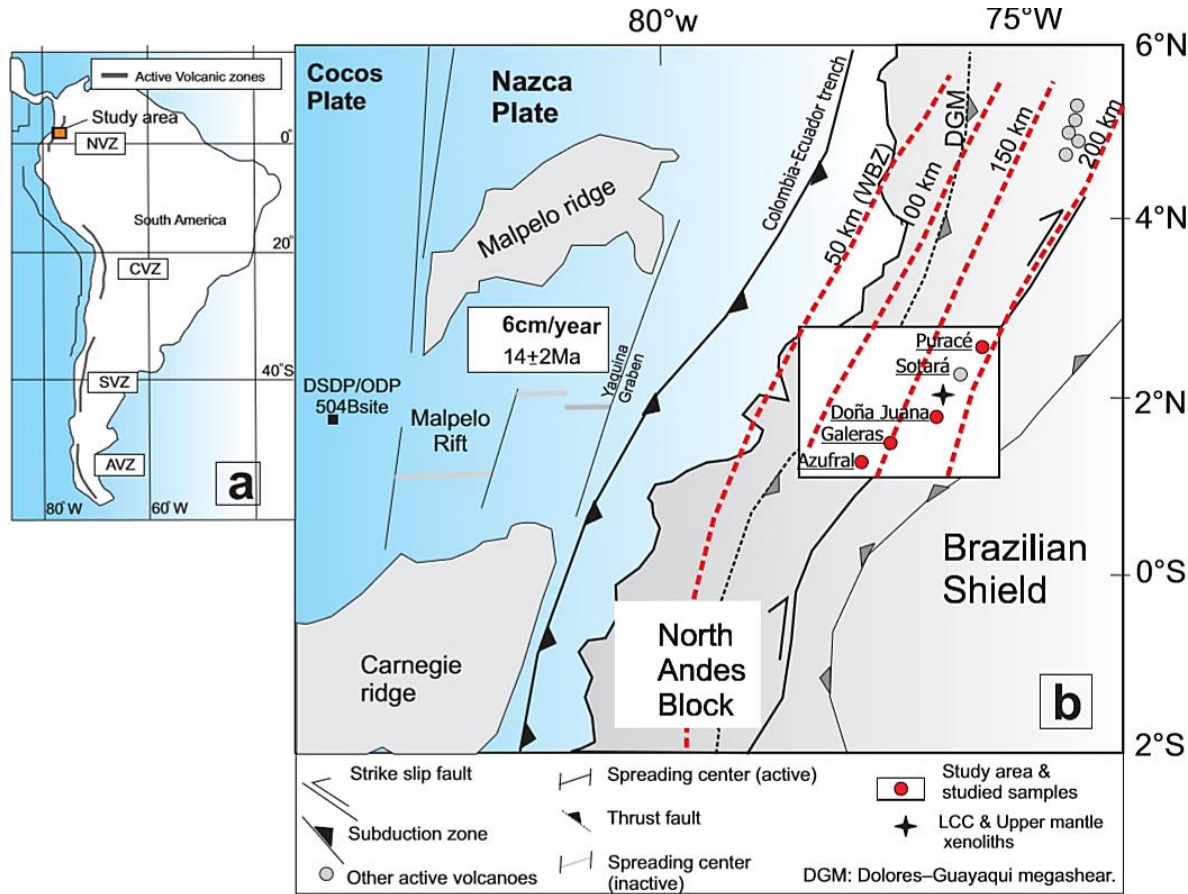


Figure 1: **a)** Active volcanism in the Andes Cordillera. **(b)** Present-day tectonic framework of SW Colombian arc. Red dotted lines are the Wadati-Benioff Zone (WBZ) contours: isobaths of the top of the deep seismic zone as a consequence of the subduction of the Nazca plate beneath the North Andes Block (Took from Marín-Cerón (2007))

The subduction of the Nazca Plate along the western margin of South America has given way to the Late Cenozoic volcanic activity (Weber, 2002). Currently, active volcanism is subdivided into four zones: the Northern Volcanic Zone (NVZ), the Central Volcanic Zone (CVZ), the Southern Volcanic Zone (SVZ) and the Austral Volcanic Zone (AVZ) (Fig. 1a). The NVZ is in Colombia and Ecuador from latitude 5°N to 2°S, the CVZ is in southern Peru and northern Chile from 16 to 27°S, the SVZ is mainly in southern Chile from 33 to 55°S and the AVZ from 46 to 49°S (Winter, 2014). Between these zones there are inactive gaps associated with small dips of the subduction slab (Best, 2003). Moreover, the volcanic character of the zones is different because of the variations in the thickness, age and angle of subduction of the oceanic plate, crustal thickness and the unlike structure and composition of the crust (Weber, 2002). The latter implicates different types of crust assimilated by the magmas in the path to the surface (Marín-Cerón, 2007).

One of the active volcanic systems of the NVZ is the Doña Juana Volcanic Complex (DJVC), located in the region of Nariño (southwest Colombia), at the Central Cordillera of the Northern Andean

Block (Cediel et al., 2003) (Fig. 1b). The DJVC is a composite volcano with a calc-alkaline dacitic composition and which activity began about 1125.4 ± 4.4 ka ago (Pardo et al., 2016). According to Marín-Cerón (2007), isotopic data of Pb, Nd and Hf pointed out strong contributions of the underlying crust in the petrogenesis of the Quaternary lavas. Moreover, Pardo et al. (2016) suggested, through petrographic and geochemical analysis of the DJVC products, an open-system magmatic evolution in which magma mixing and crustal assimilation-fractional crystallization (AFC) could have occurred. Among the possible assimilated materials are the rocks of the lower crust, found as xenoliths in the Granatifera Tuff of Mercaderes (Grosse, 1935): hornblende-rich rocks (hornblendites and pyribolites), hornblende-poor to hornblende-free rocks (pyroxenites, pyroclastites, pyrigarnites and granulites) and gneisses (Weber et al., 2002). Additionally, according to Pardo et al. (2016), the lithologic units of DJVC basement are also possible contaminants: the Pompeya Metamorphites (Ingeominas & Geoestudios, 1998), the Buesaco Schists (Murcia & Cepeda, 1984), the metamorphic and volcanic rocks of the Quebradagrande Complex (Botero, 1963), the sedimentary rocks of the Esmita Formation (León et al., 1973) and the Neogene Porphyritic Bodies (Núñez, 2003). Until now it has not been possible to study the influence of the basement in the petrography and geochemistry of CVDJ, because there is not complete data of the pre-volcanic basement in Nariño.

In this work, I aim to develop a detailed petrographic description of the lithologic units that makes up the basement of DJVC and propose hypothesis about their implications in the magmatism and whole-rock geochemistry of the DJVC rocks.

2. Conceptual Framework

2.1. Petrogenesis of continental arc magmas

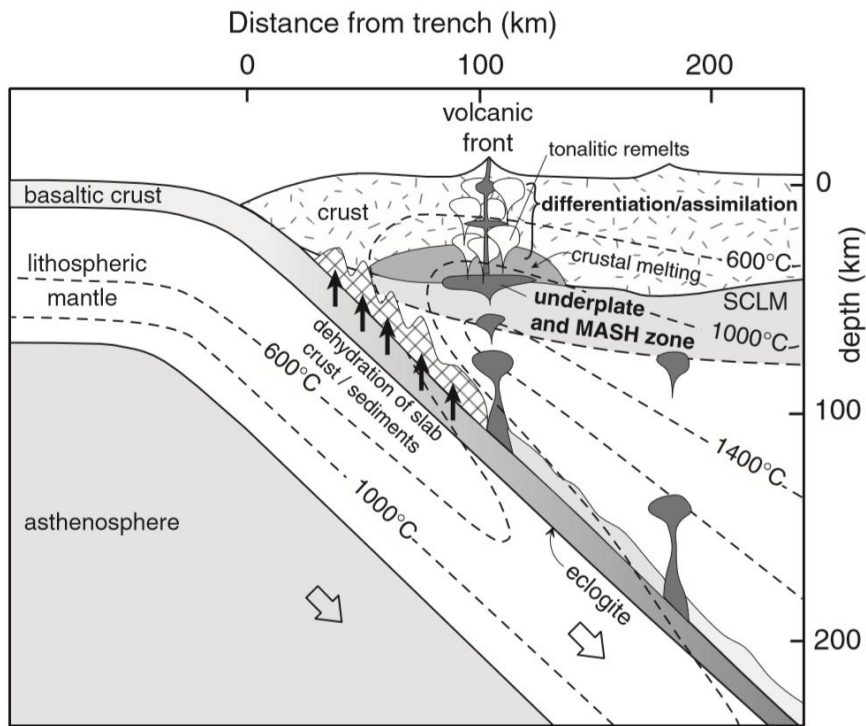


Figure 2: Cross section of a continental arc subduction zone, showing the magmatic processes involved.
From Winter (2014).

Subduction of oceanic crust and upper mantle is accompanied by the dehydration of the subducted crust and sediments and by the subsequent migration of LIL-enriched fluids from the crust to the overlying mantle wedge (Winter, 2014) (Fig. 2). This addition of fluids decreases the mantle solidus, leading to the partial melting of the mantle wedge and to the production of basaltic primary melts (LaFemina, 2015). Due to buoyancy forces, the melts rise and then underplate the base of the continental crust, suffering fractional crystallization, assimilation and melting of the less refractory crustal rocks thanks to the addition of heat (Winter, 2014). MASH is the term used to describe the process of melting, assimilation, storage and homogenization at the mantle-crust transition (Hildreth and Moorbath, 1988). Initially, primary magmas were denser than the crust; however, MASHed magmas acquire buoyancy as they become enriched and silicic. Then, they rise to shallower magma chambers (Winter, 2014). Throughout the uprise, magmas may incorporate silicic to alkalic melts and wall-rock components of the mid- to upper-crust (Winter, 2014). Additionally, in the open-system shallow magmatic chambers, they may experience fractional assimilation-fractional crystallization (AFC) and/or magma mixing (Winter, 2014).

In general, in convergent plate margins, andesites are the usual rock type, but more silicic rocks as dacites and rhyolites are mainly associated with the continental arcs (Marín-Cerón, 2007). Specifically, dacites are one of the fundamental volcanic rocks of the calc-alkaline igneous series

(Stefan et al., 1996). Their composition is similar to andesites, but with higher content of sodic plagioclase, K-feldspar and quartz (Mindat, 2006). Usually, dacites are dark-grey to black in color and have a porphyritic texture, consisting of small phenocrysts (0.1-3mm) of quartz, plagioclase (26-49% An) that may be zoned and twinned, hornblende, biotite and sparse pyroxene (augite and hypersthene) in a glassy-microcrystalline groundmass (Stefan et al., 1996).

Taking into account the difficulty of the magmatic systems, the resultant crystal populations that are found erupted in volcanic zones or in shallow intrusions are complex (Jerram and Davidson, 2007). Igneous rocks, not only have crystals from the magma involved in the eruption (phenocrysts), but also crystals foreign to it and incorporated by some physical process (xenocrysts); crystals from previous stages of the magmatic system at depth that are 'reincorporated' (antecrysts), and crystals less than a few hundred microns in size formed during degassing of the magma on eruption (microlites) (Jerram and Martin, 2008). In other words, the textural complexity of igneous rocks reflects the several processes involved in the magmatic system of continental arcs.

2.2. Open magmatic systems

On the ascending of primary magmas from the mantle and deep crustal sources, many differentiation mechanisms affect them in different degrees (Best, 2003). The differentiation refers to natural processes with the capacity to modify the composition of the magma and generate a spectrum of igneous rocks (Winter, 2014). In open systems, where energy and matter can be transferred to and from the surroundings (Winter, 2014), the principal differentiation processes are: magma mixing and assimilation (Best, 2003).

2.2.1. Magma mingling and mixing

Initially, when two or more different parent magmas blend together, they retain their contrasting identity and they are physically mingled. After mingling, if there is enough time and available thermal energy, diffusion process may begin in an atomic scale, leading to the mixing and homogenization of the magmas. The differences in composition between the hybridizing magmas can be wide as basalt and rhyolite, or hardly noticeable with small variations in the weight percentages of major elements (Best, 2003).

Mixing of the magmas is a function of the contrasting magma properties: temperature, composition, density, volatile content and viscosity. Likewise, the location and the turbulence associated to the injection of one magma into the chamber with the other are also important variables (Winter, 2014). So, when there are big differences in the properties of the magmas, the degree of mixing is limited and disequilibrium textures (complex resorption, overgrowths and corroded textures in phenocrysts) or compositional evidence (juxtaposed quartz and olivine or calcic and sodic plagioclase) can be appreciated (Best, 2003). In contrast, similar magmas may experience more extensive mixing and their evidence is less visible (Winter, 2014).

2.2.2. Assimilation

Assimilation is the process in which a magma incorporates chemical constituents from the walls or roof around the magma chamber or from the xenoliths (Winter, 2014). The degree of chemical equilibrium of the magma with the foreign rocks depends on their compositions, temperatures and time available (Best, 2003). Moreover, the magma itself must supply the heat requirements for the assimilation, by two sources: the released heat from the magma cooling and the latent heat of crystallization (Winter, 2014). Even though partial melting of the foreign rocks and ion incorporations by time and T-dependent diffusion are considered the principal mechanisms by which a magma can assimilate components, absorption of volatiles can also add constituents of the solid country rock into the magma (Patchett, 1980; Watson, 1982).

Crystals can be dissolved in the parent melt, if there is sufficient heat available and if the melt is not already saturated in that phase. For example, quartz xenocrysts can dissolve in basaltic melts in which silica activity is <1 . In addition, crystals may react with the melt if it has a lower temperature than the precipitation temperature of the crystals. For instance, xenocrysts of clinopyroxene in a granodiorite melt, in which stable hornblende is being crystallized, will react with the melt generating a reaction border of hornblende by ionic diffusion (Best, 2003).

Assimilation can modify significantly the composition of a magma, however the resulting variations in abundances of major elements in the remaining liquid may be usually undetectable, while trace elements can provide a sensitive measure of the assimilation (Winter, 2014). The concentrations of some trace elements like Rb, Cs, Ba, Th and LREE are higher in the continental crust than in mantle-derived magmas, so the assimilation of an amount of crustal material enriched in these elements may have a significant effect on a magma with initial small amounts of them (McBirney, 1979).

The combined process of assimilation and the accompanying fractional crystallization required to supply the necessary heat is known as AFC and was mathematically modeled by DePaolo (1981).

3. Geological Framework

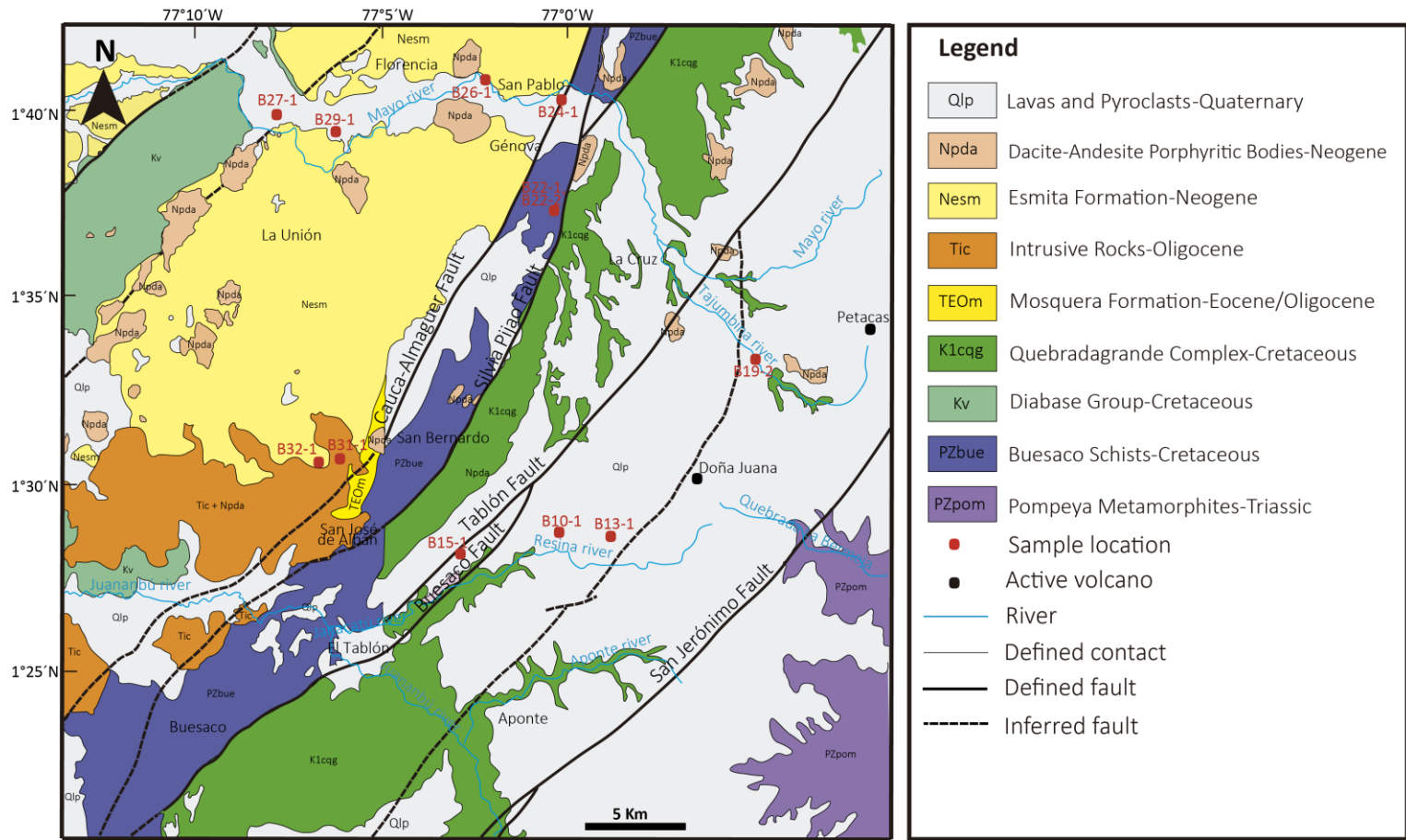


Figure 3: a) Geological map of the Doña Juana Volcanic Complex (DJVC) showing sample locations, modified from Murcia & Cepeda (1991) and Núñez (2003).

Pardo et al., (2016) defined the DJVC as constituted by three central and overlapped dacitic volcanic edifices: the Santa Helena (~1125-1097 ka), the Ancestral Doña Juana (~878-312 ka), and the Old Doña Juana (~231-77 ka). Each of the three edifices is truncated by a major volcano-tectonic depression partially filled with three dacitic lava-dome fields (<10ka) named El Filo, Totoral, and Young Doña Juana. Moreover, to the west of the Santa Helena edifice, the DJVC comprises two adventive cones (pre-Montoso and Montoso).

The DJVC have generated deposits of lava-flows, lava-domes, and volcaniclastic deposits: primary (pyroclastic) and secondary (lahars and debris avalanches), as a consequence of the constructive and destructive processes of each edifice. These volcanic deposits fill the paleotopography developed between the Silvia-Pijao and El Tablón faults to the ESE, and the San Jerónimo fault to the WNW. The volcaniclastic transport and accumulation has been mainly controlled by the Tajumina river (tributary of the Mayo river) to the NE, and the Resina river (tributary of the Janacatú and Juanambú rivers) to the SW (Fig. 3) (Pardo et al., 2016).

All the deposits of DJVC lie above a regional nonconformity that separates the lithologic units of the basement, with the Quaternary volcaniclastic deposits. According to Pardo et al. (2016), the units that make up the basement are the following, listed in chronological order from oldest to youngest:

3.1. Mesozoic Units

3.1.1. Pompeya Metamorphites (PZpom)

The Pompeya Metamorphites was defined by Ingeominas & Geoestudios (1998) as the metamorphic rock sequence, mainly schists, that crop out in the Pompeya-Aponte road on the northwestern side of the 1:100.000 geological map number 430 of the Colombian Geological Survey. Núñez (2003) established that the unit appear as a metamorphic belt orientated N45°E, limited with the Quebradagrande Complex (Botero, 1963) along the San Jerónimo fault (Fig. 3) and with the mudstones and limestones of Granadillo along the Colón fault. It consists of green and gray quartz-mica schists and quartz-sericite schists of sedimentary protolith with quartz, micas, plagioclase and secondary minerals as calcite and manganese oxides. Within the schists succession there are thin layers of gray quartzites and metarenites, with abundant quartz veins (Núñez, 2003). The best outcrops of the Pompeya Metamorphites are situated in the Quebrada La Bermeja (tributary of Cascabel river) and along the road between Pompeya and Aponte towns (Núñez, 2003). Taking in to account the lithologic similarities and the tectonic position, Barbosa-Camacho (2003) suggested the Pompeya Metamorphites as an equivalent of the Cajamarca Complex (Maya & González, 1995), which was described by Villagomez et al. (2011) as Triassic (~240-220 Ma) metasedimentary and meta-intrusive rocks.

3.1.2. Buesaco Schists (PZBue)

Initially, Murcia & Cepeda (1984) defined the Buesaco Schists with the name of "Metamorphic Sequence of Buesaco", corresponding to the lithological unit composed of green schists and micaceous schists in its western part, and by phyllites and quartzites in its eastern part. Murcia & Cepeda (1984) established the photolith of the sequence as volcanic and sedimentary rocks of a eugeosyncline environment, formed during the Upper Precambrian-Lower Paleozoic and metamorphosed to the green schist facies of baric type in the mid-Paleozoic during the Caledonian orogeny. The rocks are well exposed along the Buesaco-San José de Albán and the Buesaco-El Tablón roads. Later, Núñez (2003) renamed the unit as Buesaco Schists, following the International Stratigraphic Guide (International Subcommission on Stratigraphic Classification of IUGS, 1994) and described it as intercalations of quartz-mica schists with abundant biotite (locally graphic schists), green tremolitic and sericitic schists and black phyllites. As the Pompeya Metamorphites (Ingeominas & Geoestudios, 1998), this unit also appears as a NE-trending metamorphic belt of about 9 km wide, in faulted contact with the Quebradagrande Complex and the Esmita Formation along the Silvia- Pijao and the Cauca-Almaguer faults (Fig. 3), respectively, belonging to the Romeral Fault System (Núñez, 2003). Maya & González (1995) and Barbosa-Camacho (2003) correlated the Buesaco Schists with the Arquía Complex (Núñez, 1990), whose isotopic ages corresponds to 112 ± 3.7 Ma (Albian) (Villagomez et al., 2011).

3.1.3. Quebradagrande Complex (K1cqq)

The Quebradagrande Complex was defined by Botero (1963) as the volcanic and sedimentary lithodems that are limited to the west by the Arquía Complex (Núñez, 1990) along the Silvia- Pijao fault and to the east by the Cajamarca Complex (Maya & González, 1995) through the San Jerónimo fault (Maya & González, 1995) (Fig. 3). Nivia (2006) established that the Quebradagrande Complex is composed of volcanic and sedimentary rocks of oceanic affinity. In the eastern outcrops consists of matrix-supported conglomerates with subrounded clasts of basalts, diabases, siltstones and cherts, and in the western outcrops of massive thick layers of arenites, metarenites, siltstones and levels of basalts and diabases. Microscopically, Núñez (2003) identified foliated metarenites with fine grain and subtle schistosity with quartz, plagioclase, orthoclase, microcline and quartzite lithics; greywackes with poor selection composed by microcrystalline quartz and mood; extrusive igneous rocks (lavas and tuffs) that compositionally range between andesites and basalts. The tuffs can be crystal-lithic composed by plagioclase fragments, detrital quartz and lithics or vitric-lithic composed by plagioclase, silicic aggregates and lithics; chert with radiolarians and foraminifera. The best outcrops of this units are located along the Juanambú and the Resina rivers, and along the La Cruz-San Bernardo road (Núñez, 2003). Villagomez et al. (2011) found a zircon U-Pb age of 114 ± 3.8 Ma (Aptian) from a metatuff of the Quebradagrande Complex.

3.2. Cenozoic Units

3.2.1. Esmita Formation (Nesm)

León et al. (1973) defined the Esmita Formation as a lithostratigraphic sequence of marine-continental origin, subdivided in three members: the lower member consists of dark fossiliferous siltstones, the middle member of greenish greywackes and the upper member of polymictic conglomerates with pebbles of quartzite, chert and basalts. The type locality is ubicated on the south of Popayán in the Esmita river. Microscopically, Barbosa & Camacho (2003) found: angular grains of quartz, feldspar and lithics of quartzites and cherts in a matrix of clay with sericite in the siltstones of the lower member, and angular grains of quartz, plagioclase, amphiboles altered to chlorite and lithics of quartzites, cherts and basalts and opaques (pyrite and magnetite) in a matrix of clay with sericite and fine grains of quartz in the greywackes of the middle member. The outcrops of the Esmita Formation are situated on the San Pablo- Florencia and the San Pablo-Génova roads and it has a tectonic boundary with Buesaco Schists (Núñez, 2003) (Fig. 3). Ruiz (2002) found gastropods of the Limnaeado genus in the middle member, indicating an Early Miocene age.

3.2.2. Dacite-Andesite Porphyritic Bodies (Npda)

The porphyritic bodies have been documented by many authors in the geological maps number 386, 410 and 411 of the Colombian Geological Survey (cf. Murcia & Cepeda (1991), Álvarez (1983), Ruiz et al. (2002), Núñez (2003)). Núñez (2003) used for the first time the nomenclature of Dacite-Andesite Porphyritic Bodies (Npda) to name the lithological unit. Murcia & Cepeda (1991) described the bodies as hypabyssal with an andesitic and dacitic composition, porphyritic and holocrystalline textures, and with an aphanitic matrix. The phenocrystals size range from millimeters to 1cm of diameter and consist of zoned and twinned plagioclase (oligoclase-

andesine), green hornblende, biotite with green to brown pleochroism and bi-pyramidal quartz. The principal alteration minerals are kaolinite, sericite, calcite and iron oxides. The porphyritic rocks cut several lithological units: Buesaco Schists (Murcia & Cepeda, 1984), Diabase Group (Nelson, 1962), Mosquera Formation (León, 1973) and Esmita Formation (León, 1973) (Fig. 3). Álvarez et al. (1979) reported an age of 13 ± 3 Ma (K / Ar in biotite), in a dacitic porphyry that is intruding the Esmita Formation. Álvarez and Linares (1979) dated the stock of Minas in 8 ± 3 Ma (K / Ar in biotite), and Álvarez et al. (1978) reported an age of 6 ± 1 m.a. (K / Ar in hornblende) in the Suárez stock. According to Barbosa-Camacho (2003), these radiometric ages indicate a magmatic episode related with the subduction of the Middle Miocene-Late Miocene and with the uplift of the Central Cordillera during the Andean Orogeny, that precede the Plio-Quaternary volcanism.

3.2.3. Granatífera Tuff (tgr)

The Granatífera Tuff contains xenoliths of both crustal and mantle origin, providing insights about the composition of the lower crust and upper mantle in this area (Weber et al., 2002). For this reason, it is important to consider the Granatífera Tuff within the lithological units to study in this work. At first, Ruiz (2002) divided Mercaderes Formation, corresponding to all the rocks that make up the Mercaderes plateau, into two members: a pyroclastic Lower Member and an epiclastic Upper Member in the top. The pyroclastic member is equivalent to the Granatífera tuff defined by Grosse (1935) and Weber (1998), and the epiclastic member with the Mercaderes tuff (Murcia, 1982). However, Pardo et al. (2016) proposed the abandonment of the terms "Mercaderes Formation" and "Mercaderes tuff" and to conserve the informal character of the "Granatífera Tuff" (tgr) lithostratigraphic unit mapped by Weber (1998), associated with a local source in the surroundings of Mercaderes, until proper mapping and volcanic stratigraphy is carried on. Pardo et al. (2016) argue that the Granatífera tuff is related to a volcanism sourced around Mercaderes town, in agreement with Weber (1998), whereas the "Mercaderes tuff" is actually linked to the Áimas volcano and is not genetically related to the Mercaderes volcanism. According to Weber (2002), the Granatífera tuff contains crustal and mantle xenoliths, and also yields normal igneous lithics (volcanic fragments and bombs of dacitic, andesitic and lamprophyric compositions). Crustal xenoliths include hornblendites, pyroxenites, granulites, amphibolites and gneisses (Weber, 2002). Additionally, based entirely on its stratigraphical relationships, Weber (1998) defined the age of the Granatífera Tuff as at least 1.5 (± 0.1) Ma old. In the Fig. 3, the Granatífera Tuff is mapped within the Quaternary lavas and pyroclasts unit (Qlp).

Although, the Diabase Group (Kv), the Oligocene intrusive rocks (Tic) and the Mosquera Formation (TEOm) are units reported by Murcia & Cepeda (1991) in the 1:100.000 geological map number 410 of the Colombian Geological Survey (Fig. 3), they are not considered among the lithologic units of the basement because of their distance to the DJVC.

4. Methodology and Analytical techniques

4.1. Petrography

The samples were collected in the field by Natalia Pardo (advisor of the present contribution). Subsequently, twelve (12) thin sections with a thickness of 30 µm were done in the Investigation Laboratory of Geosciences Department at Universidad de Los Andes. Eight (8) of these samples were polished. The thin sections include: one (1) sample from the Buesaco Schists unit (PZBue), four (4) from the Quebradagrande Complex (Kcqg), three (3) from the Esmita Formation (Nesm), one (1) from the Intrusive and subvolcanic bodies of the Neogene (Npda), one (1) from the Granatífera Tuff (tgr) and two (2) from the lavas of the DJVC (Table 1). It is important to make clear that there are not samples from the Pompeya Metamorphites because of the complexity to access to its outcrops in the field. Each of the thin sections were described using the transmitted light microscopes Olympus CX-31 of the mineralogy laboratory at Universidad de Los Andes.

Table 1: Locations of the samples selected to the petrographic analysis

Sample	Lithologic unit	Latitude N	Longitude W	Altitude (m.a.s.l)
B15-1	Buesaco Schists (PZBue)	1° 28.092'	77° 02.792	1818
B10-1	Quebradagrande Complex (Kcqg)	1° 28.669'	77° 00.177'	2295
B13-1		1° 28.652'	76° 58.882'	2694
B19-2		1° 33.514	76° 54.866	2684
B31-1		1° 30.701	77° 06.176	2354
B24-1		1° 40.233	77° 00.110	1749
B29-1	Esmita Formation (Nesm)	1° 39.311	77° 06.176	1194
B32-1		1° 30.524	77° 06.601	2311
B26-1	Intrusive and subvolcanic bodies of the Neogene (Npda)	1° 40.864	77° 02.202	1665
B27-1	Granatífera Tuff (tgr)	1° 39.881	77° 07.838	1315
B22-1 and B22-2	Lavas Doña Juana Volcanic Complex (DJVC)	1° 37.206	77° 00.201'	2264

The characterization of each sample consists in their macroscopic and microscopic description. Specifically, the petrography includes the mineral (modal) composition obtained through counting of 380 points in 10x for the igneous rocks and with comparison charts for the metamorphic and sedimentary rocks; the description of the general texture, the characterization of each of their components, the classification given to the sample and a photographic register.

Petrographic descriptions of the thin sections were constantly guided by the books of Castro (2015), Mackenzie (1982) and Passchier et al. (2005) in the case of the igneous and metamorphic rocks, and Boggs (2009) and Adams et al. (1984) for the sedimentary rocks.

5. Results

5.1. Buesaco Schists (PZBue)

5.1.1. Sample B15-1

Microscopic description: The sample has a grano-lepidoblastic texture with metamorphic foliation. The modal mineral assemblage is: quartz (67%), muscovite (11%), graphite (9%), calcite (6%), opaques minerals (3%), zoisite (2%) and epidote (2%). The paragenesis of the rock is: quartz + muscovite + graphite.

Quartz: it is the dominant mineral phase found as subhedral to anhedral grains in aggregates, ranging in size from 60 µm to 0.3 mm with wavy extinction. Grain boundaries are irregular and lobate with some 120° triple junctions. They define the granoblastic texture in mosaic (Fig. 4a,b). There are few grains orientated due to the foliation.

Muscovite: anhedral and rarely subhedral elongated sections, ranging in size from 20 µm to 0.4 mm, colorless and in some cases with a weak pleochroism to light green or grayish orange pink. Muscovite crystals have a planar preferred orientation that defined the lepidoblastic texture and the foliation of the sample (Fig. 4a,b).

Graphite: anhedral crystals found as aggregates making up non-continuous bands locally microfolded that extend throughout the sample parallel to the foliation of the rock (Fig. 4a,b).

Calcite: euhedral free crystals ranging in size from 32 µm to 0.2 mm with rhombohedral habit, or anhedral crystals in aggregates ranging in size from 0.1 to 0.3 mm. In both cases, they are colorless, with lamellar twinning and their borders are oxidized. Calcite is disseminated in the sample without a preferred orientation (Fig. 4c,d).

Opaque minerals: anhedral free crystals smaller than 0.1 mm. They are usually following the foliation and are interlocked with the graphite (Fig. 4c,d).

Zoisite: fine-grained anhedral free crystals, colorless and disseminated in specific areas of the sample.

Epidote: fine-grained anhedral free crystals, smaller than zoisite and colorless or with a yellowish color. They also appear disseminated in specific areas of the sample.

Classification: The sample corresponds to a quartz-muscovite-graphite schist following Fettes et al. (2007).

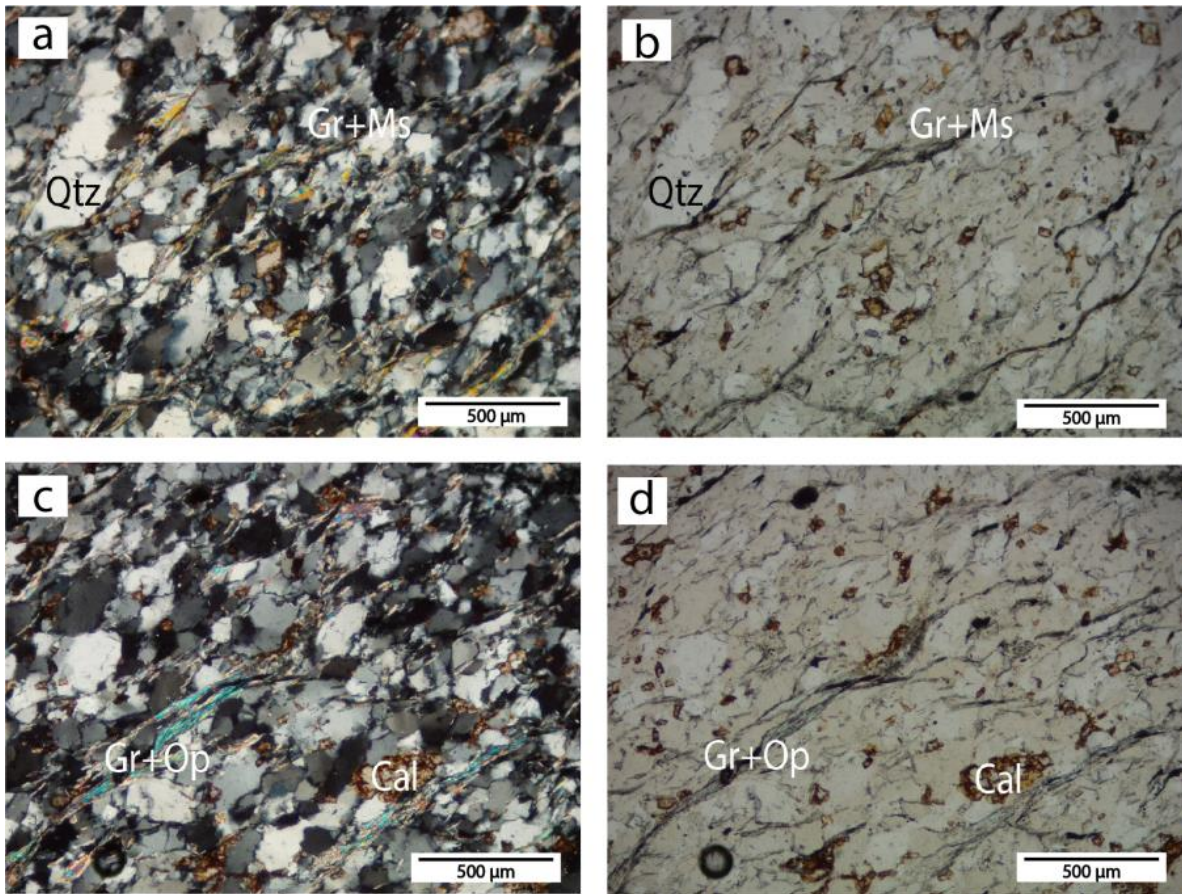


Figure 4: **a)** XPL. Overview of the sample B15-1. The granoblastic texture in mosaic defined by quartz grains, while the lepidoblastic texture and the foliation of the sample is defined by muscovite and graphite crystals. Note the non-continuous bands of graphite locally microfolded. **b)** a) in PPL. **c)** XPL. Disseminated calcite without a preferred orientation. Opaque minerals interlocked with the graphite following the foliation. **d)** c) in PPL.

5.2. Quebradagrande Complex (K1cqg)

5.2.1. Sample B10-1

Macroscopic description:

Fully altered sample possibly with aphanitic texture. Identifiable minerals include microcrystals of subhedral tabular amphibole. Recognized alteration minerals consist of chlorite, opaque minerals and white micas (Fig. 5).



Figure 5: Hand specimen of Sample B10-1

Microscopic description:

The sample is highly altered. The identified mineral assemblage consists of plagioclase and amphibole. Additionally, the alteration is given by the chlorite, opaque minerals, sericite, calcite, epidote and quartz.

Plagioclase: mesocrystals of around 1 mm in length found as free crystals or in crystalline aggregates. Free crystals are subhedral with tabular habit and polysynthetic or Carlsbad twinning. They are altered to sericite and they have irregular fractures filled by chlorite with anomalous birefringence (Fig. 6a,b). Microaggregates are composed of subhedral mesocrystals with elongated tabular habit and polysynthetic twinning. They are strongly altered to sericite (Fig. 6c,d).

Amphibole: mesocrystals ranging in size from 0.1 to 0.5 mm. They are euhedral free crystals with tabular or prismatic (mainly rhombohedral) habit. They have colorless to grayish pink pleochroism and high birefringence. In basal sections, cleavages intersect at 120°/60°. They are altered to sericite and chlorite (Fig. 6e,f). Some free crystals are completely altered and replaced by anomalous chlorite, calcite or opaque minerals giving up to pseudomorphs after amphibole (Fig. 6g,h,i,j).

Alteration minerals

Chlorite: anhedral crystals with colorless to pale green pleochroism and anomalous birefringence. Chlorite can be found in three ways along the sample: filling fractures of the mesocrystals, filling veins (Fig.6k,l) or as pseudomorphs after amphibole.

Opaque minerals: subhedral crystals with prismatic habit in aggregates ranging in size from 30 µm to 0.1 mm. They have a fluidal texture.

Sericite: it occurs disseminated in the rock.

Calcite: anhedral crystals. it occurs disseminated in the rock.

Epidote: anhedral free crystals with pale yellowish orange to moderate yellow pleochroism and high birefringence. It is disseminated in the rock.

Quartz: subhedral to anhedral free crystals of around 70 µm in size. They have parallel or wavy extinction and occur in association with chlorite.

Classification: Considering that the sample is highly altered, it is not possible to classify it. Furthermore, taking into account the mineral assemblage, the alteration is classified as propylitic.

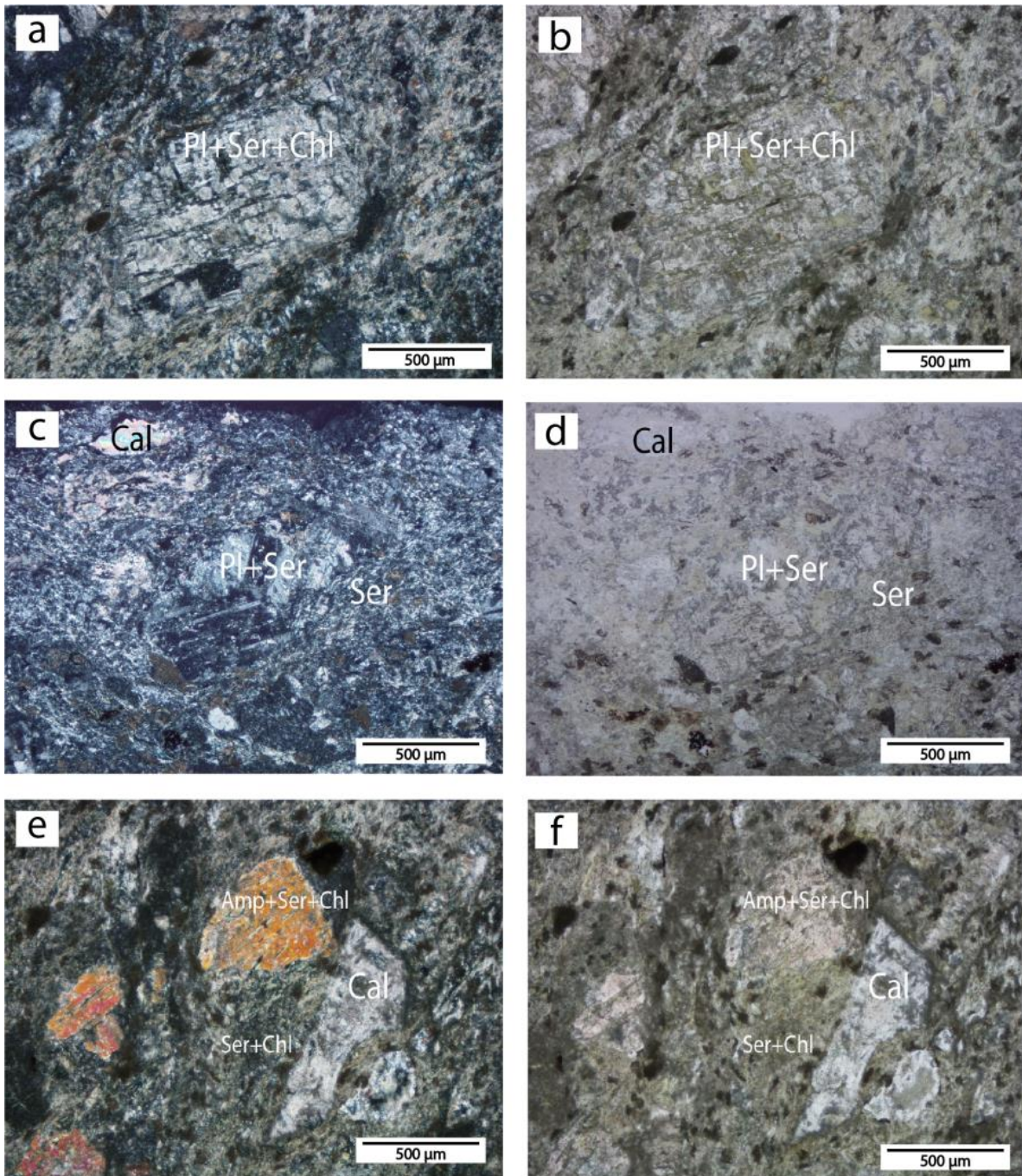


Figure 6: a) XPL. Plagioclase free mesocrystal with polysynthetic or Carlsbad twinning. It is altered to sericite and its fractures are filled by chlorite with anomalous birefringence. b) a) in PPL. c) XPL. Plagioclase microaggregates of mesocrystals with polysynthetic twinning. They are strongly altered to sericite. d) c) in PPL. e) XPL. Amphibole free mesocrystals with rhombohedral habit. It has colorless to grayish pink pleochroism and high birefringence. Note the sericite and chlorite alteration. f) e) in PPL.

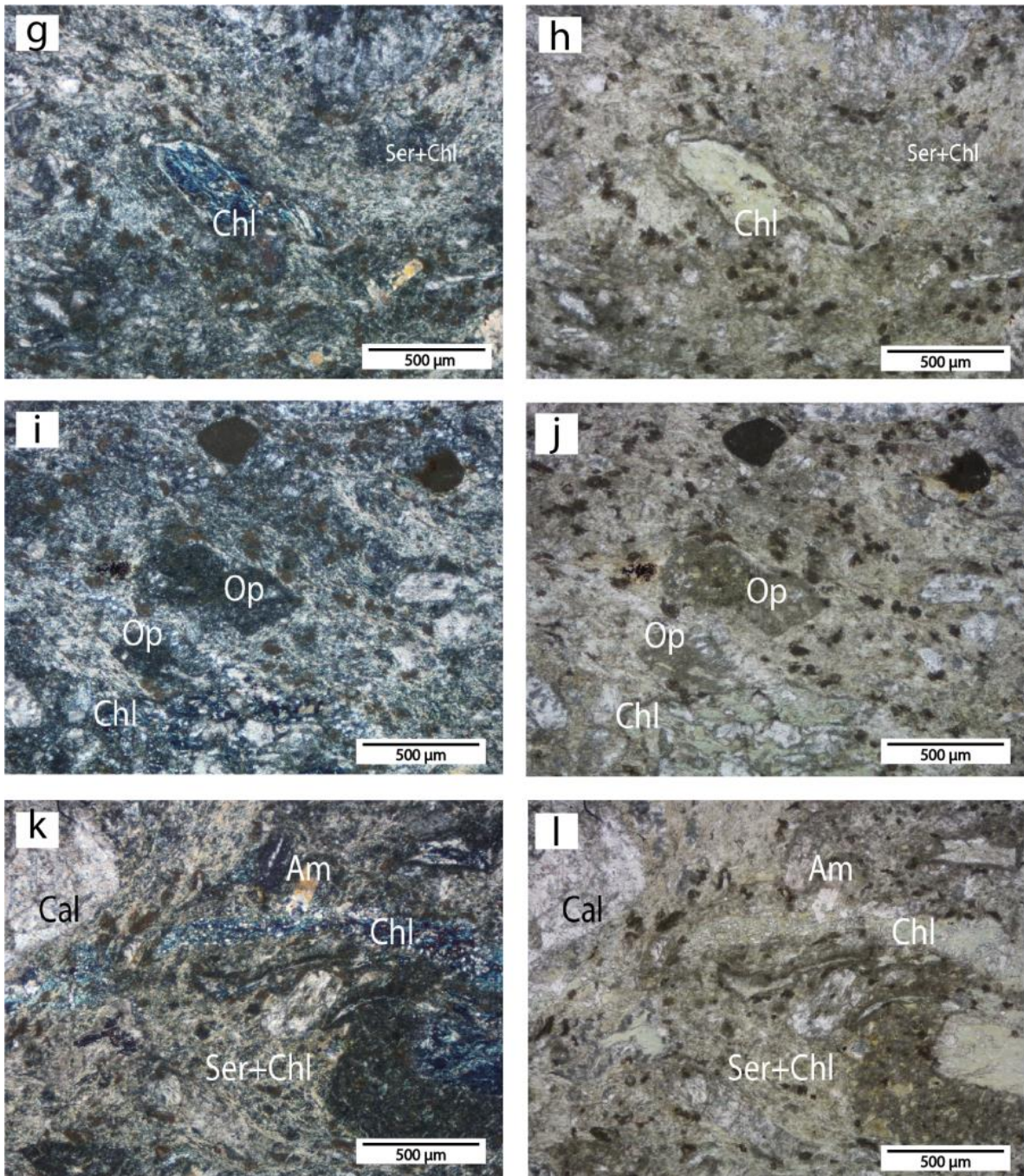


Figure 6: g) XPL. Chlorite pseudomorphs after amphibole. h) g) in PPL. i) XPL. Opaque minerals pseudomorphs after amphibole. j) i) in PPL. k) XPL. Chlorite with anomalous birefringence found as veins. l) XPL. k in PPL.

5.2.2. Sample B13-1

Macroscopic description:

Medium gray, matrix-supported and well sorted (very fine sand-fine sand) sample with dominant subangular to subspherical grains. It consists of quartz, plagioclase, white micas, clay minerals and rock fragments grains. Moreover, it has an incipient foliation given by thin planes that are not fully defined (Fig. 7).



Figure 7: Hand specimen of Sample B13-1

Microscopic description: The sample has a remanent matrix-supported sedimentary texture with metamorphic foliation. The framework consists of individual mineral grains of quartz (28%), plagioclase (6%), epidote (3%) and clinozoisite (0.6%), and sedimentary rock fragments (11.4%) in a clay matrix (26.6%). Additionally, the metamorphic foliation is defined by the graphite (13%), chlorite (4%), stilpnomelane (4%), and muscovite (3.4%). Secondary minerals include chlorite.

Framework

Quartz: anhedral monocrystalline quartz, ranging in size from 23 to 67 μm . Crystals may have or not wavy extinction and some of them exhibit a thin rim of iron oxide with syntaxial overgrowth (Fig. 8g,h). There is also polycrystalline quartz ranging in size from 34 μm to 0.1 mm, with wavy extinction and irregular grain boundaries (boundary migration).

Plagioclase: subhedral to anhedral free crystals with tabular habit in a maximum length of 0.1 mm. Only in specific cases, deformation polysynthetic twinning is appreciable. Plagioclase is strongly altered to sericite among all the crystal.

Sedimentary rock fragments: rounded grains orientated according to the foliation of the sample, ranging in size from 70 μm to 0.1mm. They are totally composed by cryptocrystalline aggregates of clay minerals with low birefringence (Fig. 8i,j).

Epidote: anhedral crystals, less than 60 μm in maximum dimensions and colorless or with a very pale green color (Fig. k,l).

Clinozoisite: subhedral crystals, less than 57 µm in maximum dimensions and with a weak pleochroism from colorless to light yellow.

Matrix

Clay minerals: cryptocrystalline aggregates with low birefringence filling the spaces between the framework (Fig. 8e,f).

Foliation markers

Graphite: anhedral and elongated crystals in aggregates which make up non-continuous bands, locally microfolded. The graphite determines the foliation (Fig. 8c,d).

Chlorite: anhedral platelets ranging in size from 95 µm to 0.1 mm, pale green colored, and with very-low birefringence (black). They are following the foliation of the sample.

Stilpnomelane: anhedral elongated crystals of 0.1 µm with moderate yellowish brown to pale pink pleochroism. They follow the foliation of the sample.

Muscovite: anhedral and rarely subhedral elongated sections, ranging in size from 72 µm to 0.1 mm and colorless.

Secondary minerals

Chlorite: anhedral radial aggregates, less than 0.1 mm in maximum dimensions, pale green colored and low birefringence (green and yellow). They are filling spaces of the sample.

Classification: The sample corresponds to a meta-quartz arenite indicating very low grade of metamorphism.

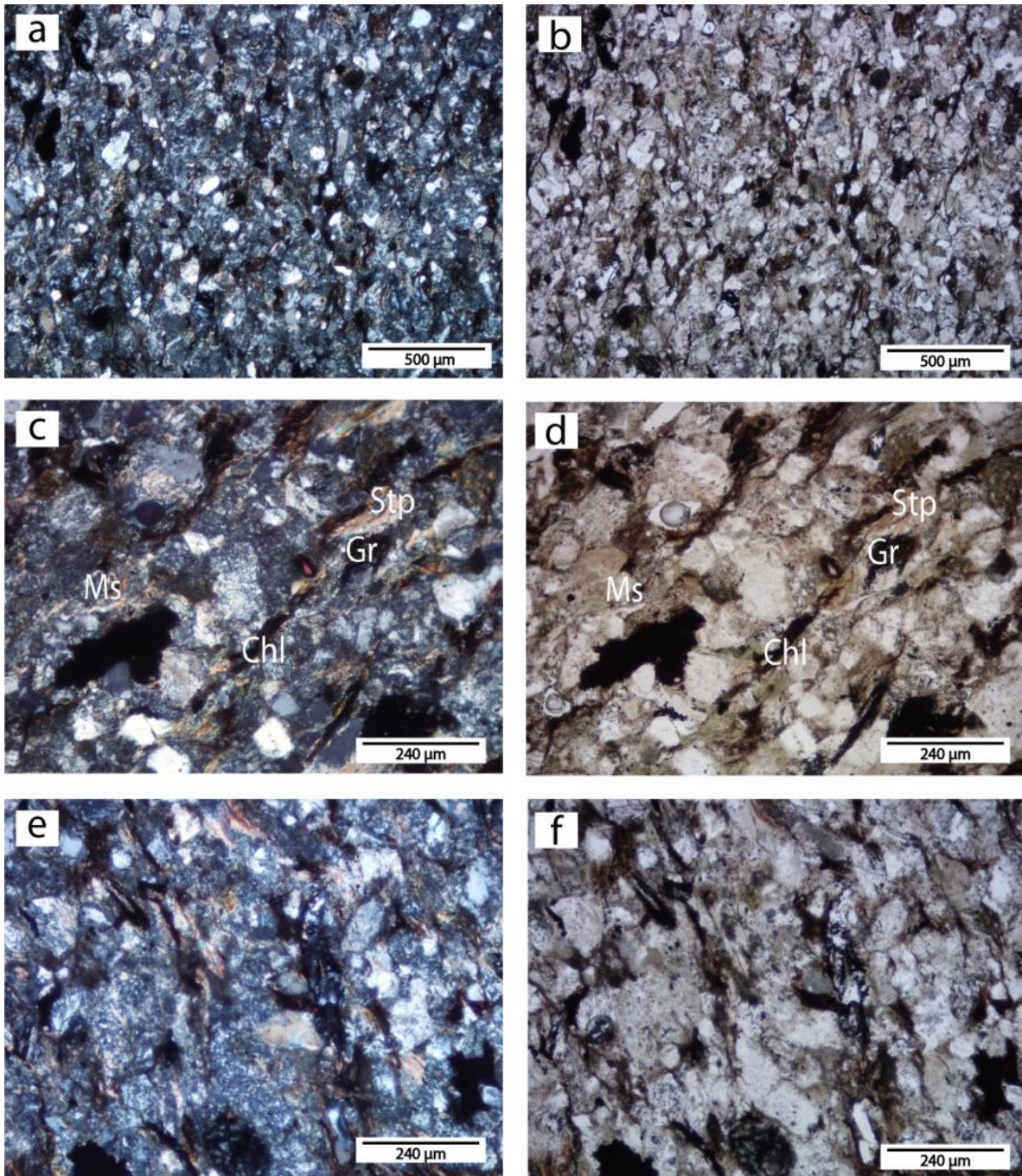


Figure 8: a) XPL. Overview of the sample B13-1. Remanent matrix-supported sedimentary texture with metamorphic foliation. b) a) in PPL. c) XPL. Foliation markers: elongated crystals of graphite, chlorite, stilpnomelane and muscovite. d) c) in PPL. e) XPL. Matrix filling the spaces between the framework. f) e) in PPL.

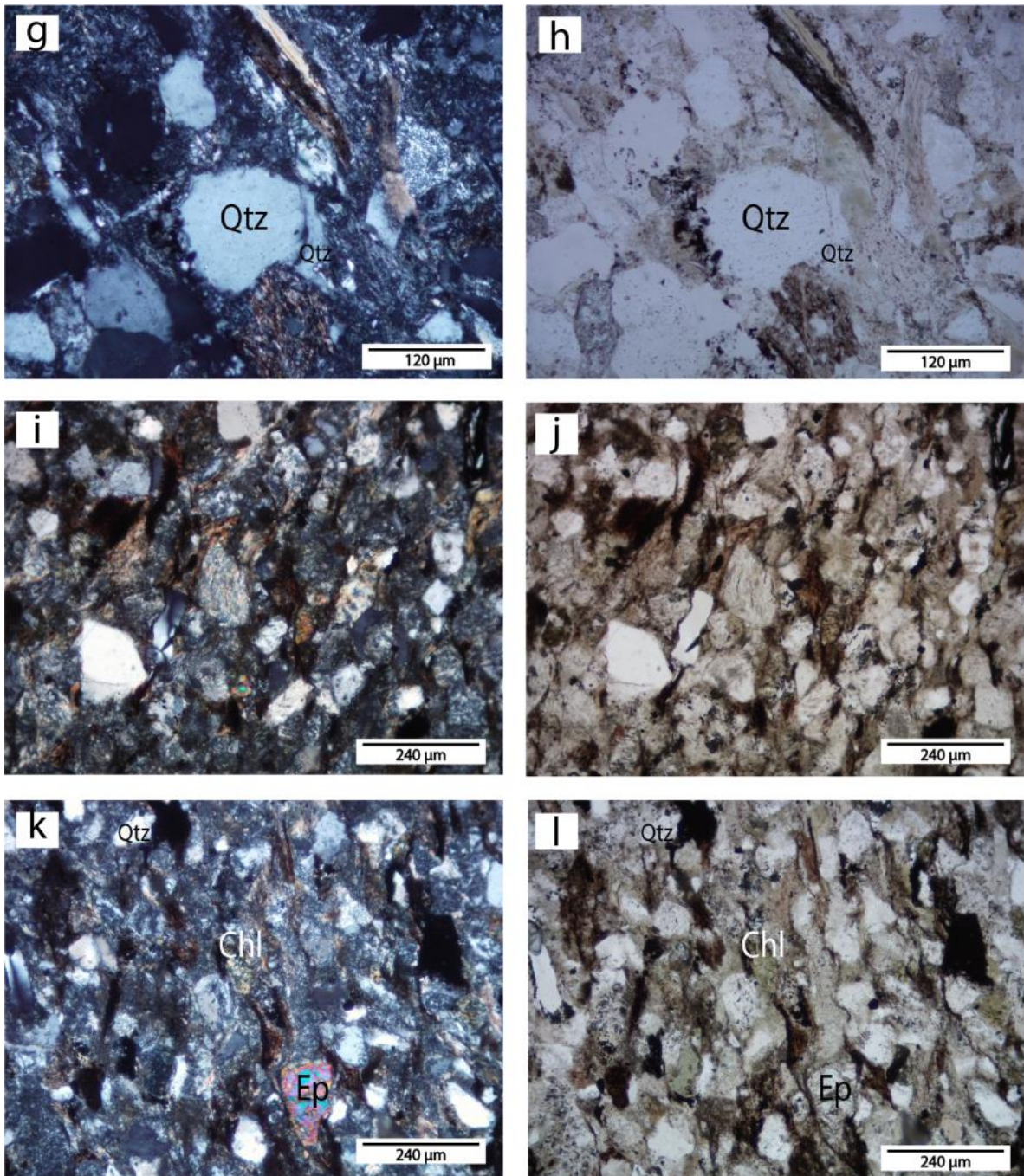


Figure 8: **g)** XPL. Monocrystalline quartz with an iron oxide rim followed by a syntaxial overgrowth. **h)** **g)** in PPL. **i)** XPL. Sedimentary rock fragments of cryptocrystalline aggregates of clay minerals. **j)** **c)** in PPL. **k)** XPL. Secondary chlorite in radial aggregates filling spaces and anhedral crystal of epidote. **l)** **e)** in PPL.

5.2.3. Sample B19-2

Macroscopic description:

Dark greenish gray, clast-supported and well sorted (predominantly silt grains) sample with high harness and conchoidal fracture. The sample has planar lamination that range in thickness from 0.3 cm to 1cm (Fig. 9a).



Figure 9: a) Hand specimen of Sample B19-2. **b)** Identified sections in the lamination of the sample

There are ten appreciable sections in the sample (Fig. 9b) described below, from top to bottom:

I Internal thin planar-parallel lamination with lenses of lighter sediment (Fig. 10j).

H-I Planar contact

H Gradational laminae (Fig. 10i).

G-H Wavy contact

G Internal thin discontinuous and wavy parallel lamination with similar sorting and grains size (Fig. 10h).

F-G Planar contact

F Gradational laminae (Fig. 10g).

E-F Planar contact

E Internal thin planar-parallel lamination with appreciable variations of grain size (Fig. 10f).

D-E wavy contact with flume structures

D Internal thin planar-parallel lamination (Fig. 10e) with oval-shaped lenses of lighter sediment.

C-D Wavy contact

C Internal thin parallel lamination with aligned and oriented dark lenses (Fig. 10d).

B-C Planar contact with associated bioturbation structures (Fig. 10c).

B Ungraded laminae (without sedimentary structures) with a lens of darker sediment (Fig. 10b).

A-B Planar contact

A Ungraded laminae (without sedimentary structures) (Fig. 10a).

Microscopic description:

Table 2: Modal mineral assemblage for each of the identified sections

Section	Clay minerals	Quartz	Plagioclase	White Mica	Igneous rock fragment	Calcite	Chlorite
A, B	78	5	3	<1	1	7	5
B lens	95	3	1	-	1	-	-
C	81	4	2	1	<1	8	3
D, F	89	2	1	<1	-	4	3
D lenses	96	1	-	-	-	2	1
E	86	5	1	-	-	7	1
H, I	72	15	3	<1	1	3	5
G, K	89	2	1	1	-	6	1

The mineral properties are similar for the recognized sections.

Clay Minerals: with the petrographic microscope it could only be identified sericite among the minerals of clay. The other require specific instruments to be classified.

Quartz: angular grains with low or high sphericity. They have parallel extinction.

Plagioclase: subangular grains with low or high sphericity. They may have polysynthetic twinning and are subtly altered to sericite.

White mica: angular with low sphericity

Igneous rock fragment: angular with high sphericity. They have a holocrystalline porphyritic texture. Crystals consist of subhedral plagioclase with tabular habit and Carlsbad twinning in groundmass altered to chlorite.

Calcite: anhedral crystals in aggregates without twinning. They are replacing plagioclase grains.

Chlorite: euhedral to subhedral free crystals. They have colorless to pale green pleochroism and anomalous birefringence.

Classification: The sample correspond to a laminated siltstone.

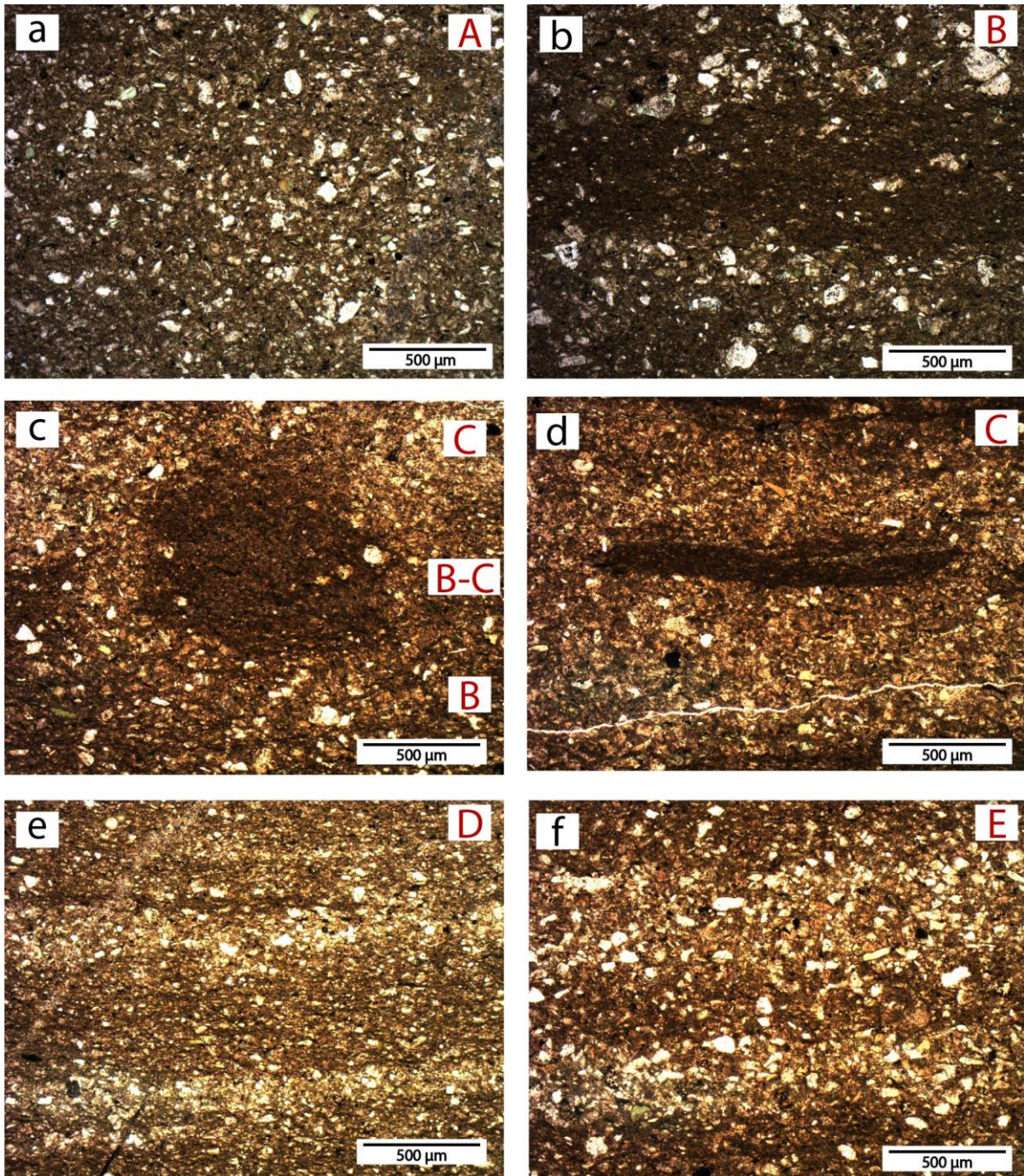


Figure 10: a) XPL. A ungraded laminae. b) PPL. B ungraded laminae with lens of darker sediment. c) PPL. Bioturbation structure in the contact between B and C. d) C section with lenses of darker sediment. e) PPL. D section with internal planar-parallel lamination. f) PPL. E section with internal planar-parallel lamination. Note the variations in grain-size between the laminae.

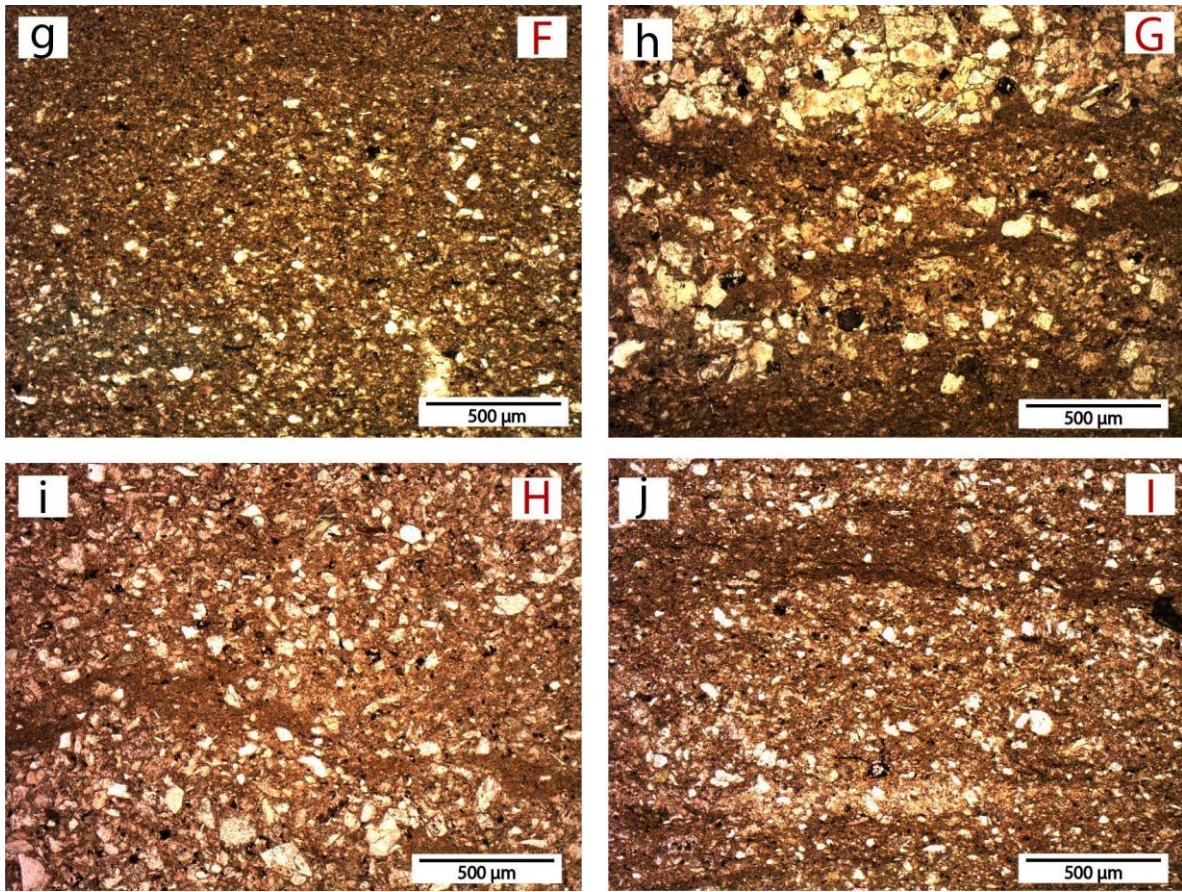


Figure 10: g) PPL. F gradational laminae. h) PPL. G section with internal thin discontinuous and wavy parallel lamination. i) PPL. H gradational laminae with lens of darker sediment. j) PPL. I section with thin planar-parallel lamination and lenses of lighter sediment.

5.2.4. Sample B31-1

Microscopic description: The sample is a holocrystalline porphyritic rock with mesocrystals of plagioclase and microcrystals of pyroxene in a groundmass made up by microlites of plagioclase. The mineral assemblage is: plagioclase (61%) and clinopyroxene (32%). Accessory minerals consist of opaque minerals (4%), quartz (2%) and clinozoisite (1%). Secondary minerals include sericite, chlorite, opaque minerals and calcite. Vesicles represent less than 1% of the sample.

Plagioclase: mesocrystals (ranging in size from 0.5 mm to 1.3 mm) and microcrystals (<0.5 mm). Mesocrystals can be subdivided in four types according to their texture: (A) Free crystals with euhedral to subhedral core, tabular habit and without twinning or zoning. They have a subhedral to anhedral overgrowth rim of maximum 30 µm. They are altered to sericite along all the crystal (Fig. 11a). (B) It is the dominant type. Euhedral to subhedral tabular free crystals with deformation polysynthetic twinning on the albite law and only in some cases combined with pericline law or Carlsbad law. They are not zoned and they are altered to sericite along all the crystal (Fig. 11b). (C)

With the same textural characteristics of (B), but polysynthetic twinning is not deformed. Based on Michel-Levy method, this plagioclase is compositionally classified as albite/andesine. (D) Free crystals with anhedral core, deformation polysynthetic twinning that is sometimes combined with Carlsbad twinning and concentric zoning. They are surrounded by a sericite rim, followed by subhedral to anhedral overgrowth border of maximum 90 µm (Fig. 11c).

Microcrystals are subhedral to anhedral crystals in aggregates. Rarely, they present polysynthetic twinning. They are between the mesocrystals of plagioclase and mafic minerals.

Clinopyroxene: microcrystals (<0.5 mm) are found as free crystals or in aggregates: (A) Subhedral to anhedral free crystals with tabular or prismatic (4 or 8 sided) habit, colorless and with a maximum extinction angle of 45°. They exhibit irregular fractures and crystals are partially or totally altered to chlorite and opaque minerals (Fig.11e,f). (B) Free crystals with anhedral core, colorless and with high birefringence. They are surrounded by a reaction border of cryptocrystalline opaque minerals, followed by a subhedral to anhedral overgrowth border of maximum 60 µm (Fig. 11g,h). (C) Aggregates of subhedral and anhedral mesocrystals, colorless and with high birefringence. They can be altered to cryptocrystalline opaque and clay minerals in the borders and along the fractures (Fig. I,j).

Opaque minerals: subhedral to anhedral free crystals of less than 0.1 mm in length. They appear as free crystals scattered in the groundmass or replacing clinopyroxenes with the chlorite .

Quartz: anhedral free crystals less than 32 µm in maximum dimensions. They are rarely located with the microcrystals of plagioclase in the groundmass.

Clinozoisite: subhedral prismatic free crystals of less than 30 µm in length.

Chlorite: anhedral platelets <0.5 mm in length, pale green colored and with very-low birefringence (black). They alter mafic minerals and in some cases produce chlorite pseudomorphs after pyroxenes.

Calcite: anhedral free crystals infilling interstitial spaces of the sample.

Classification: Modal classification of the sample is a basalt.

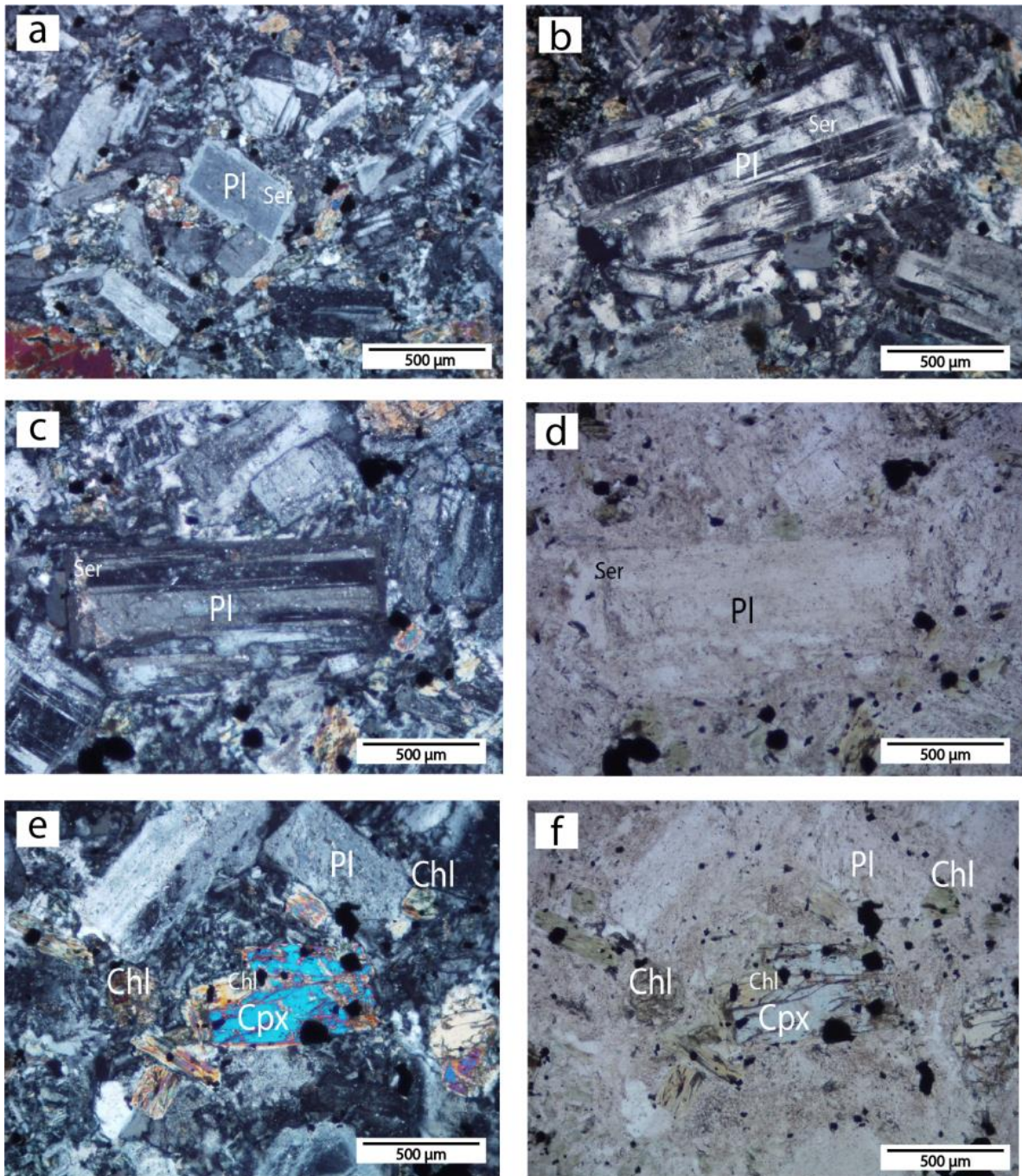


Figure 11: **a)** XPL. Type (A) plagioclase free mesocrystal with euhedral to subhedral core and without twinning or zoning. It has a subhedral overgrowth border. Note the alteration to sericite along all the crystal. **b)** XPL. Type (B) plagioclase free mesocrystal with deformation polysynthetic twinning. It is altered to sericite along all the crystal. **c)** Type (D) plagioclase free mesocrystal with anhedral core and deformation polysynthetic twinning. It is surrounded by a sericite rim, followed by subhedral to anhedral overgrowth border. **e)** Type (A) clinopyroxene free mesocrystal with irregular fractures and partial alteration to chlorite and opaque minerals. Additionally, there are pseudomorphs of chlorite after pyroxenes. **f)** e) in PPL.

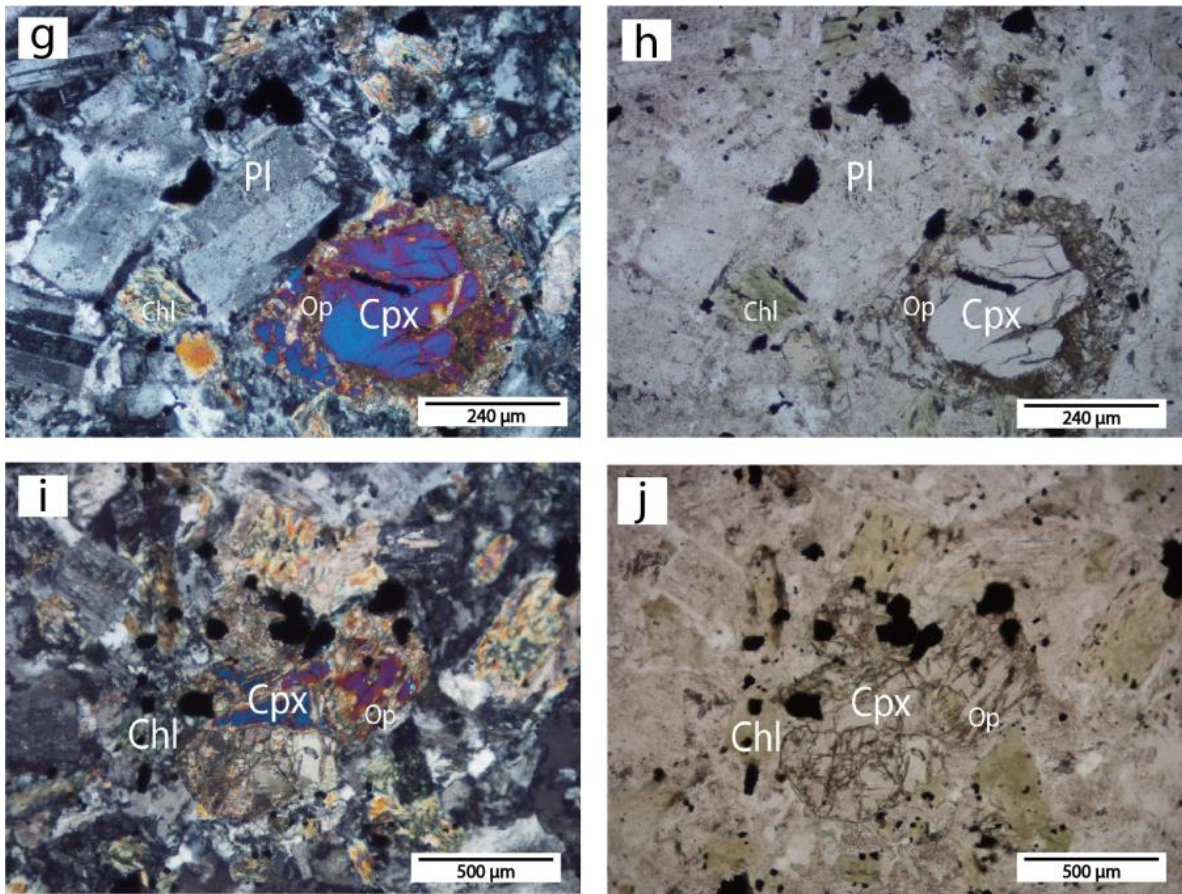


Figure 11: g) XPL. Type (B) clinopyroxene free mesocrystal with anhedral core surround by a reaction border of cryptocrystalline opaque minerals, followed by a anhedral overgrowth border. h) g) in PPL. i) XPL. Type (C) Aggregates of clinopyroxene mesocrystals. It is altered to cryptocrystalline opaque and clay minerals in the borders and along the fractures. j) i) in PPL.

5.3. Esmita Formation (Nesm)

5.3.1. Sample B24-1

Microscopic description:

The sample is massive, poorly sorted, submature and clast-supported. The framework consists of individual grains of polycrystalline quartz (28%), monocrystalline quartz (14%), plagioclase (8.4%), sedimentary rock fragments (28%), igneous rock fragments (14%), and metamorphic rock fragments (0.7%). The matrix fraction represents the 1% of the sample, while cement represents the 4%. Additionally, the porosity of the sample is 2%.

Framework fraction

Detrital Minerals

Monocrystalline Quartz: ranging in size from 0.2 to 0.4 mm. It is subdivided in two types: (A) Subrounded grains with high sphericity and parallel extinction (B) Subangular to subrounded grains with low or high sphericity and wavy extinction

Polycrystalline Quartz: subangular to rounded with high sphericity grains ranging in size from 0.3 to 0.5 mm. According the aggregate textural characteristics, polycrystalline quartz is subdivided in five types: (A) Inequigranular size distribution of quartz subgrains with irregular boundaries and wavy extinction (chessboard texture). There may be muscovite included on quartz subgrains or along their contacts, without a preferential orientation (Fig. 12a). (B) Inequigranular size distribution of quartz subgrains with polygonal boundaries and parallel extinction. Along the subgrains boundaries there are few elongated micas (Fig. 12b). (C) Equigranular size distribution of quartz subgrains with irregular boundaries and wavy extinction. Along the subgrains boundaries there are bands of fine anhedral quartz grains with wavy extinction formed by bulging recrystallisation, anhedral opaque minerals and calcite (Fig. 12c). (D) Inequigranular size distribution of quartz subgrains with amoeboid boundaries and wavy extinction (Fig. 12d). (E) Equigranular size distribution of quartz subgrains with irregular boundaries, wavy extinction and deformation lamellae (Fig. 12g).

Schistose Quartz (6): subrounded grains with low sphericity and a maximum length of 1 mm. Inequigranular size distribution of quartz subgrains with irregular boundaries and wavy extinction. There is muscovite in the contacts between subgrains that show a preferential alignment resulting in a schistose texture (Fig. 12e).

Plagioclase: ranging in size from 0.1 to 0.4 mm. It is subdivided in six types according to its textural characteristics: (A) Angular grains with low sphericity. They have wavy extinction without twinning (Fig. 12h). (B) Subangular grains with high sphericity and polysynthetic twinning. They can be faulted giving up to non-continued and displaced polysynthetic twinning. In some cases, grains are subtly altered to sericite and calcite (Fig. 12i). (C) Angular grains with low or high sphericity. They have deformation polysynthetic twinning and they are altered to sericite, calcite and chlorite (Fig. 12j). (D) Subangular grains with high sphericity. They have symplectitic texture and are altered to epidote (Fig. 12k). (E) Angular grains with low sphericity. They have coarse-sieve in the core and fine-sieve towards the rim. Moreover, they are altered to sericite (Fig. 12l). (F) Subrounded grains

with high sphericity. They are aggregates of plagioclase with polysynthetic twinning in different directions and sericite alteration (Fig. 12m).

Rock fragments

Metamorphic rock fragments: rounded grains with low sphericity of maximum 0.4 mm in length. They have lepidoblastic texture with folded metamorphic foliation defined by anhedral elongated white micas, graphite and anhedral opaque minerals. Locally, there are equigranular aggregates of quartz with wavy extinction and irregular subgrain boundaries (Fig. 12n).

Igneous rock fragments: ranging in size from 0.1 to 0.5 mm. They can be subdivided in three types according to their textural characteristics: (A) subrounded grains with high sphericity. They are hialocrystalline. Crystals consist of euhedral to subhedral free microcrystals of plagioclase with tabular habit, polysynthetic or Carlsbad twinning, sericite alteration and without a preferential orientation. Moreover, there are anhedral opaque minerals and calcite. Glass is locally devitrified and, in some grains, it is totally oxidized (Fig. 12o). (B) subrounded grains with low sphericity. They have the same characteristics of (A), but microcrystals are totally aligned and anhedral chlorite with radial habit is filling interstitial spaces (Fig. 12p). (C) angular grains with low sphericity. They are hialocrystalline with porphyritic texture. Crystals include free mesocrystals of euhedral to subhedral plagioclase with tabular or prismatic habit, polysynthetic, Carlsbad or deformation polysynthetic twinning, in some cases with coarse sieve texture in the core and sericite alteration. The groundmass is vitric-crystalline with tabular or acicular plagioclase microcrystals and oxidized glass (Fig. 12q,r).

Sedimentary rock fragments: ranging in size from 0.7 to 2.1 mm. They can be subdivided in four types according to their textural characteristics and components: (A) subrounded with low sphericity. They are constituted by angular and subangular plagioclase grains with polysynthetic and Carlsbad twinning and altered to sericite in a fully oxidized matrix (Fig. 12s). (B) subrounded with high sphericity. They are principally composed by very fine-grained quartz with angular grains of white mica and rounded calcite. Along the grains there are oxide stylolites. In some cases, grains are more oxidized in the border than in the center (Fig. 12u). (C) subrounded with high sphericity. They are made up by clay minerals and coarse rounded calcite (Fig. 12v). (D) subrounded with high sphericity. They are predominantly made up by radial and fibrous clay minerals with subrounded grains of quartz and subangular micas (Fig. 12t).

Matrix

It is constituted by fine material with a maximum size of 0.03mm. Likewise, it is made up by clay minerals with low birefringence (Fig. 12x).

Authigenic minerals

Quartz: comb quartz infill vein (Fig. 12w).

Cement

Calcite: anhedral and locally with lamellar twinning.

Classification: The sample corresponds to a submature lithic conglomeratic sandstone

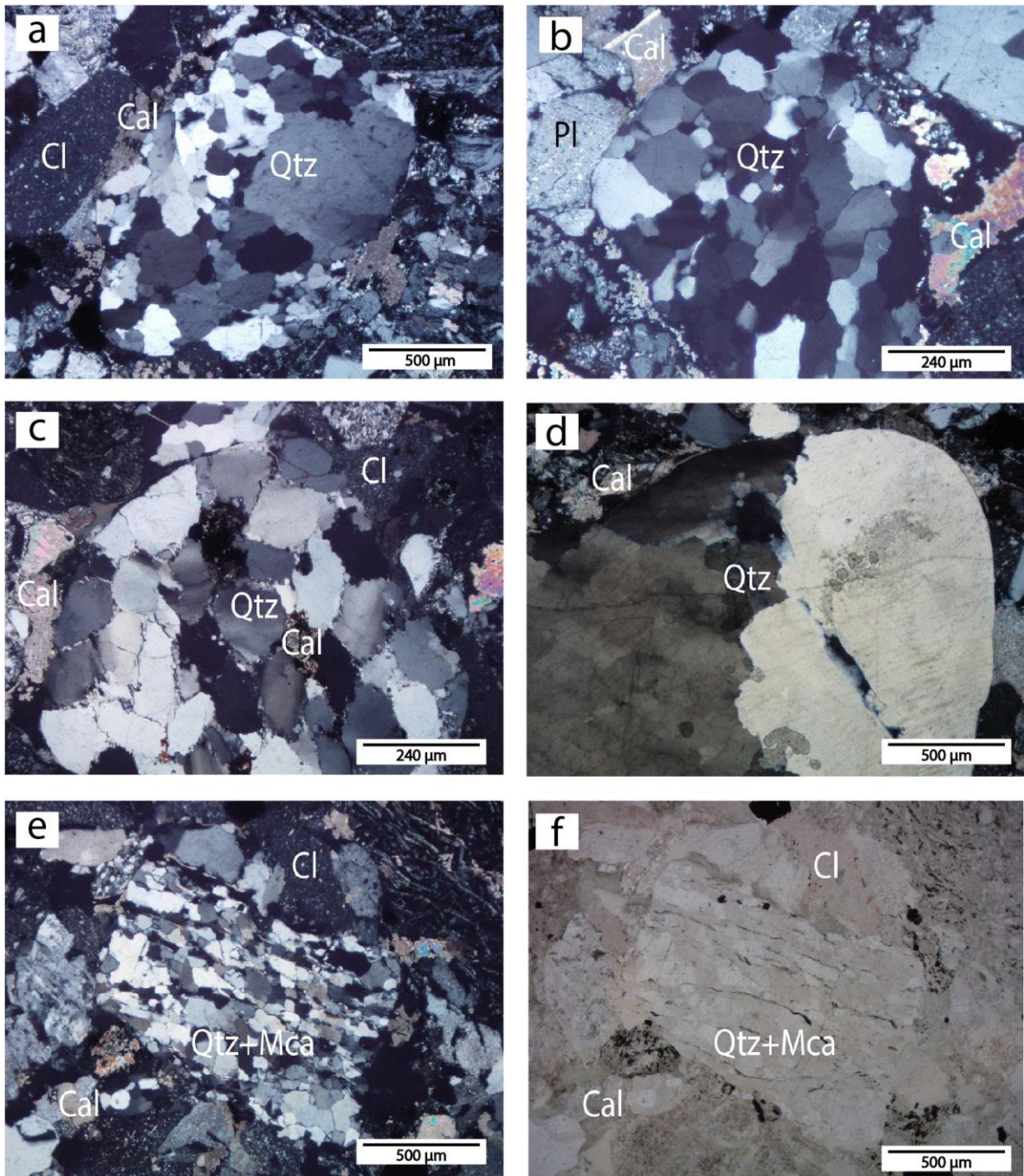


Figure 12: **a)** XPL. Type (A) Polycrystalline quartz with irregular boundaries and wavy extinction. **b)** XPL. Type (B) Polycrystalline quartz with polygonal boundaries and parallel extinction. **c)** XPL. Type (C) Polycrystalline quartz with irregular boundaries and wavy extinction. Note the bands of fine quartz grains with wavy extinction formed by bulging recrystallisation. **d)** XPL. Type (D) Polycrystalline quartz with amoeboid boundaries and wavy extinction. **e)** XPL. Schistose quartz. **f)** e) in PPL.

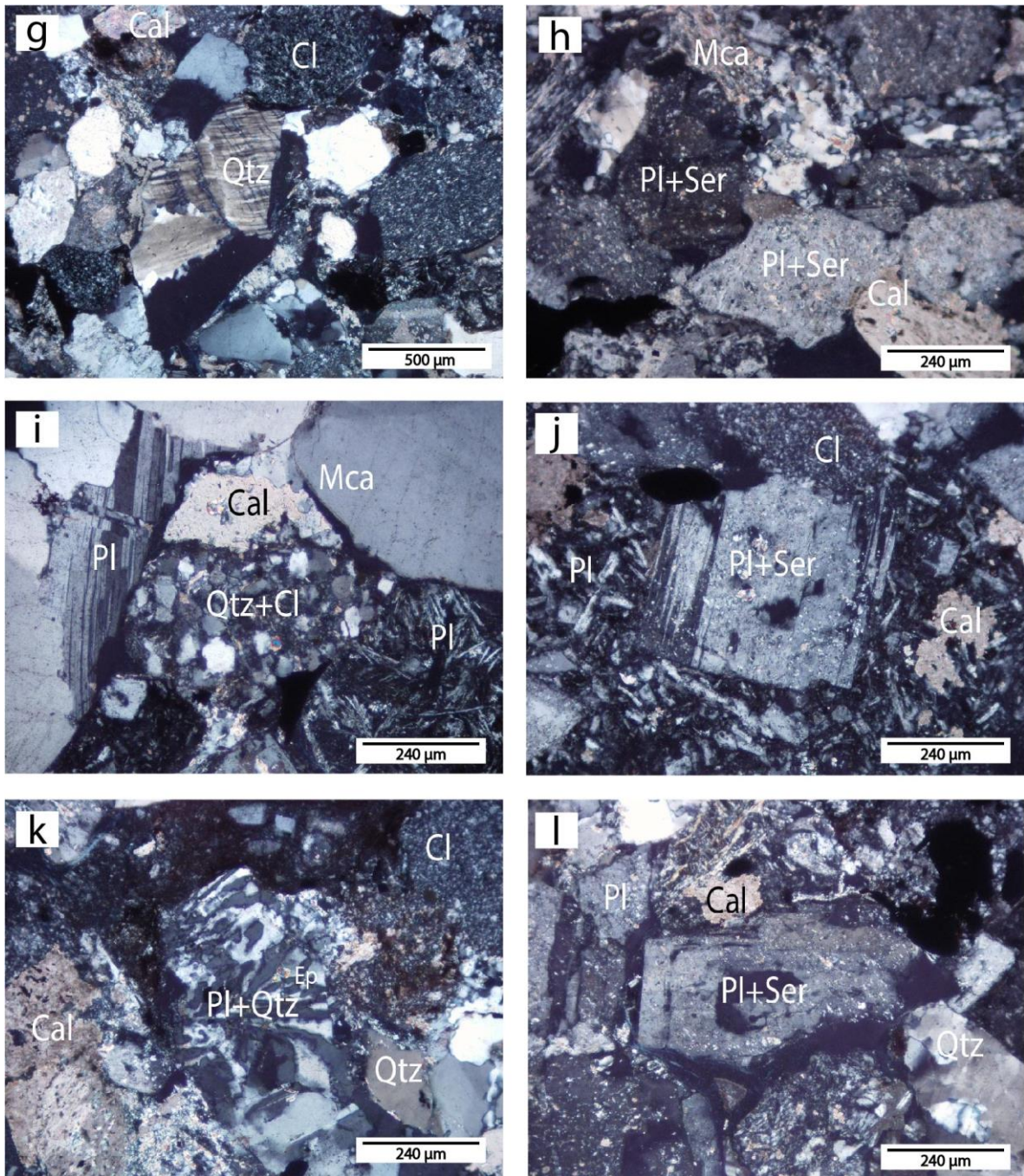


Figure 12: g) XPL. Type (E) Polycrystalline quartz with irregular boundaries, wavy extinction and deformation lamellae. h) XPL. Type (A) plagioclase grain with wavy extinction without twinning. i) XPL. Type (B) plagioclase grain. It is faulted giving up to non-continued and displaced polysynthetic twinning (it is not centered in the optic field). j) Type (C) plagioclase grain with deformation polysynthetic twinning. It is altered to sericite, calcite and chlorite. k) XPL. Type (D) plagioclase grain with symplectitic texture. It is altered to epidote. l) XPL. Type (E) plagioclase grain with coarse-sieve in the core and fine-sieve towards the rim. It is altered to sericite.

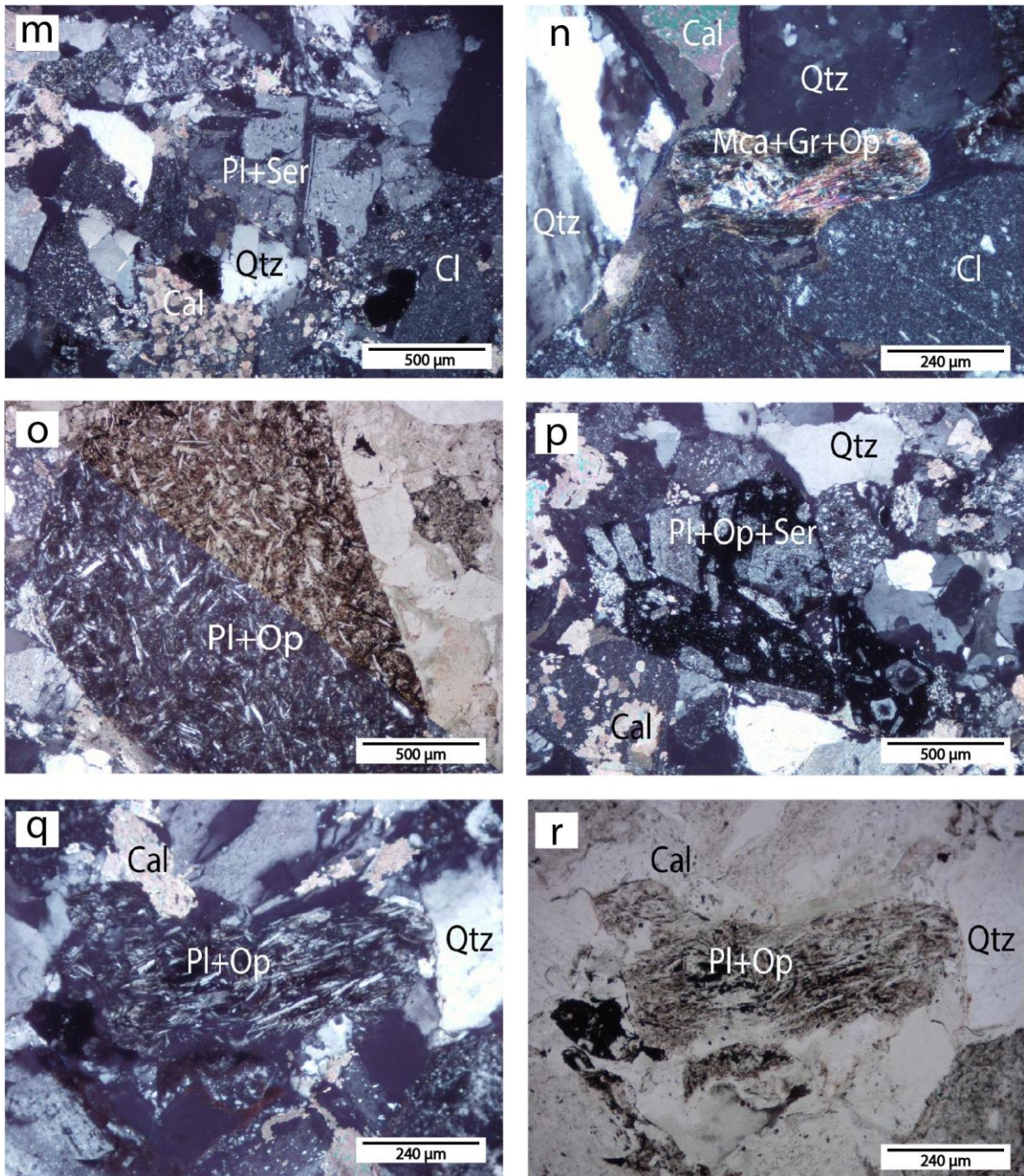


Figure 12: **m)** XPL. Type (F) aggregates of plagioclase with polysynthetic twinning in different directions. Note the sericite alteration. **n)** XPL. Metamorphic rock fragment grain with lepidoblastic texture and folded metamorphic foliation defined by white micas, graphite and opaque minerals. **o)** XPL/PPL. Type (A) igneous rock fragment grain with haliocystalline texture. It consists of plagioclase microcrystals without a preferential orientation, opaque minerals and calcite. Glass is locally devitrified. **p)** XPL. Type (B) igneous rock fragment grain with haliocystalline texture and aligned microcrystals. **q)** XPL. Type (C) igneous rock fragment grain with haliocystalline and porphyritic texture. It is made up by mesocrystals of plagioclase in a vitric-crystalline groundmass of plagioclase microcrystals and glass. **r)** **q)** in PPL.

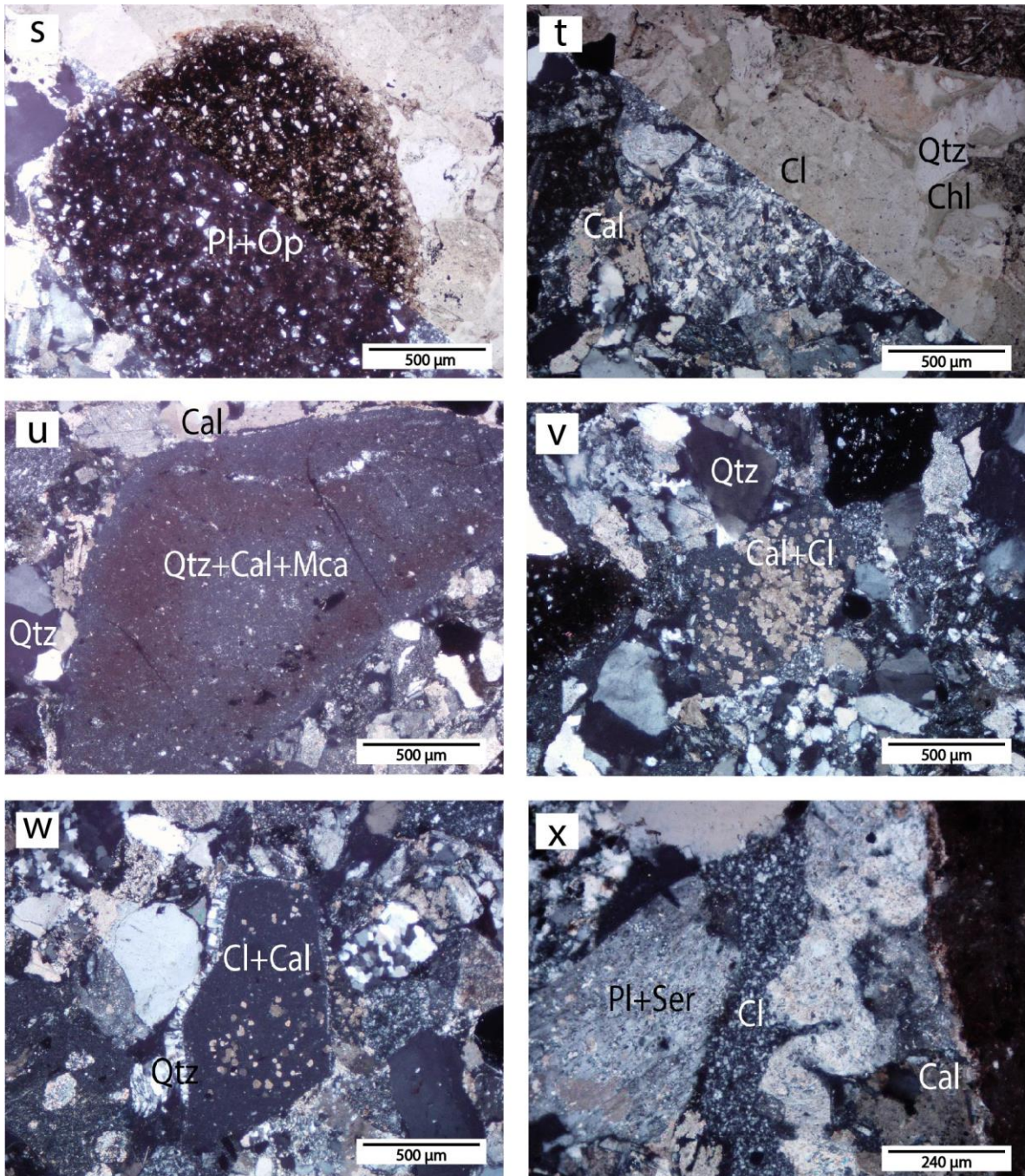


Figure 12: **s)** XPL. Type (A) sedimentary rock fragment grain with plagioclase grains in a fully oxidized matrix. **t)** XPL/PPL. Type (D) sedimentary rock fragment grain made up by radial and fibrous clay minerals with grains of quartz and micas. **u)** XPL. Type (B) sedimentary rock fragment grain composed by vey fine-grained quartz, white mica and calcite. **v)** XPL. Type (C) sedimentary rock fragment grain may up by clay minerals and coarse rounded calcite. **w)** XPL. Comb quartz infill vein. **x)** XPL. Matrix made up by clay minerals.

5.3.2. Sample B29-1

Macroscopic description:

Pale brown, clast-supported and well sorted (very fine sand to fine sand) sample constitute by subrounded grains with high sphericity. It consists of quartz, plagioclase, white micas, rock fragments and rarely potassic feldspar (Fig. 13).



Figure 13: Hand specimen of Sample B29-1

Microscopic description:

Framework fraction

The sample is homogeneous, well sorted, mature and clast-supported. The framework consists of individual grains of monocrystalline quartz (30.9%), polycrystalline quartz (10.8%), plagioclase (4.6%), opaque minerals (3.1%), amphibole (1.5%), epidote (1.5%), orthoclase (0.8%), titanite (0.8%), sedimentary rock fragments (23.2%), igneous rock fragments (4.6%) and metamorphic rock fragments (3.1%). The matrix fraction represents the 6% of the sample, while the cement represents the 3%. Authigenic minerals consist of calcite (1%). Moreover, the porosity of the sample is the 5%.

Detrital Minerals

Monocrystalline Quartz: ranging in size from 50 µm to 0.3 mm. As in sample B24-1, monocrystalline is subdivided in types (A) and (B).

Polycrystalline Quartz: subrounded with high sphericity grains ranging in size from 0.2 to 0.3 mm. According the aggregate textural characteristics, polycrystalline quartz is subdivided in two types: (A) (See description (A) in Sample B24-1). Within the polycrystalline quartz there is also plagioclase with polysynthetic twinning. (F) Inequigranular size distribution of quartz subgrains with polygonal boundaries and wavy extinction. There is some muscovite in the contacts between subgrains.

Schistose Quartz: (See description in Sample B24-1) subrounded grains with low sphericity and a maximum length of 0.4 mm.

Plagioclase: ranging in size from 0.2 to 0.3 mm. It is subdivided in five types according to its textural characteristics: (A) (See description (A) in Sample B24-1) Subangular grains with high sphericity. (B) (See description (B) in Sample B24-1) Subrounded grains with low sphericity. They are only altered to sericite. (C) (See description (C) in Sample B24-1) Subrounded grains with low sphericity. They are only altered to sericite. (G) Subrounded grains with high sphericity. They are untwined and concentrically zoned (Fig. 14a,b). (H) Subrounded grains with high sphericity. They have polysynthetic twinning with irregular patchy pattern of alteration (Fig. 14c,d).

Orthoclase: subrounded grains with high sphericity and a maximum length of 0.2 mm. They are untwined and with perthite unmixing texture in the form of irregular veinlets (Fig. 14e).

Amphiboles: angular to subangular grains with low sphericity ranging in size from 0.1 to 0.3 mm. They have light green to light olive pleochroism and grayish yellow or yellowish gray interference colors. In basal sections, amphiboles expose cleavage in two sets: 56° and 124° and extinction is symmetrical (Fig. 14g).

Epidote: detrital epidote is found as angular to subangular grains with a maximum length of 0.3 mm. They have grayish yellow to light blue green pleochroism and high interference colors. Additionally, grains are fractured (Fig. 14f).

Titanite: rounded with high sphericity. They are colorless and high birefringence (moderate orange pink). Likewise, grains are fractured.

Opaque minerals: rounded to subrounded grains with low or high sphericity.

Rock fragments

Igneous rock fragments: subrounded grains with high sphericity ranging in size from 0.2 to 0.3 mm. They have a hialocrystalline porphyritic texture. Additionally, crystals consist of euhedral plagioclase with tabular habit and polysynthetic twinning, and smaller subhedral plagioclase crystals with acicular habit set in a very-fined oxidized groundmass in which it can only be recognized devitrified glass (Fig. 14i).

Metamorphic rock fragments: subangular to subrounded grains with a maximum size of 0.5 mm. They are foliated and, in some cases, folded. Although, they are constituted by fine-grained material, it can be identified micas, graphite and opaque minerals following the foliation.

Sedimentary rock fragments: ranging in size from 0.1 to 0.3 mm. They can be subdivided in three types according to their textural characteristics: (E) subangular to subrounded grains with low or high sphericity and an oxidized border. They are composed by clay minerals, rounded quartz with wavy or parallel extinction, subrounded opaque minerals and very fine chlorite (Fig. 14j). (F) subangular to subrounded grains with high sphericity. Their composition is really similar to type (E), but opaque minerals are aligned. Furthermore, their core is more oxidized than the border (Fig. 14K). (G) subrounded grains with low sphericity. They are only constituted by clay minerals with irregular fractures infilled by iron oxide (Fig. 14m,n).

Matrix

It is constituted by fine material with a maximum size of 30 µm. Likewise, it is made up by quartz, feldspars and clay minerals.

Authigenic minerals

White mica: euhedral to subhedral free crystals with tabular habit with a maximum size of 70 µm. They have bluish white or pale greenish color and high birefringence. They appear as an alteration product of plagioclase grains; however, they are not classified as sericite taking into account their size (Fig. 14l).

Calcite: anhedral crystals, colorless and locally present lamellar twinning.

Epidote: anhedral crystals in aggregates. They have grayish yellow to light blue green pleochroism and high interference colors. Moreover, they are altering plagioclase grains (Fig. 14 o,p).

Cement

Authigenic Quartz: in the form of overgrowths on detrital quartz minerals. The overgrowth and the detrital cores are in optical continuity as they show the same color and uniform interference colors. Usually, the border of the detrital quartz can be recognized by the presence of small specks of hematite and clay. The overall shape of the detrital grains changes with the overgrowth from subrounded to subangular.

Silicic Cement: it postdates the authigenic quartz overgrowths and infills pores. In contrast to the authigenic quartz, silicic cement is not in optical continuity with the detrital cores (Fig. 14q,r).

Classification: The sample corresponds to a mature lithic sandstone

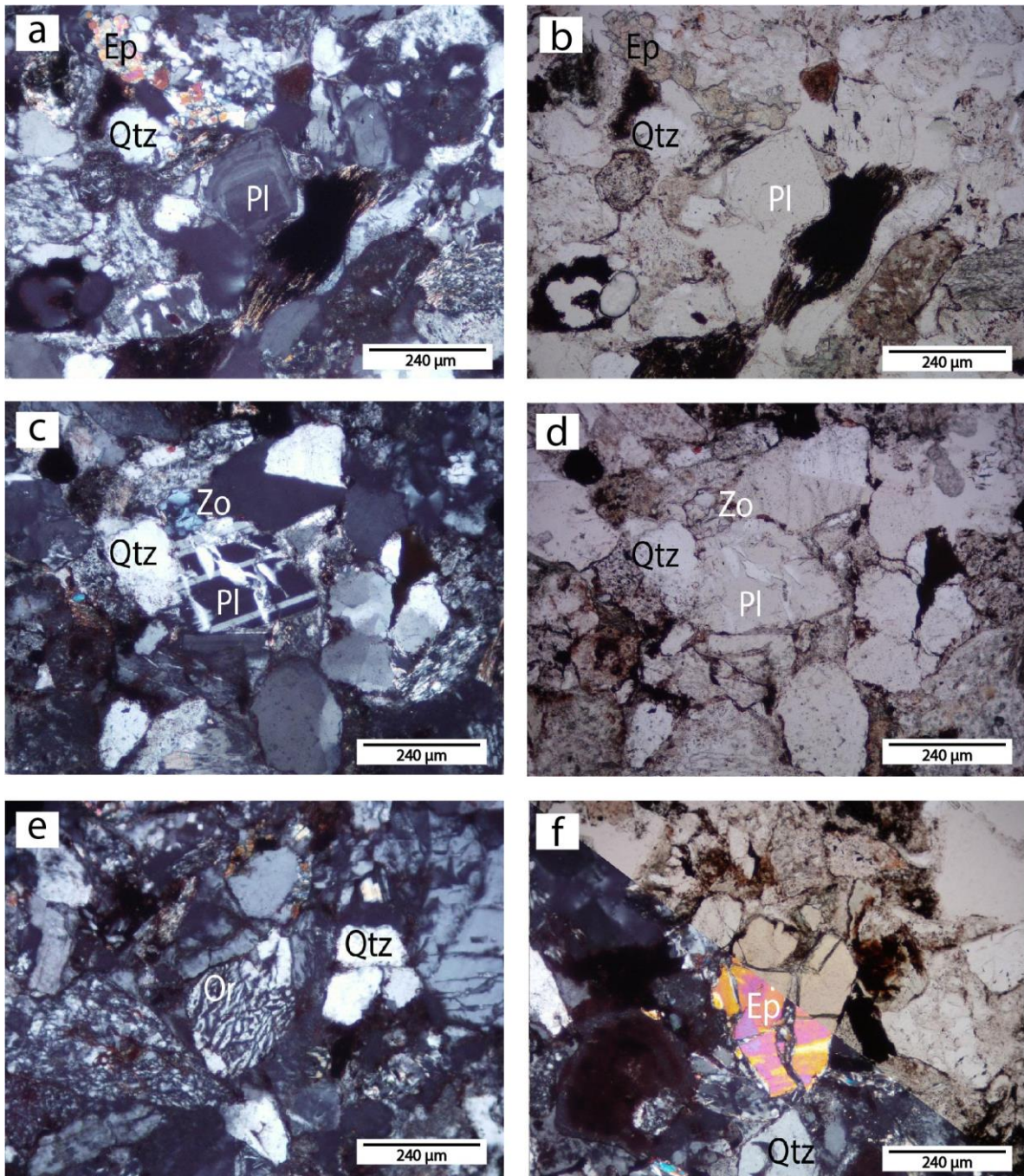


Figure 14: a) XPL. Type (G) plagioclase grain untwinned and concentrically zoned. b) a) in PPL. c) XPL. Type (H) plagioclase grain with polysynthetic twinning and irregular patchy pattern of alteration. d) c) in PPL. e) XPL. Orthoclase grain untwinned and with perthite unmixing texture in the form of irregular veinlets. f) XPL/PPL. Detrital epidote.

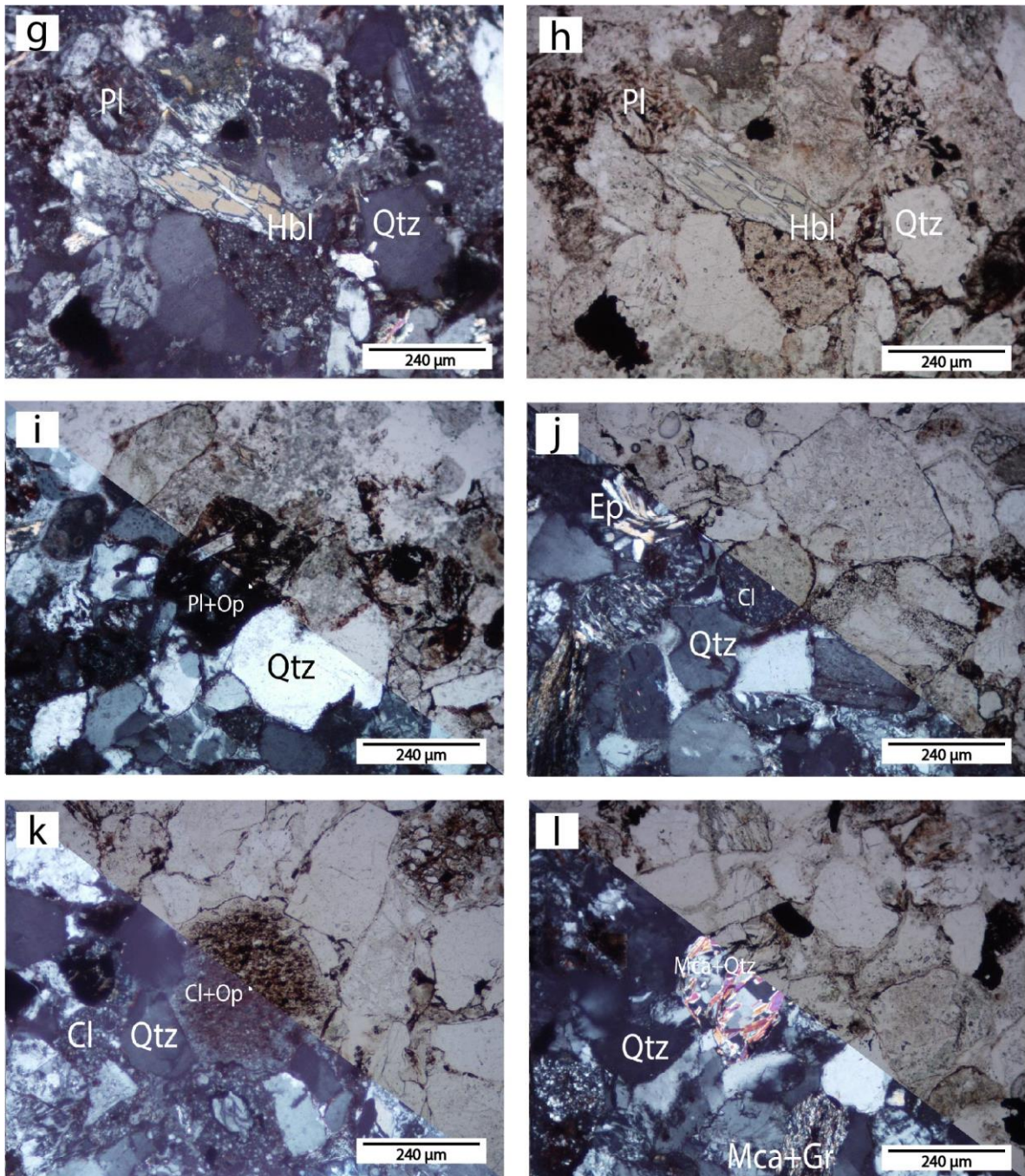


Figure 14: g) XPL. Angular amphibole grain. h) in PPL. i) XPL/PPL. Igneous rock fragment grain with hancrystalline porphyritic texture. It consists of plagioclase crystals set in a very-fined oxidized groundmass in which it can only be recognized devitrified and oxidize glass. j) XPL/PPL. Type (E) sedimentary rock fragment grain composed by clay minerals, quartz, opaque minerals and very fine chlorite. k) XPL/PPL. Type (F) sedimentary rock fragment grain. Note the alignment of opaque minerals. l) XPL/PPL. Authigenic white mica.

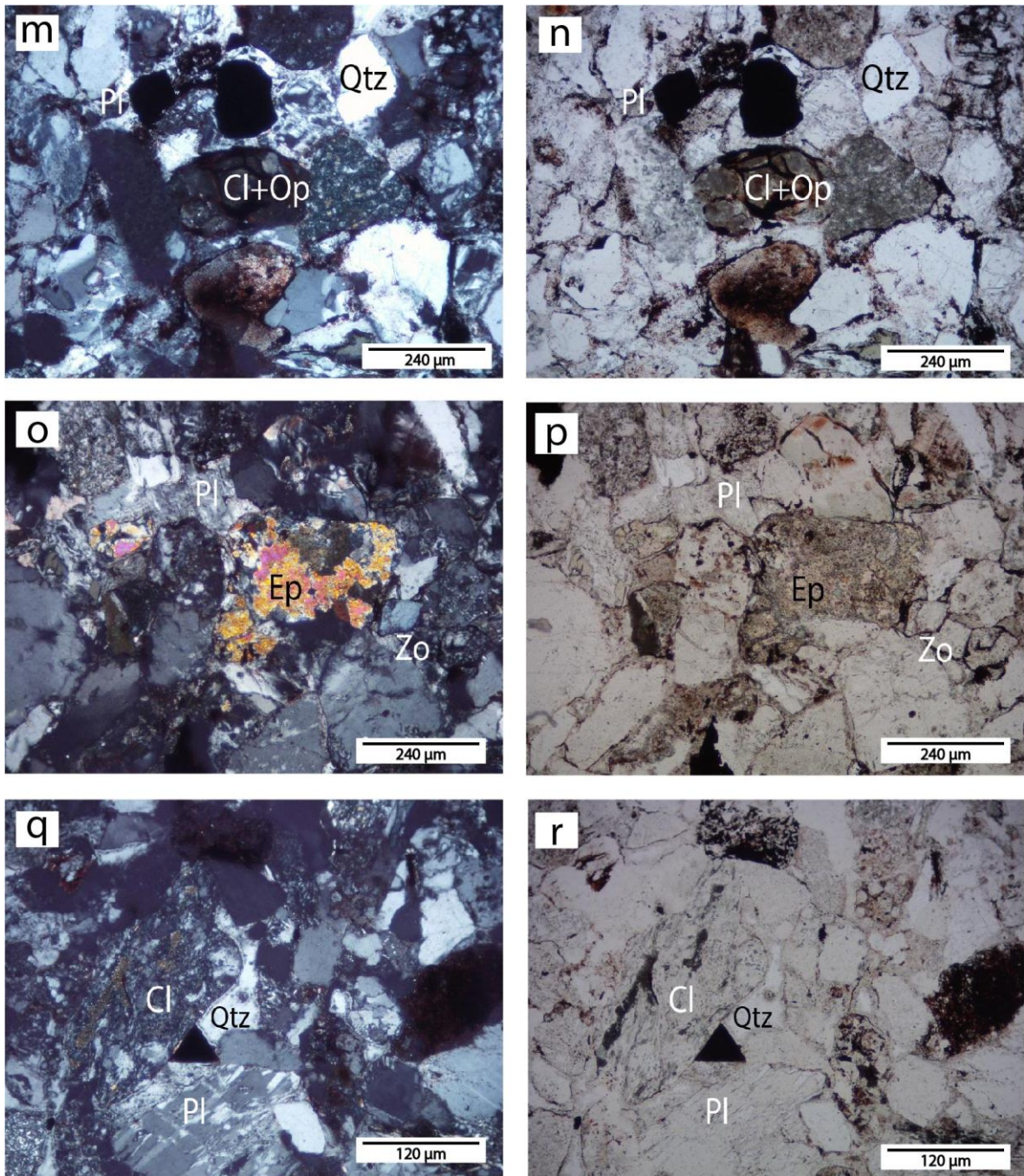


Figure 14: **m)** XPL. Type (G) sedimentary rock fragment grain. It is made up by clay minerals with irregular fractures infilled by iron oxide. **n)** **m)** in PPL. **o)** XPL. Authigenic epidote. **p)** **o)** in PPL. **q)** Silicic cement. **r)** **q)** in PPL.

5.3.3. Sample B32-1

Macroscopic description:

Medium gray, clast-supported and poorly sorted (~94% of sand and ~6% of pebble grains). Sand grains are subrounded with high sphericity and are constituted by quartz, plagioclase and rock fragments. Pebble grains (5-12 mm) are subangular to subrounded with high sphericity and are composed by quartz, plagioclase and rock fragments (Fig. 15).



Figure 15: Hand specimen of Sample B32-1

Microscopic description:

The sample is homogeneous, poorly sorted, submature and clast-supported. The framework consists of individual grains of monocrystalline quartz (30.7%), polycrystalline quartz (7.7%), plagioclase (3.1%), opaque minerals (4.6%), sedimentary rock fragments (26.1%), igneous rock fragments (7.7%) and metamorphic rock fragments (3.1%). Matrix fraction represent the 5% of the sample, while cement the 2%. Authigenic minerals consist of calcite and white micas (6%). Moreover, the porosity of the sample is the 4%.

Detrital Minerals

Monocrystalline Quartz: ranging in size from 0.1 to 0.5 mm. As in samples B24-1 and B29-1, monocrystalline is subdivided in types (A) and (B).

Polycrystalline Quartz: subrounded with low sphericity grains ranging in size from 0.3 to 0.6 mm. According to the aggregate textural characteristics, the dominant polycrystalline quartz is type (A) (See description (A) in Sample B24-1).

Schistose Quartz: (See description in Sample B24-1) subrounded grains with low sphericity and a maximum length of 0.3 mm.

Plagioclase: ranging in size from 0.3 to 0.4 mm. Textures of the plagioclase grains of these samples were already described in Sample B24-1: (A) Subrounded grains with low sphericity. They are altered to sericite. (B) Subangular grains with low sphericity. They are not altered but have few irregular fractures. (C) Subrounded grains with low sphericity. They are only altered to sericite (Fig. 16a). (D) Subangular grains with low sphericity. They are not altered to chlorite. (F) Rounded grains with high sphericity.

Opaque minerals: rounded to subrounded grains with low or high sphericity, ranging in size from 0.1 to 0.2 mm (Fig 16c).

Rock fragments

Metamorphic rock fragments: subrounded grains with low sphericity and a maximum size of 0.4 mm. (See description in Sample B29-1).

Igneous rock fragments: subangular to subrounded grains with high sphericity ranging in size from 0.3 to 0.4 mm. (See description in Sample B29-1).

Sedimentary rock fragments: ranging in size from 0.3 to 0.7 mm. They are rounded grains with high sphericity. Their textural characteristics are the same of (A) type sedimentary rocks fragments of sample B24-1.

Matrix

It consists of detrital minerals with a maximum size of 30 µm, low birefringence and locally altered to sericite. Moreover, it has subrounded opaque minerals.

Authigenic minerals

White mica: anhedral crystals in aggregates with a maximum size of 0.4 mm. They are colorless or with a subtle pleochroism to pinkish gray. They are associated with calcite aggregates.

Calcite: anhedral crystals in aggregates, colorless and without lamellar twinning. They are filling the spaces and the fractures of detrital minerals and rock fragments.

Cement

Cement in the sample is rarely found. Identifiable cement consists of authigenic quartz (See description in Sample B29-1).

Classification: The sample corresponds to a submature lithic conglomeratic sandstone

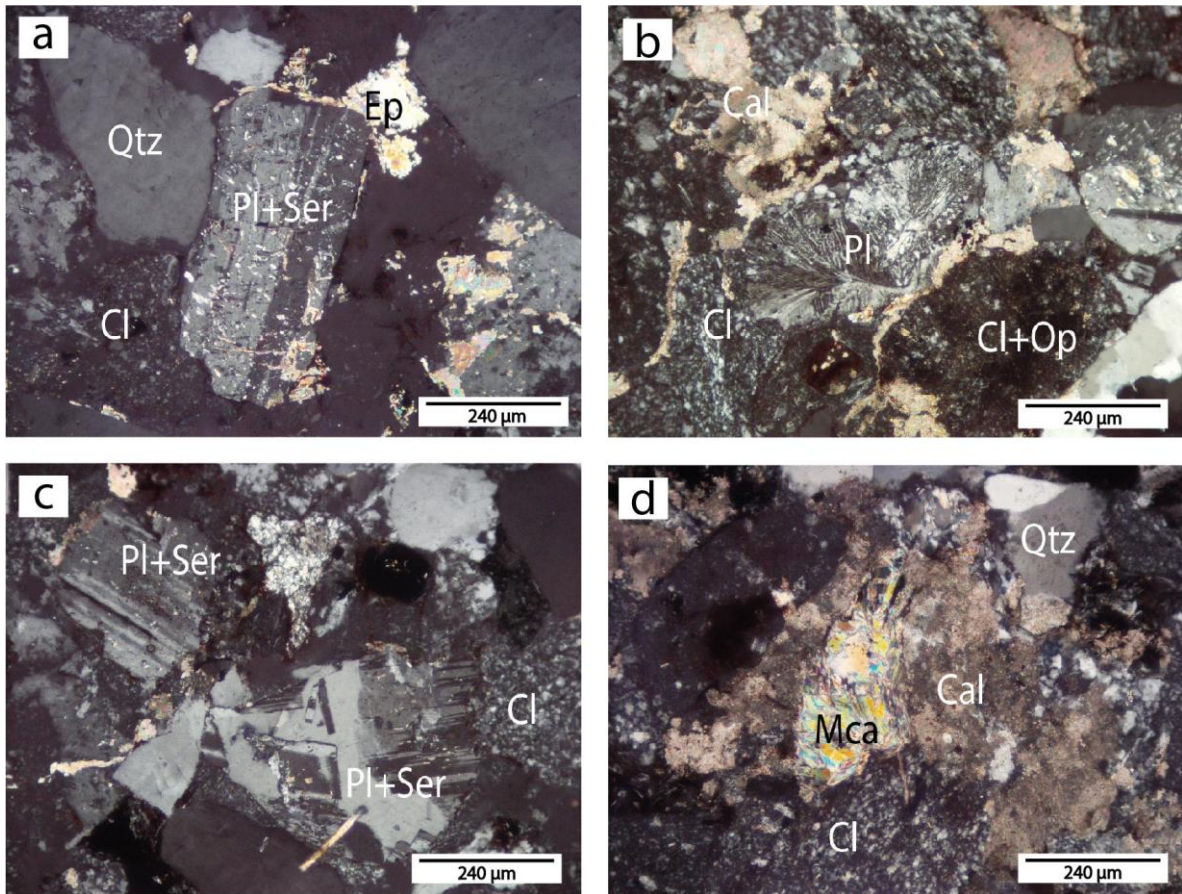


Figure 16: a) XPL. Type (C) plagioclase grains in Sample B32-1. b) XPL. Type (D) plagioclase grains in Sample B32-1. c) XPL. Type (F) plagioclase grains in Sample B32-1. d) XPL. Authigenic white mica associated with calcite aggregates.

5.4. Dacite-Andesite Porphyritic Bodies (Npda)

5.4.1. Sample B26-1

Macroscopic description:

Fresh porphyritic rock with macrocrystals of euhedral tabular plagioclase (2 mm-1.4 cm) and subhedral tabular or hexagonal hornblende (2-5 mm), and mesocrystals (0.5-2 mm) of anhedral plagioclase, subhedral to anhedral tabular hornblende, and subhedral to anhedral quartz. Macrocrystals and mesocrystals are embedded in a greenish gray cryptocrystalline groundmass with anhedral microcrystals of hornblende. The sample is noticeably altered to epidote (Fig.17).



Figure 17: Hand specimen of Sample B26-1

Microscopic description: Holocrystalline porphyritic rock with seriate texture. Macrocrystals and mesocrystals consist of plagioclase, hornblende and quartz scattered in an equigranular microcrystalline groundmass of plagioclase, quartz and hornblende, with spherical vesicles. The mineral assemblage is made up of plagioclase (46%), hornblende (32%), quartz (18%) and apatite (3%). Secondary minerals consist of epidote, clinozoisite, chlorite and calcite. Vesicularity is low and corresponds to 1% of the sample.

Plagioclase: macrocrystals (ranging in size from 2 to 3 mm), mesocrystals (ranging in size from 0.5 mm to 2 mm) and microcrystals (<5 mm). Macrocrystals and Mesocrystals are found as free crystals or aggregates. There are three types according to their texture: (A) It is the most common. Subhedral to euhedral free crystals with prismatic or tabular habit and patchy zoning. They are untwinned and without zoning. Additionally, they are strongly altered to sericite and saussurite: overgrowth of epidote, chlorite, clinozoisite and hornblende spread through the plagioclase crystals or located in the margin. (Fig. 18a,b). (B) Anhedral free crystals untwinned and without zoning. Near the borders, crystals have anhedral to subhedral thin reaction rims of sericite and microcrystals of Fe-Ti opaque minerals (Fig 18. c). (C) Euhedral to subhedral crystals with prismatic habit found as aggregates with a maximum length of 7mm. The twinning is complex: on albite, pericline and Carlsbad laws. In some crystals, the albite and pericline laws are deformed. They are zoned and the borders of the aggregates are more fractured than the cores. Among the grains there is sericite and saussurite alteration (Fig. 18d,e).

Microcrystals are found as anhedral to subhedral crystals in aggregates with quartz. They are altered to sericite and saussurite.

Hornblende: It is the dominant mafic mineral. Macrocrystals (ranging in size from 2 to 6 mm), mesocrystals (ranging in size from 0.5 mm to 2 mm) and microcrystals (<5 mm).

Macrocrystals and Mesocrystals are euhedral to subhedral free crystals with tabular, prismatic or skeletal habit (Fig. 18i,j). They have highly pleochroic green color and lamellar or simple twinning. Moreover, crystals are not zoned and present opaque minerals inclusions (Fig. 18g). They can be partially replaced by chlorite along the borders and cleavages. As some of the plagioclase macrocrystals and mesocrystals, epidotes and clinozoisite altered the borders of the hornblende crystals too.

Microcrystals are not as abundant as microcrystals of plagioclase and quartz. They are found as subhedral to anhedral free crystals with tabular, prismatic or skeletal habit. As mesocrystals, they can also be partially replaced by chlorite along the borders and cleavages.

Biotite: all the crystals observed are subhedral pseudomorphs with tabular habit of chlorite, epidote and magnetite after biotite of maximum in 0.1 mm length (Fig. 18k).

Quartz: mesocrystals (ranging in size from 0.5 mm to 1.5 mm) and microcrystals (<0.5 mm) (Fig 18l).

Mesocrystals can be subdivided in two types: (A) anhedral and rounded free crystals with parallel extinction. They are embayed, corroded and with a reaction border. (B) subhedral free crystals with tabular habit and parallel extinction.

Microcrystals are anhedral free crystals with wavy extinction scattered among the groundmass.

Apatite: trace mineral that is present as euhedral to subhedral free crystals with prismatic habit ranging in size from 0.1 mm to 0.3 mm. They are in the groundmass or as inclusions in hornblende phenocrysts (Fig. 18f).

Epidote/Clinozoisite: found as free crystals or aggregates. In both cases, they are subhedral to anhedral alteration minerals with prismatic habit, ranging in size from 0.3 to 0.6 mm. They are in association with chlorite.

Chlorite: anhedral with pale green pleochroism and without anomaly interference colors. They are altering plagioclases or replacing mafic minerals.

Calcite: anhedral free crystals less than 60 µm in size. They are found filling interstitial spaces in the groundmass.

Interpretation: Modal classification of the sample is a tonalite.

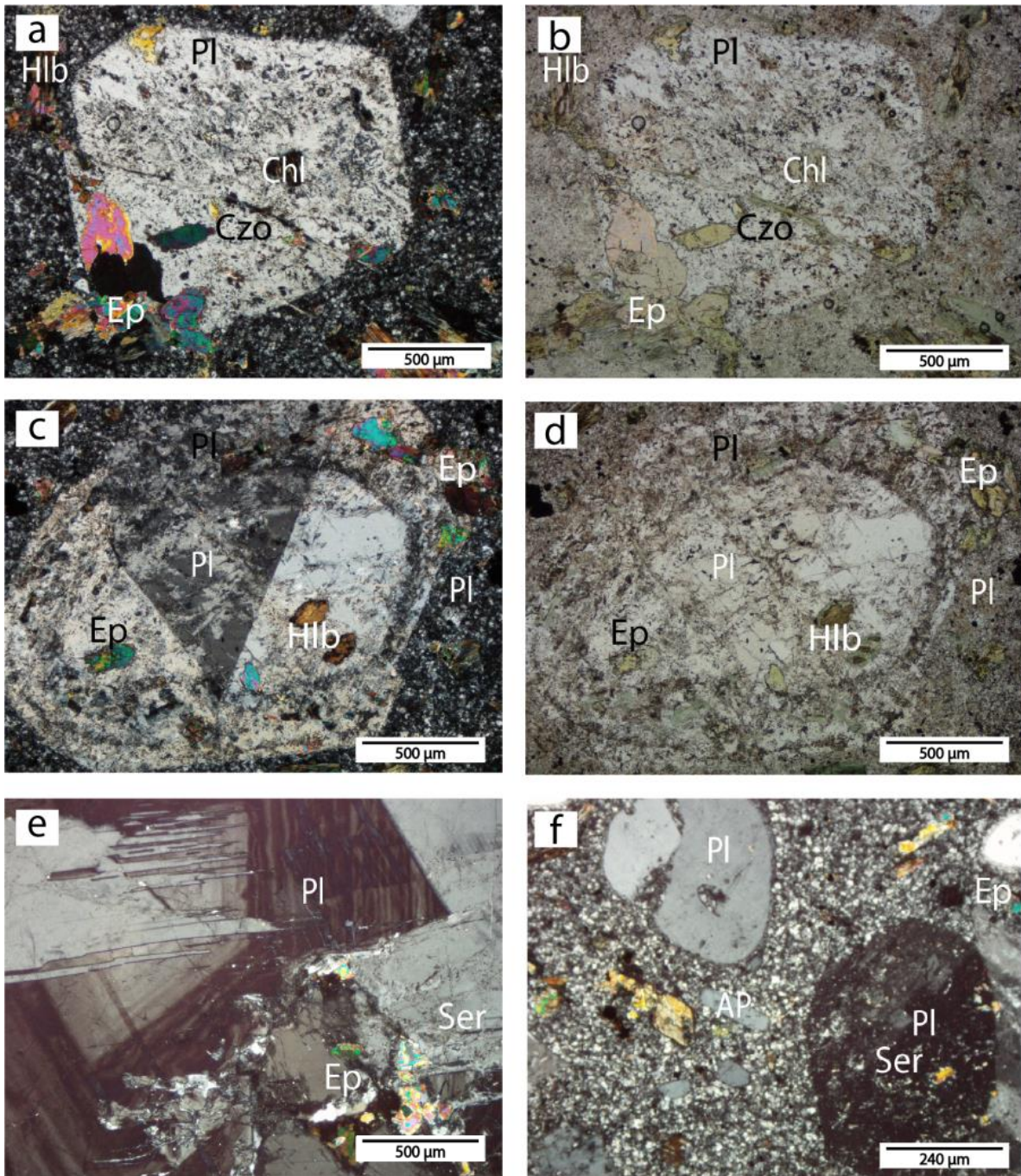


Figure 18: **a)** XPL. Type (A) plagioclase free mesocrystal with patchy extinction. It is untwinned and without zoning. Strong alteration to sericite and saussurite: overgrowth of epidote, chlorite, clinozoisite and hornblende spread through the plagioclase crystals or located in the margin. **b)** a) in PPL. **c)** XPL. Type (B) plagioclase free crystals untwinned and without zoning. Note the reaction rims Fe-Ti opaque minerals. **d)** c) in PPL. **e)** XPL. Type (C) aggregate of plagioclase mesocrystal with deformation polysynthetic twinning. It is concentric zoned and altered to sericite and saussurite (The aggregate completely covers the optical field). **f)** XPL. Apatite free crystals disseminated in the groundmass.

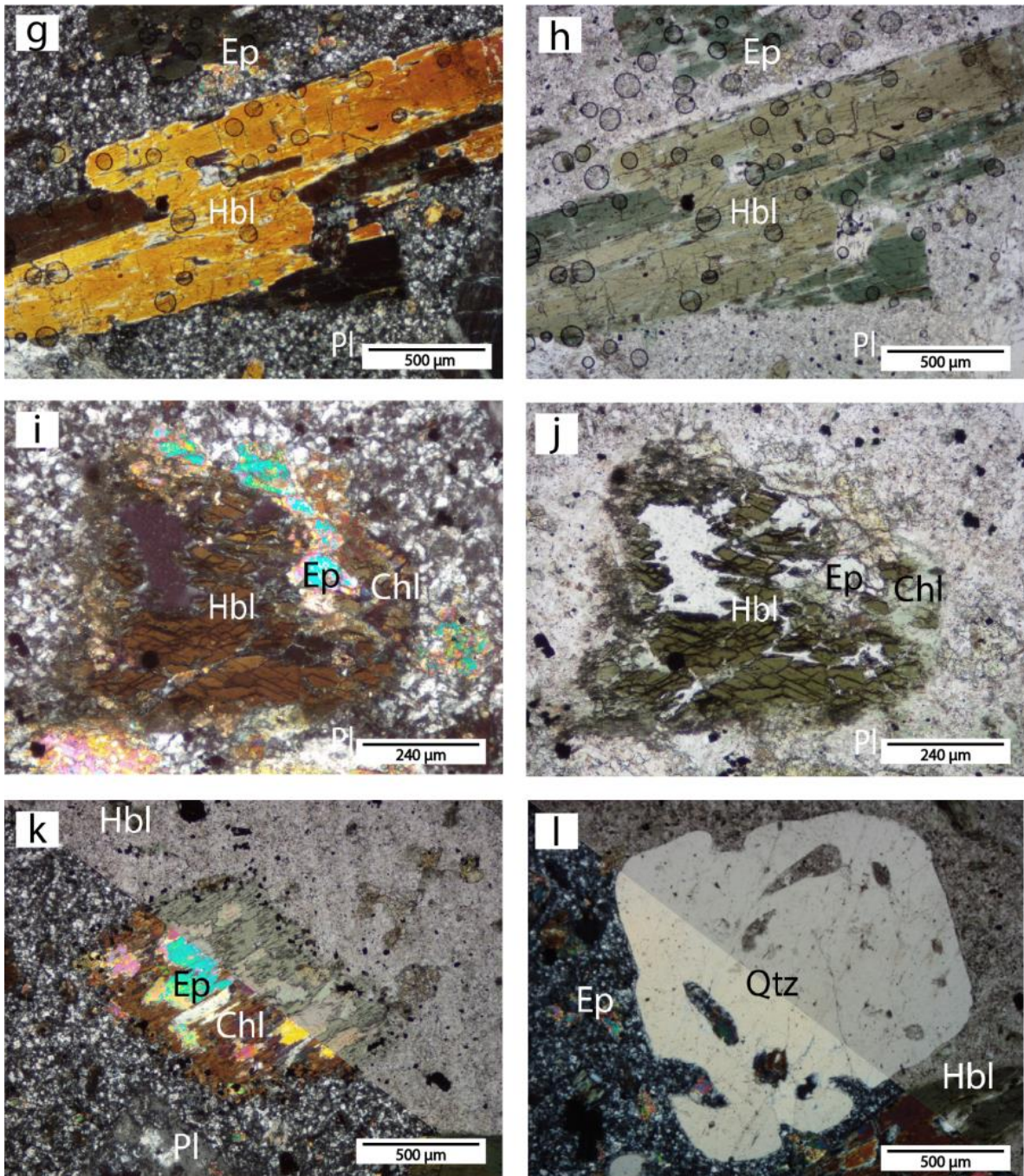


Figure 18: **g)** XPL. Hornblende free macrocrystal with highly pleochroic green color. It has opaque minerals inclusions. **h)** a) in PPL. **i)** XPL. Hornblende free mesocrystal with skeletal habit and highly pleochroic green color. It has opaque minerals inclusions partially replaced by chlorite epidotes and clinozoisite along the borders. **j)** i) in PPL. **k)** XPL/PPL. Pseudomorphs of chlorite, epidote and magnetite after biotite. **l)** XPL/PPL. Type (A) quartz free mesocrystal corroded and embayed.

5.5. Granatífera Tuff (tgr)

5.5.1. Sample B27-1

Microscopic description:

Glass represent the 43.3% of the sample, while lithic clasts represent the 32.12% (metamorphic rock fragments: 21.16%, igneous rock fragments: 10.44% and others: 0.52%). Modal assemblage of free crystals is given by: hornblende (7.28%), quartz (3.4%), plagioclase (3.4%), opaque minerals (2.9%), white mica (0.3%), zoisite (0.3%) and epidote (0.2%). Vesicle content is high and represent the 6.8% of the sample.

Free Crystals

Hornblende: mesocrystals (ranging in size from 0.5 to 0.7 mm) and microcrystals (<0.5 mm).

There are three types according to their texture: (A) Subhedral free crystals with prismatic habit (rhombohedral). They present moderate reddish orange to pale greenish yellow pleochroism and moderate birefringence. Crystal sections show 60°/120° cleavages, without twinning or zoning. Some crystals have symplectitic intergrowths with quartz (Fig. 19b). (B) Subhedral free crystals with tabular or prismatic habit (rhombohedral). Pleochroism is different in the core and in the border: in the core it varies from dusky yellow to pale yellowish orange and in the border to light brown. They have moderate birefringence with symmetric extinction in basal sections. Crystals have simple zoning without twinning (Fig. 19c). (C) Euhedral to subhedral free crystals with tabular habit. Pleochroism and birefringence is the same of (A) hornblende. Crystals have simple twinning without zoning.

Plagioclase: microcrystals (<0.3 mm). Plagioclase is found as subhedral free crystals with tabular habit. They have polysynthetic twinning and are slightly altered to sericite.

Quartz: microcrystals (<0.4 mm). They are subhedral to anhedral free crystals with parallel extinction and irregular fractures (Fig. 19a).

White Mica: microcrystals (<50 µm). White mica is found as anhedral free crystals. They are colorless with high birefringence.

Zoisite and Epidote: as microcrystals (<50 µm). They are subhedral to anhedral free crystals that rarely occur in the sample

Opaque Minerals: microcrystals (<0.1 mm). They are subhedral to anhedral free crystals.

Glass particles

Glass particles can be classified in three categories according to their texture: (A) Subrounded with irregular borders. They are hialocrystalline with fluidal texture, isotropic in PPL with moderate brown color in PPL, and embedding mesocrystals. The latter are subhedral to anhedral hornblende free crystals or aggregates, and euhedral orthopyroxene free crystals. Embedded microcrystals comprise subhedral hornblende, plagioclase and euhedral orthopyroxene free crystals. Additionally, lithic fragments include equigranular polycrystalline quartz with polygonal boundaries and wavy extinction. Vesicles are abundant, ranging from 0.1 to 0.6 mm in length,

predominantly subspherical or irregular due to the coalescence processes (Fig. 19g,h). (B) Subrounded hialocrystalline fragments without preferential orientation of crystals and exhibiting irregular outlines. Embedded microcrystals consist of subhedral hornblende and plagioclase free crystals. Vesicles are also abundant, ranging from 0.1 to 0.6 mm in length, with the same shape that vesicles described in (A) (Fig. 19d). (C) Rounded glass particles similar to B-type, but hosting mesocrystals of subhedral hornblende free crystals and less abundant plagioclase microcrystals. Vesicles are not as abundant as in (A) and (B) but have the same shape.

Rock fragments

Igneous rock fragments: Subrounded to rounded rock fragments, ranging in size from 0.6 to 2 mm. There are three types according to their textural characteristics and components: (A) Hialocrystalline porphyritic rock fragments with seriate texture. They consist of subhedral hornblende and plagioclase free crystals scattered in a crystal-vitric groundmass made up by microcrystals of the same mineralogy. They can locally be oxidized. (B) Hialocrystalline rock fragments in which microcrystals are dominant and consist of subhedral plagioclase free crystals with tabular habit with few hornblende altered free crystals (Fig. 19i,j). (C) Holocrystalline porphyritic rock fragments. Mesocrystals of anhedral hornblende are scattered in a microcrystalline groundmass of subhedral plagioclase with tabular habit and anhedral opaque minerals (Fig. 19k).

Metamorphic rock fragments: Subrounded to rounded rock fragments, in some cases elongated, ranging in size from 1 mm to 3 mm. There are four types according to their textural characteristics and components: (A) Grano-lepidoblastic texture with metamorphic foliation. Granoblastic texture is defined by subhedral and anhedral quartz crystals with irregular boundaries and wavy extinction and by anhedral zoisite. Additionally, lepidoblastic texture is given by anhedral elongated white micas with pale greenish yellow color and high birefringence (Fig. 19m,n). (B) Grano-lepidoblastic texture with metamorphic foliation. Granoblastic texture is defined by subhedral and anhedral quartz crystals with irregular boundaries and wavy extinction. Rarely, quartz is with anhedral plagioclase with polysynthetic twinning. Lepidoblastic texture is given by anhedral elongated white micas with high birefringence and by graphite bands. They can locally be oxidized (Fig. 19l). (C) Polycrystalline quartz with inequigranular size distribution of quartz subgrains with irregular boundaries and wavy extinction. Along the subgrains there are bands of smaller anhedral quartz grains with wavy extinction formed by bulging recrystallisation (Fig. 19o,p). (D) It is also polycrystalline quartz with inequigranular size distribution of quartz subgrains with irregular boundaries and wavy extinction, but subgrains are bigger than in (C) and along the grains there are microcrystalline aggregates of subhedral to anhedral opaque minerals (Fig. 19q,r).

Others: Subrounded rock fragment with granoblastic and inequigranular texture. It consist of subhedral to anhedral mesocrystals and microcrystals of amphibole, anhedral microcrystals of plagioclase and few subhedral microcrystals of pyroxene (Fig. 19e,f).

Interpretation: The sample correspond to a lithic-bearing, vitric lapilli tuff.

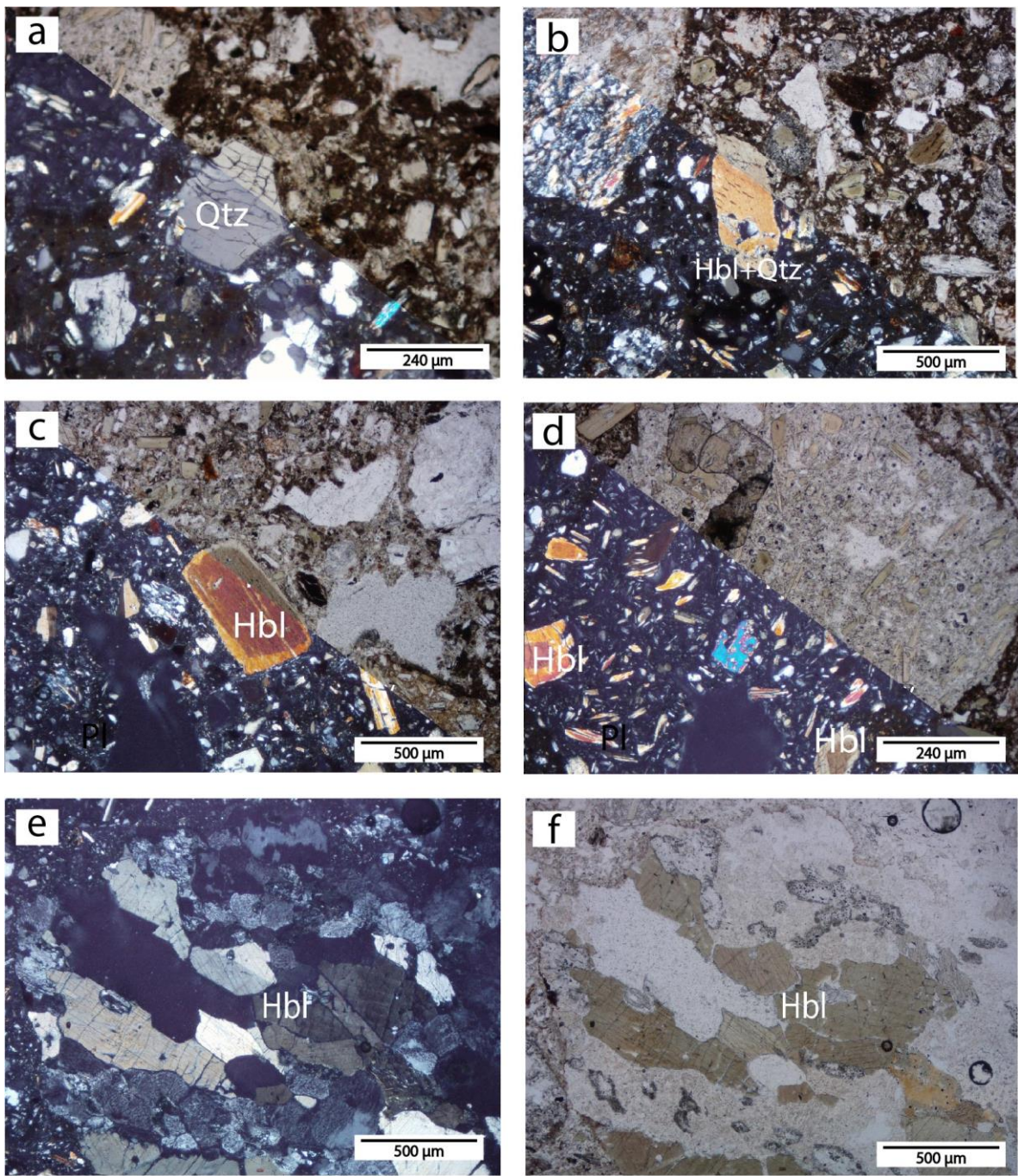


Figure 19: a) XPL/PPL. Quartz mesocrystal with irregular fractures. b) XPL/PPL. Type (A) hornblende free mesocrystal with symplectitic intergrowths with quartz. c) XPL. Type (B) hornblende free mesocrystal noticeable zoned without twinning d) XPL/PPL. Glass type (B). e) XPL. Subrounded rock fragment with granoblastic and inequigranular texture of hornblende, plagioclase and pyroxene. f) e) in PPL.

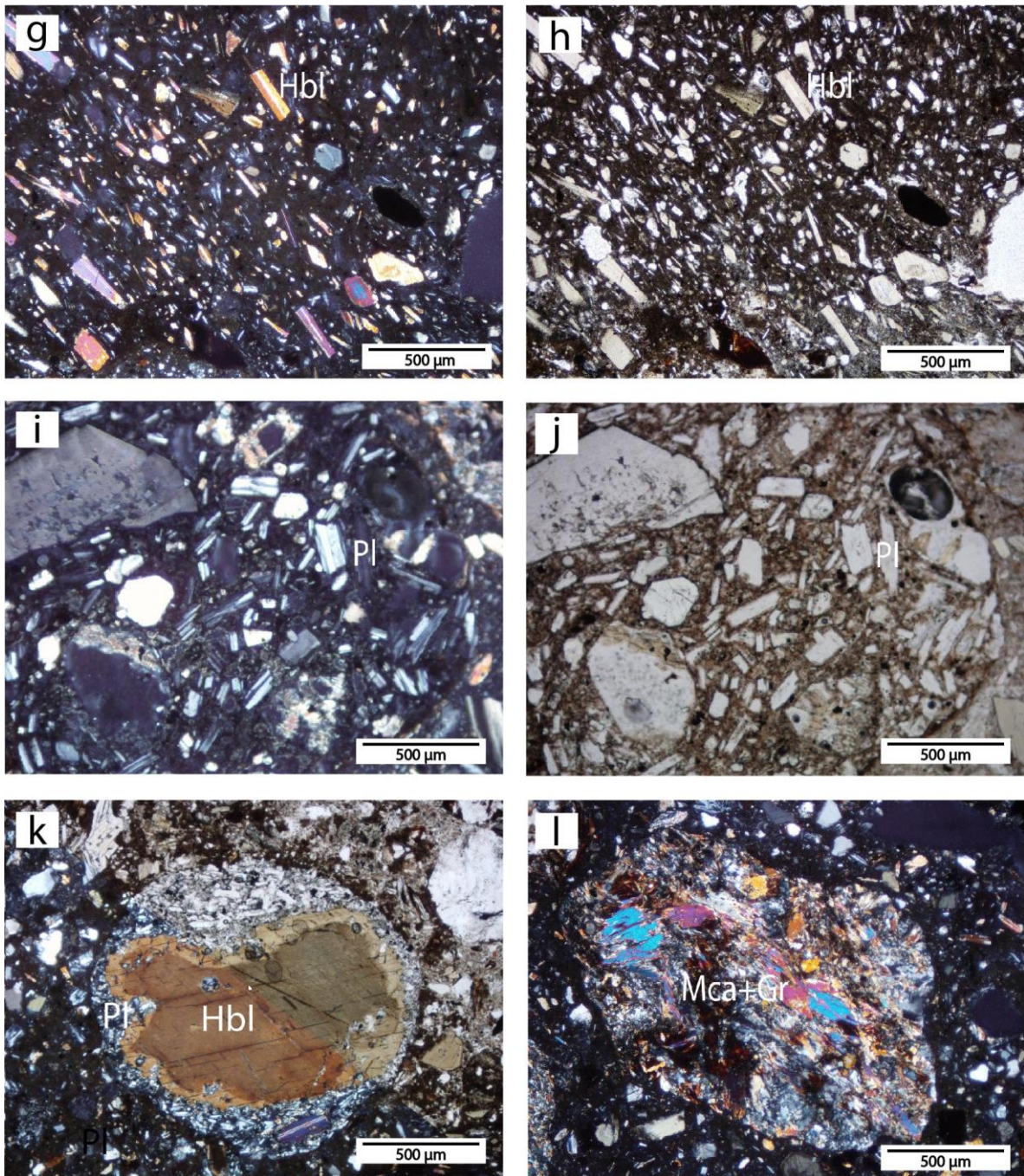


Figure 19: g) XPL. Glass Type (A). h) g) in PPL. i) XPL. Type (B) igneous rock fragment with hialocrystalline texture. Plagioclase microcrystals are dominant. j) i) in PPL. k) XPL. Type (C) igneous rock fragment with holocrystalline porphyritic texture. l) XPL. Type (B) metamorphic rock fragment with grano-lepidoblastic texture and metamorphic foliation. Granoblastic texture is defined by quartz crystals with wavy extinction. Lepidoblastic texture is given by anhedral elongated white micas and by graphite bands.

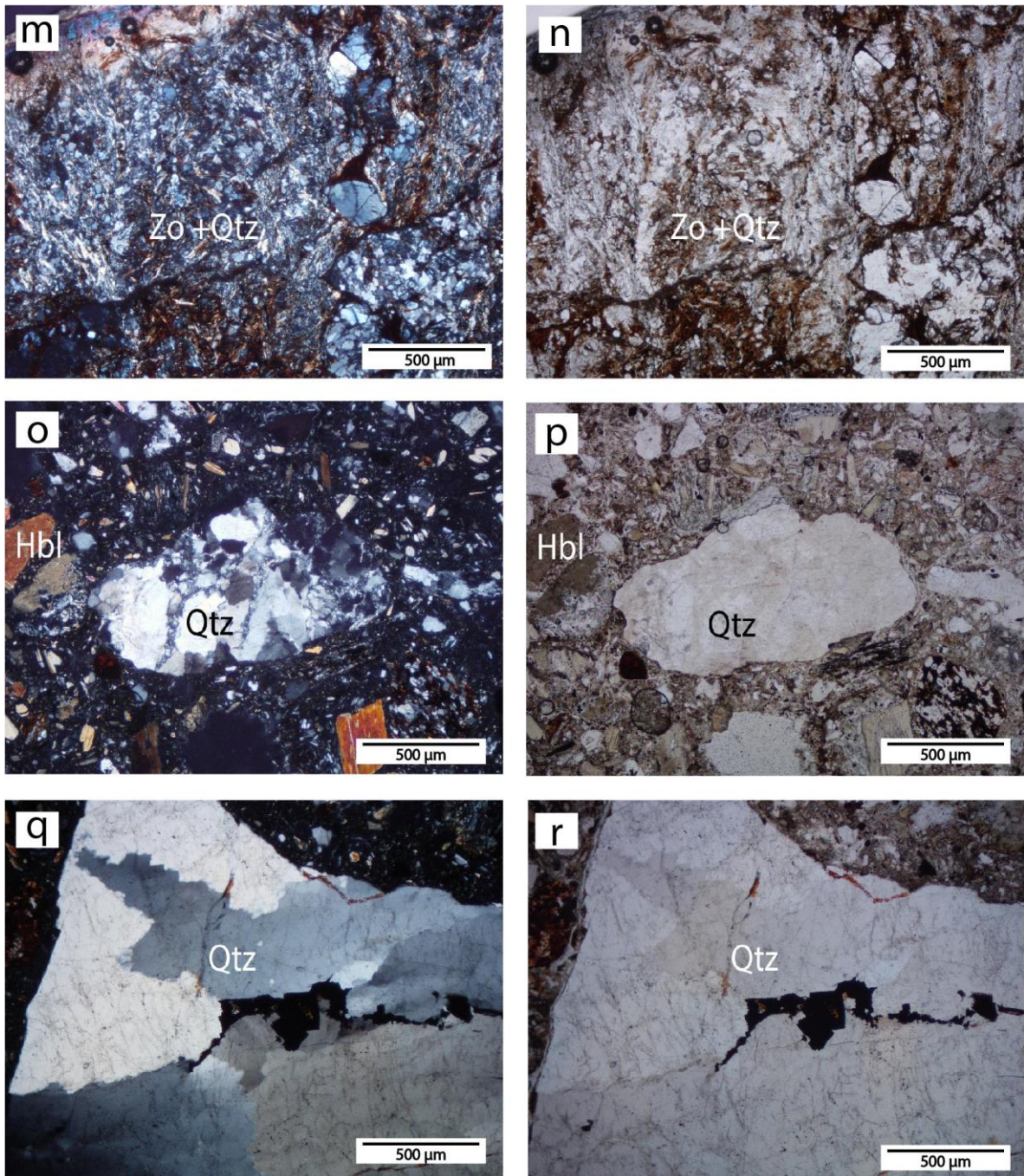


Figure 19: **m)** Type (A) metamorphic rock fragment with grano-lepidoblastic texture and metamorphic foliation. Granoblastic texture is defined by quartz and zoisite crystals. Lepidoblastic texture is given by white micas. **n)** **m)** in PPL. **o)** Type (C) metamorphic rock fragment. Polycrystalline quartz with irregular boundaries and wavy extinction. Note the bands of smaller quartz grains as a result of bulging recrystallisation. **p)** **o)** in PPL. **q)** XPL. Type (D) metamorphic rock fragment. Polycrystalline coarse quartz subgrains with irregular boundaries and wavy extinction. Note the opaque minerals in the subgrain boundaries. **r)** **q)** in PPL.

5.6. Doña Juana Volcanic Complex (DJVC)

5.6.1. Sample B22-1

Macroscopic description:

Fresh porphyritic rock with macrocrystals (2-3 mm) of subhedral plagioclase, euhedral to subhedral tabular hornblende and euhedral hexagonal biotite, and mesocrystals of euhedral to subhedral tabular hornblende (~1.5 mm), subhedral biotite (~0.8 mm) and subhedral quartz (~0.7 mm) in an aphanitic medium light gray groundmass. It has low vesicularity and vesicles are predominantly surrounded with low sphericity infilled with subhedral quartz (3-5 mm) (Fig. 20).



Figure 20: Hand specimen of Sample B22-1

Microscopic description: the sample is a hialocystalline porphyritic rock with seriate texture. It consists of mesocrystals of plagioclase, hornblende, biotite and quartz scattered in a crystal-vitric groundmass made up by microcrystals of the same mineralogy, mineral opaques, devitrified glass and subspherical or irregular vesicles. The mineral assemblage consists of plagioclase (40%), hornblende (11%), biotite (8%) and quartz (3%); accessory minerals include opaque minerals (1.5%). The groundmass represents the (26.5%) of the sample, while vesicles are the (10%).

Plagioclase: mesocrystals (ranging in size from 0.5 mm to 2 mm), microcrystals (ranging in size from 60 µm to 0.5 mm) and microlites (<60 µm)

Mesocrystals are found as aggregates of maximum 5 mm in size. There are two types according to their texture: (A) Aggregates with irregular subgrains boundaries conformed by anhedral and subhedral mesocrystals with coarse sieve texture in the core, deformation polysynthetic twinning or Carlsbad twinning, concentric oscillatory zoning and subtle alteration to sericite. The border of the aggregate is locally embayed (Fig. 21a). (B) Aggregates with irregular subgrains boundaries made up by mesocrystals with the same characteristics of (A). The difference is that individual crystals have anhedral cores that are surrounded by a reaction rim of maximum 70 µm in length followed by a subhedral overgrowth border of maximum 60 µm in length (Fig. 21b).

Microcrystals are present as free crystals. There are two types according to their texture: (A) Euhedral to subhedral free crystals with coarse sieve texture in the core, deformation polysynthetic twinning and subtle alteration to sericite (Fig. 21c). (B) Subhedral free crystals with coarse sieve texture in the core, without polysynthetic twinning or zoning (Fig. 21d).

Microlites are anhedral to subhedral crystals in aggregates. They may have polysynthetic twinning and are slightly alter to sericite.

Hornblende: mesocrystals (ranging in size from 0.5 mm to 1.1 mm) and microcrystals (<0.5 mm). In all the sizes, hornblende is found as euhedral to subhedral free crystals with tabular or prismatic (mainly hexagonal) habit; mesocrystals have skeletal habit too. There are two types according to its pleochroism: (A) pale greenish yellow to moderate yellow pleochroism (B) dark yellowish orange to light brown pleochroism. They have an opacitic rim and inclusions of anhedral opaque minerals. Rarely, (A) hornblende is zoned (Fig. 21e,f).

Although, the majority of the hornblende mesocrystals are found as free crystals, they can also be found as aggregates of maximum 1.5 mm in size. Individual crystals are subhedral to anhedral with tabular or prismatic (mainly hexagonal) and skeletal habit. They have the two types of pleochroism mentioned before and are locally oxidized (Fig. 21g).

Biotite: macrocrystals (ranging in size from 2 to 5 mm), mesocrystals (ranging in size from 0.5 mm to 0.8 mm) and microcrystals (<0.5 mm). Macrocrystals are found as subhedral free crystals with prismatic (hexagonal) and skeletal habit or as mineral fragments, while meso and microcrystals consists of euhedral to subhedral free crystals with tabular habit and skeletal habit. There are two types according to its pleochroism: (A) dusky yellow to yellowish gray (Fig. 21i,j). (B) dusky red to moderate reddish brown. They may have opacitic rim and inclusions of anhedral opaque minerals (Fig. 21k). Moreover, some of the (B) biotite crystals have a reaction crown formed by microcrystalline amphiboles and opaque minerals.

Quartz: There is primary and secondary quartz. Primary quartz is found as microcrystals (<0.3 mm). They are anhedral free crystals without wavy extinction and may be embayed (Fig 10). Secondary quartz is subhedral with parallel extinction and is filling the vesicles of the sample (Fig. 21l).

Opaque minerals: anhedral free crystals of less than 0.1 mm in length. They appear as free crystals scattered in the groundmass or as inclusions.

Classification: Following Streckeisen, the sample corresponds to an effusive andesite. However, according to Pardo et al. (2018), the geochemistry indicates that samples of the DJVC are dacites, so the groundmass must be very silic.

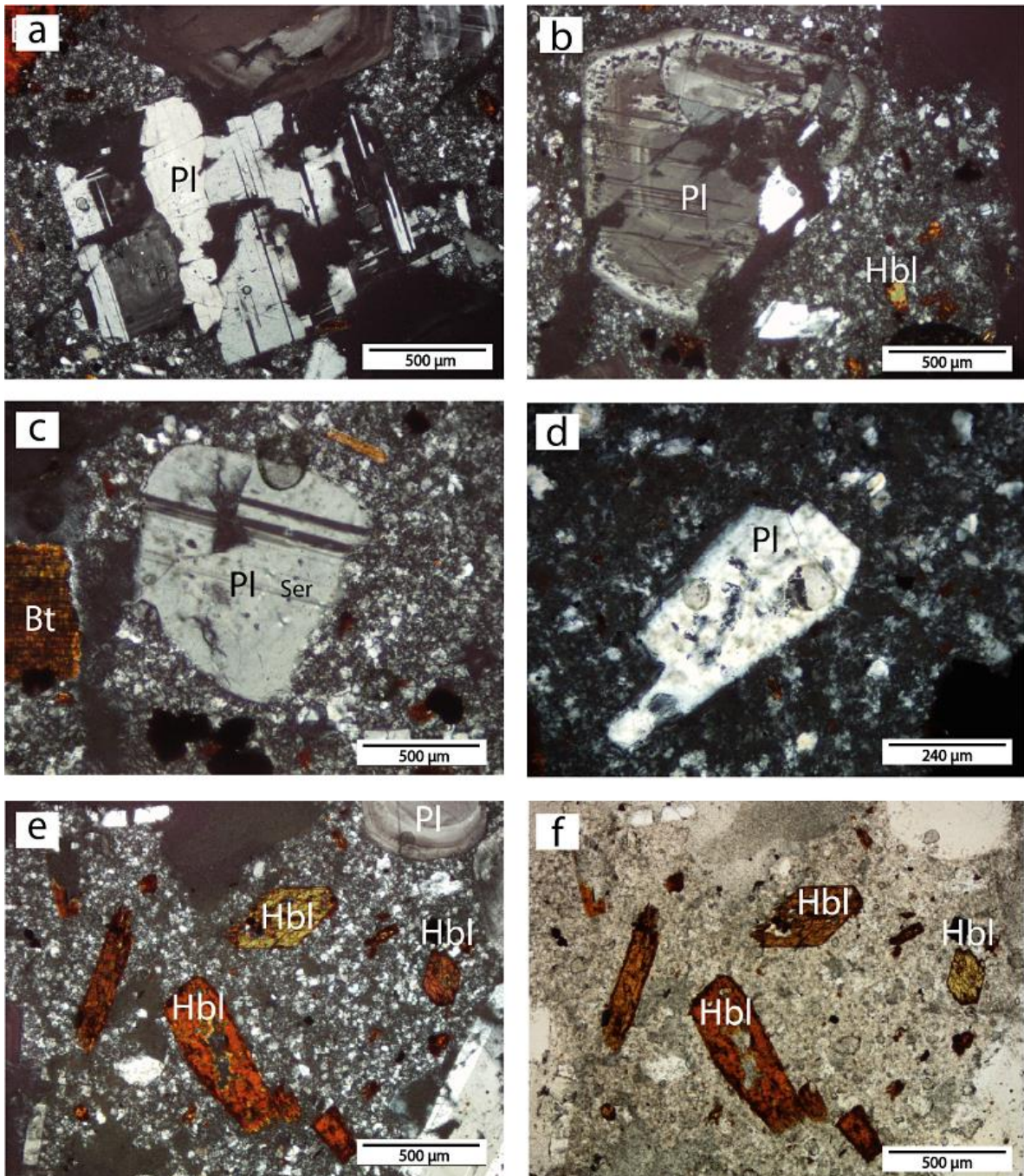


Figure 2: a) XPL. Type (A) aggregate of plagioclase mesocrystals with coarse sieve texture in the core, deformation polysynthetic twinning or Carlsbad twinning, concentric oscillatory zoning and subtle alteration to sericite. Note that the border of the aggregate is locally embayed. b) XPL. Type (B) aggregate of plagioclase mesocrystals with a reaction rim followed by a subhedral overgrowth border. c) XPL. Type (A) plagioclase free microcrystals with coarse sieve texture in the core, deformation polysynthetic twinning and subtle alteration to sericite. d) XPL. Type (B) plagioclase free microcrystals with coarse sieve texture in the core, without polysynthetic twinning or zoning. e) XPL. Hornblende free mesocrystals and microcrystals. Type (A) with pale greenish yellow to moderate yellow pleochroism and type (B) with dark yellowish orange to light brown pleochroism. Note the opacitic rim and the inclusions of anhedral opaque minerals. f) e) in PPL

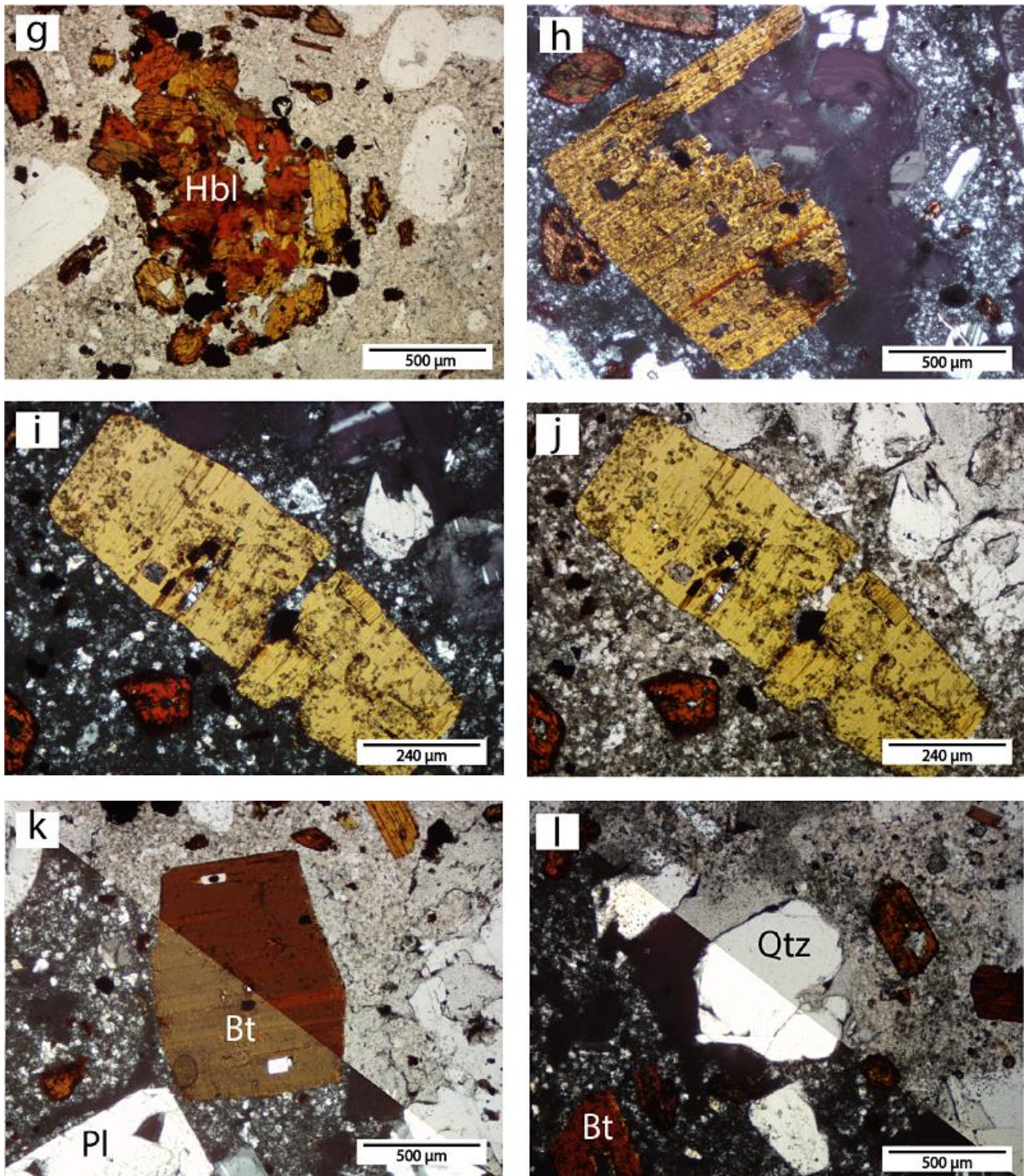


Figure 21: g) PPL. Aggregates of hornblende mesocrystals. h) XPL. Biotite macrocrystal fragment. i) XPL. Type (A) biotite mesocrystal with dusky yellow to yellowish gray pleochroism. It is fractured and has inclusions of opaque minerals. j) i) in PPL. k) XPL/PPL. Type (B) biotite mesocrystal with dusky red to moderate reddish brown and a reaction crown formed by microcrystalline amphiboles and opaque minerals. l) XPL/PPL. Secondary free crystal of quartz with parallel extinction filling vesicles.

5.6.2. Sample B22-2

Macroscopic description:

Fresh porphyritic rock with macrocrystals of subhedral tabular plagioclase (2-5 mm), euhedral to subhedral tabular hornblende (2-4 mm) and subhedral hexagonal biotite (2-4 mm), and mesocrystals (0.5-2) of the same mineralogy with similar characteristics of macrocrystals in an aphanitic very light gray groundmass (Fig.). It has low vesicularity and vesicles are predominantly subrounded with low sphericity. Locally, minerals are oxidized.



Figure 22: Hand specimen of Sample B22-2

Microscopic description: the sample is a hialocystalline porphyritic rock with seriate texture. It consists of mesocrystals of plagioclase, hornblende, biotite and quartz scattered in a crystal-vitric groundmass made up by microcrystals of plagioclase and hornblende with fluidal texture, devitrified glass and subspherical or irregular vesicles. The mineral assemblage consists of plagioclase (16%), biotite (10%) and hornblende (8%). Accessory minerals include opaque minerals (3%) and quartz (1%), and secondary minerals consist of epidote and clinozoisite. Additionally, the sample contains a few (2%) rounded and subangular enclaves without reaction rims. The groundmass represents the (58%) of the sample, while vesicles are the (2%).

Plagioclase: mesocrystals (ranging in size from 0.5 mm to 2 mm), microcrystals (ranging in size from 0.1 mm to 0.5 mm) and microlites (<0.1 mm)

Mesocrystals are found as aggregates of maximum 7 mm in size. There are three types according to their texture: (A) (See description in Sample B22-2) (Fig. 23a,b). (B) Aggregates with irregular or longitudinal subgrains boundaries conformed by mesocrystals with deformation polysynthetic twinning and subtle alteration to sericite. Individual crystals have anhedral cores that are surrounded by a reaction rim of maximum 0.2 mm in length (Fig. 23c,d)

Microcrystals are present as free crystals. There are three types according to their texture: (C) Euhedral to subhedral free crystals with patchy zoning, coarse sieve texture in the core, inclusions of anhedral opaque minerals and subtle alteration to sericite. Additionally, they have embayed borders (Fig. 23e,f). (D) Free crystal with an anhedral core, patchy zoning, reaction border and euhedral overgrowth border (Fig. 23g,h). (E) Free crystal with anhedral core reaction border and

euhedral overgrowth border (Fig. 23i). (F) Free crystals without twinning or zoning and with subtly altered to sericite. They have anhedral cores totally covered by fine sieve texture with a euhedral overgrowth border of maximum 40 µm in length (Fig. 23j).

Microlites are euhedral to subhedral free crystals with tabular or acicular habit. They are subtly altered to sericite.

Hornblende: mesocrystals (ranging in size from 0.5 to 1 mm) and microcrystals (< 0.5 mm). In all the sizes, hornblende is found as subhedral free crystals with prismatic habit or as anhedral elongated free crystals. They have a pale greenish yellow to light brown pleochroism. Mesocrystals may present simple or lamellar twinning, with an opacitic rim and inclusions of anhedral opaques minerals. They are partially altered to epidote and clinzoisoite. Microcrysts sometimes are found with lamellar twinning, with or without opacitic rim and inclusions of anhedral opaques minerals (Fig. 23k).

Even though the majority of the hornblende mesocrystals are found as free crystals, it can also be in aggregates of maximum 1 mm in size. Individual crystals are subhedral to anhedral with tabular or prismatic (mainly hexagonal) and skeletal habit. They have inclusions of anhedral opaques minerals and their borders are locally embayed (Fig. 23l).

Biotite: macrocrystals (ranging in size from 2 mm to 3 mm) and mesocrystals (ranging in size from 0.5 to 2 mm). Biotite is found as euhedral to subhedral free crystals with tabular habit and yellowish brown to dark brown pleochroism. Macrocrystals have the reaction crown constituted by microcrystalline amphiboles and opaque minerals (Fig. 23m), while mesocrystals are surrounded by an opacitic rim (Fig. 23n). In all sizes, biotite has a symplectitic intergrowth with quartz and inclusions of anhedral opaque minerals.

Quartz: microcrystals (<0.3 mm). They are anhedral free crystals with parallel extinction. It is found scattered in the matrix or intergrowing the biotite.

Opaque minerals: as in Sample B22-1, opaque minerals are anhedral free crystals of less than 0.1 mm in length. They appear as free crystals scattered in the groundmass or as inclusions.

Epidote and clinzoisoite: crystals present as aggregates with a maximum size of 90 µm. Individual crystals are subhedral with prismatic habit or anhedral elongated crystals. They are colorless and are altering hornblende.

Enclave: subangular to subrounded igneous enclave exhibiting a microphaneritic texture with elongated anhedral microcrystals of epidote (Fig. 23p).

Interpretation: Following Streckeisen, the sample corresponds to an effusive andesite. However, according to Pardo et al. (2018), the geochemistry indicates that samples of the DJVC are dacites, so the groundmass must be very silicic.

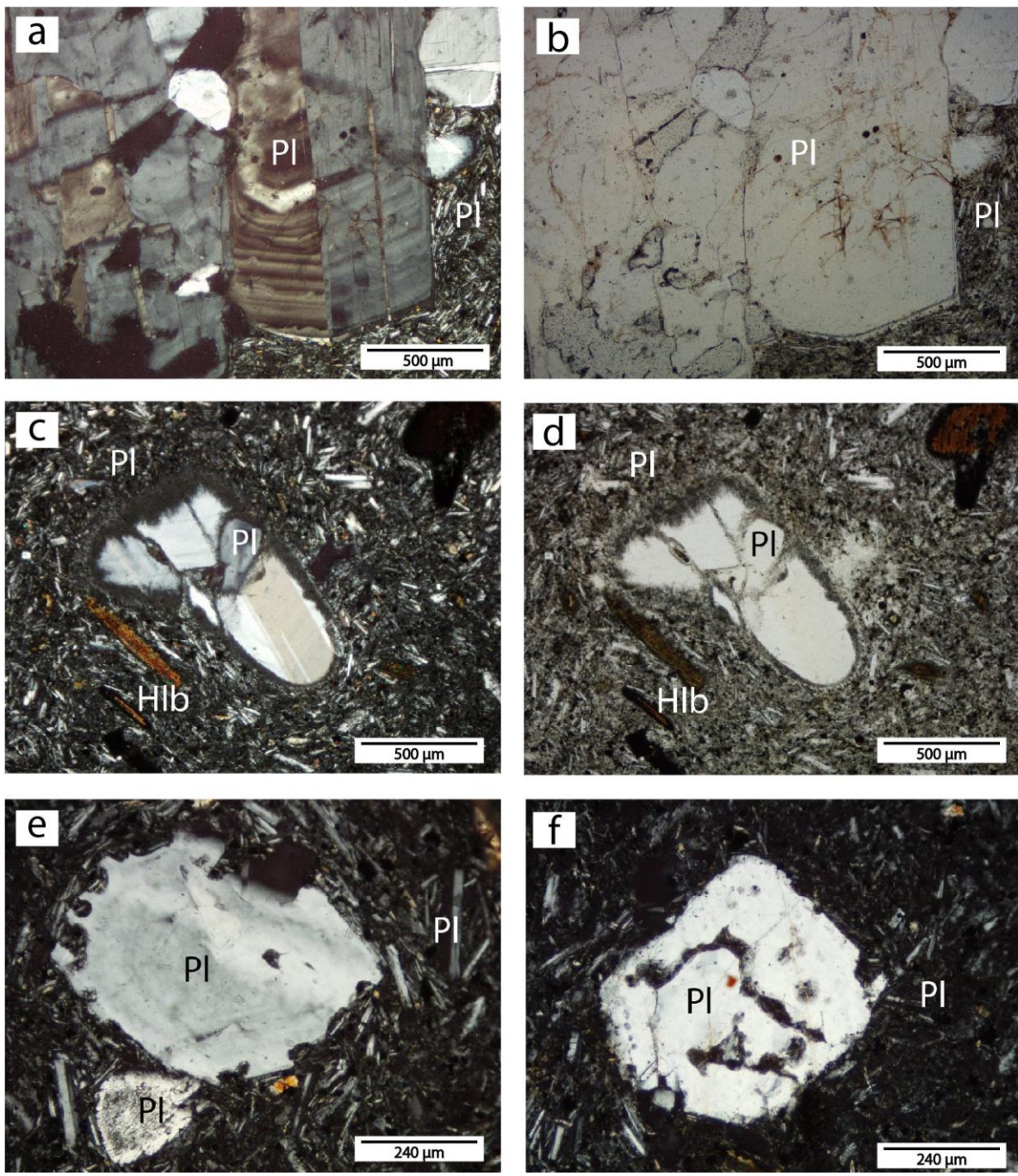


Figure 23: **a)** XPL. Type (A) aggregate of plagioclase mesocrystal with subhedral to anhedral cores that are surrounded by a thin reaction rim of maximum 20 µm in length followed by a euhedral overgrowth border. **b)** a) in PPL. **c)** XPL. Type (B) aggregate of plagioclase mesocrystal anhedral cores that are surrounded by a reaction rim without a subsequent overgrowth border. **d)** c) in PPL. **e)** and **f)** XPL. Type (C) plagioclase free microcrystal with coarse sieve texture in the core and subtle alteration to sericite. **e)** Note the embayed border and **f)** Note the coarse sieve texture.

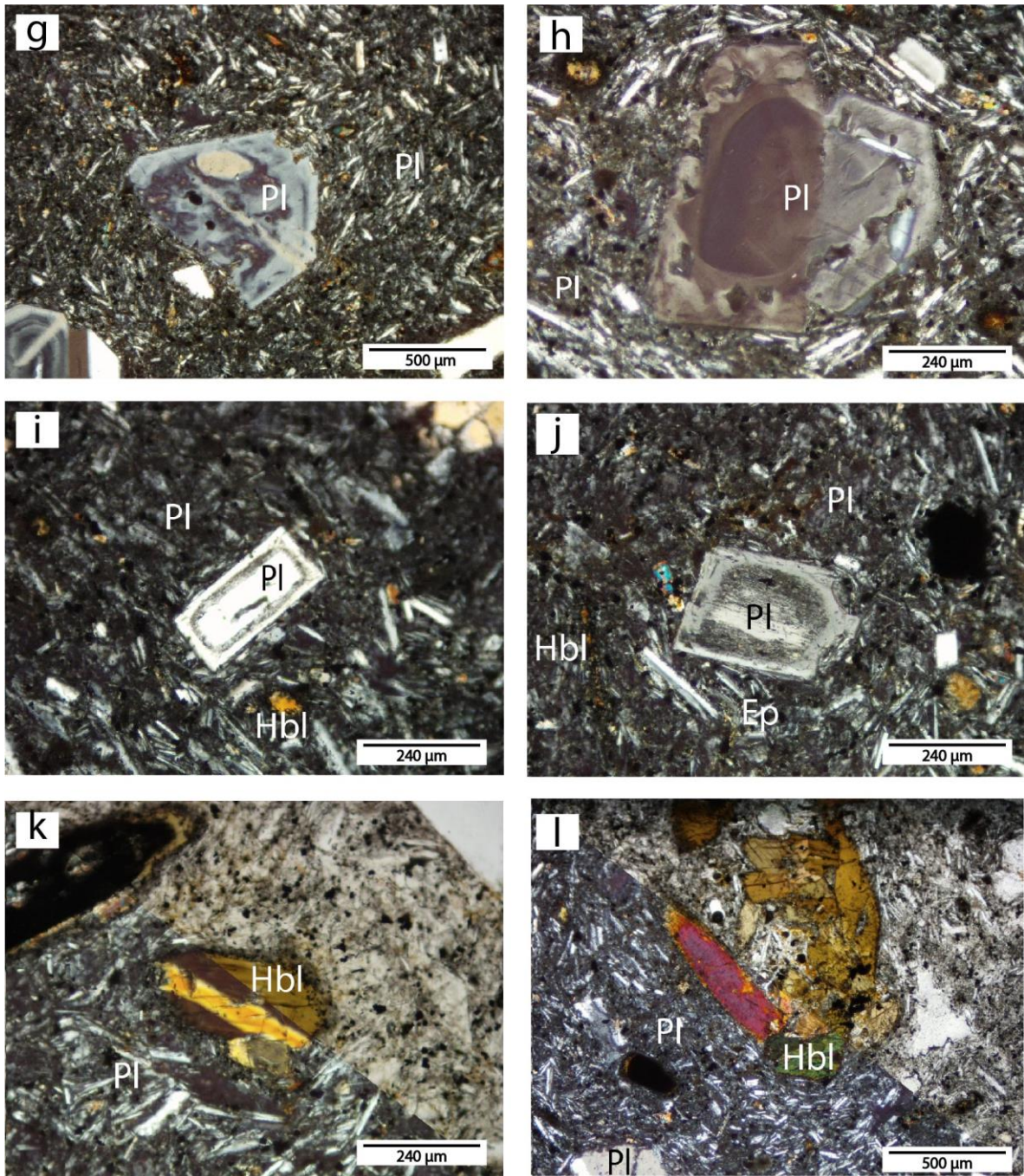


Figure 3: g) and h) XPL. Type (D) plagioclase free microcrystal with an anhedral core, patchy zoning, reaction border and euhedral overgrowth border. **i)** XPL. Type (E) plagioclase free microcrystal with anhedral core reaction border and euhedral overgrowth border. **j)** XPL. Type (F) plagioclase free microcrystal without twinning or zoning. It has anhedral cores totally covered by fine sieve texture with a euhedral overgrowth border. **k)** XPL/PPL. Hornblende free microcrystal with lamellar twinning and opacitic rim. **l)** XPL/PPL. Aggregate of hornblende mesocrystals with tabular or prismatic (mainly hexagonal) and skeletal habit. It has inclusions of anhedral opaques minerals and their borders are locally embayed.

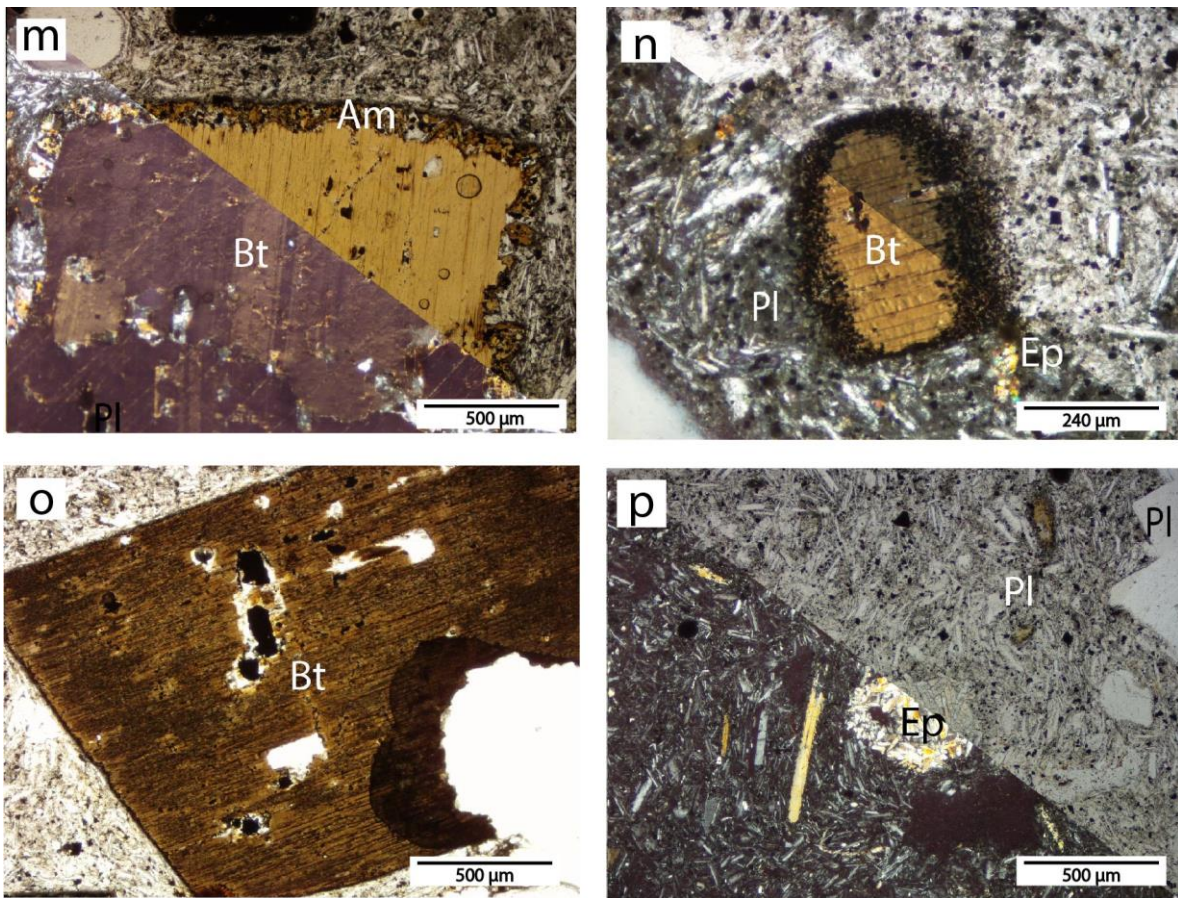


Figure 23: **m)** XPL/PPL. Biotite free macrocrystals with a crown constituted by microcrystalline amphiboles and opaque minerals. **n)** XPL/PPL. Biotite free mesocrystal surrounded by an opacitic rim. **o)** PPL. Fragment of a biotite macrocrystal. **p)** XPL/PPL. Subangular to subrounded igneous enclave exhibiting a microphaneritic texture with elongated anhedral microcrystals of epidote.

6. Discussion

6.1. Buesaco Schists (PZBue)

6.1.1. Interpretation Sample B15-1

Mineral assemblage indicates that the protolith of the sample is a sedimentary rock, possibly a quartz arenite, which suffered low-grade metamorphism.

6.2. Quebradagrande Complex (K1cqg)

6.2.1. Interpretations Samples B10-1, B13-1, B19-2 and B31-1

Petrographic descriptions evidence the lithologic variety of the Quebradagrande Complex. From these sample it can only be conclude that the effusive rock suffered propylitic hydrothermal alteration associated with the outermost alteration zone of the porphyry systems at intermediate to deep level (e.g., Allen et al., 1996). B13-1 sample corresponds to a meta-arenite that suffered very low-grade metamorphism evident on the remnant sedimentary textures of the rock. It is still possible to clearly see the framework of the sample constitute by quartz, plagioclase, epidote and clinozoisite, and sedimentary rock fragments in a matrix of clay minerals (Fig. 8a,b). The indicators of the metamorphism corresponds to the foliation defined by the graphite bands and elongated crystals of chorite, stilpnomelane and chlorite (Fig 8 c,d). Sample B19-2 is a siltstone with lamination and bioturbation. It is associated with a fluvial environment of low energy. Finally, sample B31-1 is a basalt in which it could not be recognized either olivine, nor orthopyroxene.

6.3. Esmita Formation (Nesm)

6.3.1. Interpretations Samples B24-1, B29-1 and B32-1

Textural maturity concept is useful in order to characterize sediments. It is used to describe the approach of a sediment to the most inert end state possible, through the operation of both physical processes (tending to produce a perfectly sorted and rounded sediment) and chemical processes (tending to produce a sediment containing only the most stable minerals) (Folk, 1951). According to Folk (1951), textural maturity in sandstones is given by three textural parameters: (1) the amount of clay-size sediment in the rock, (2) the sorting of the framework grains and (3) the roundness of the framework grains. When this concept is applied to the sedimentary rocks of the Esmita Formation, it can be concluded that samples B24-1 and B32-1 are submature as none of them contain more than 5% of matrix, they are poorly sorted and the majority of the grains of the framework are subrounded with few rounded grains. On the other hand, sample B29-1 is mature as matrix represent the 6% of the sample, it is well sorted and grains are predominantly subrounded. Maturity is also an indicator of the input of modifying energy (Folk, 1951) or the length of time that the sediment has been in the sedimentary cycle (Nelson, 2018). So, Sample B29-1 in comparison with the other samples is possibly further away from the source. In the three cases, igneous rock fragments are more abundant than metamorphic ones, which give insights about the source.

6.4. Dacite-Andesite Porphyritic Bodies (Npda)

6.4.1. Interpretation Sample B26-1

Plagioclase crystals were organized in different groups according to their size and texture. Size variations give information about the order of crystallization, while the different textures reveal details of the magmatic environment. A simplified magma plumbing model is proposed for the described sample B26-1 (Fig. 24).

In the first stage, water-saturated magma was located in a deep chamber on a stable magmatic environment. Crystallization of euhedral macrocrystals and mesocrystals of amphiboles and plagioclase occurred.

In the second stage, magma could rise from the deep chamber. Plagioclase stability could be reduced, so the crystals started to develop the reaction borders and lose their euhedral shape (Fig. 18a,b,c,d). Similarly, amphibole stability could be reduced and acquired skeletal habits (Fig. 18i,j).

In the third stage, magma could stall in a shallower chamber. Plagioclase crystals started to arrange in aggregates (Fig. 18e) as a consequence of the dissolution they suffered, which generated a boundary melt layer around the grains, that subsequently cooled and joint the closely spaced crystals (e.g., Renjith, 2014). The plagioclase aggregates correspond to Type (C) plagioclase in the petrographic description of the sample. Two textural characteristics are important to remark: these aggregates are euhedral to subhedral without reaction borders. It means that they were in equilibrium with the melt. Additionally, they have deformation polysynthetic twinning in the albite and pericline laws that may be accompanied with Carlsbad twinning. Deformation twins can be differentiated as they are commonly tapper and incomplete toward the crystal center (e.g., Passchier et al., 2005). According to Passchier et al. (2005), when a crystal of plagioclase is subjected to a strain, deformation twinning accommodates only a limited amount of the strain and operates in specific crystallographic directions. Higher strains are accommodated by dislocation creep or recrystallization. Moreover, in plagioclase, deformation twinning on albite and pericline law planes is generally associated with temperatures lower than 400°C (Passchier et al., 2005). So, this kind of twinning suggests that once the aggregates developed, they were under a strain field. The latter is possibly linked with the forces that the last crystallized phases made over the aggregates thanks to the reduced available space. Another event related with this stage is the start of crystallization of biotite macrocrystals following the Bowen Series.

In the fourth stage, the last decompression could occur. Possibly, the melt could have assimilated quartz grains from the host rock. The latter is evidenced in the embayed and corroded forms of the quartz mesocrystals (Fig. 18l). Considering that these crystals are described with parallel extinction, it is possible that they could be from the Esmita formation rather than the metamorphic formations. Additionally, in this stage microcrystals could grow and magma fully crystallized generating subvolcanic bodies.

Finally, many secondary processes related to hydrothermal alteration are evidenced in the textures of the sample: highly alteration of plagioclase crystals to sericite and saussurite (Fig. a,b), replacement of amphiboles by chlorite (Fig. i,j), subhedral pseudomorphs of chlorite, epidote and magnetite after biotite (Fig. 18k), and calcite filling spaces in the groundmass.

Sample B26-1

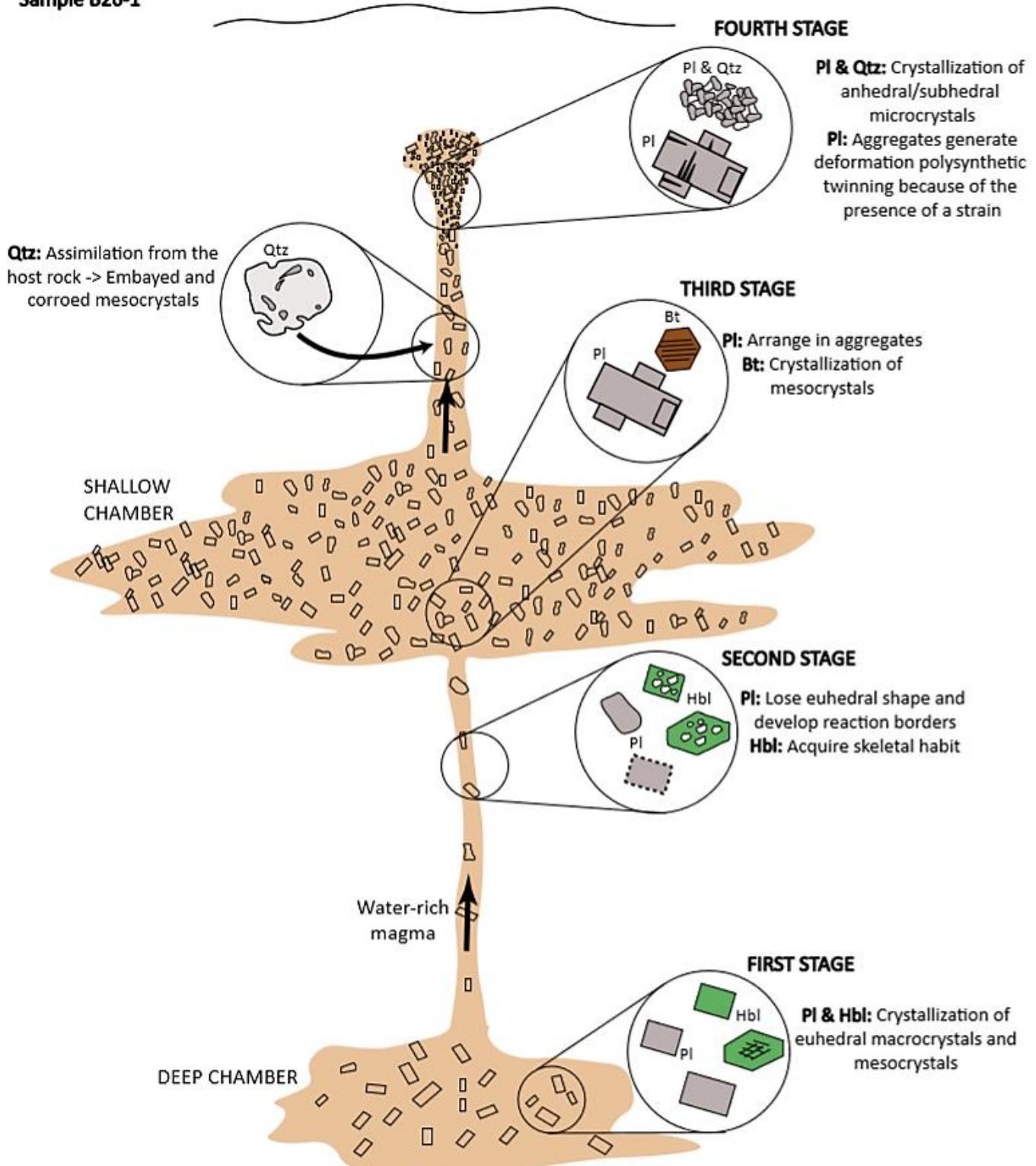


Figure 24: Schematic model Sample B26-1

6.5. Granatífera Tuff (tgr)

6.5.1. Interpretation Sample B27-1

Crystal fraction of the Granatífera Tuff sample evidence at least four stages of crystallization: the first inferred stage is associated with the crystallization of euhedral amphibole macrocrystals. Then, oxygen fugacity of the melt must be changed in a second stage in order to generate the simple zoning observed in the amphibole crystals (Fig. 19c). Specifically, at higher fO_2 , the Mg-number is strongly increased (e.g., Humphreys et al., 2006). So, differences in pleochroism described in the core vs. the border of amphibole crystals could be explained as an increased Mg-number, Na and Si from the core to the rim after the modification of fO_2 . In the third stage, crystallization of microlites occurred. Simultaneously or nearly after, the melt with the crystallized phase and gas bubbles was transformed into a gas phase with dispersed magma fragments. Likewise, there was a transformation in energy: potential energy of the expanding magma was converted to the kinetic energy of the gas phase and individual pyroclasts (Cashman et al., 2005).

Also, the rock fragments of the tuff are very important to characterize the basement of the DJVC (Fig.25). According to Weber (1998) the xenoliths of the Granatífera Tuff xenoliths can be subdivided in three groups: mantle-derived, lower crystal and igneous xenoliths. The mantle derived xenoliths range from garnet peridotite to websterite and pyroxenite. Lower crustal xenoliths comprise pyribolites, hornblendites, granulite, pyroxenites and gneisses. And igneous xenoliths consist of volcanic rocks with andesitic, dacitic and lamprophytic petrographic characteristics or plutonic xenoliths of dioritic composition (Weber, 1998). In the analyzed sample, no mantle nor dioritic xenoliths were found. From the lower crust, it was only identified a possible xenolith (Fig. 19e,f) named as “other” within the description of the rock fragments of the sample. Taking into a count that it was feldspar rich, with ferromagnesian minerals>30% and Hornblende/Pyroxene>1, it was classified as a pyribolite based on the rock classification scheme made by Weber (2002). Furthermore, there were found volcanic xenoliths with different textures (Type (A) and type (B)) (Fig. 19i,j). In spite of their textural differences, their mineral assemblage was similar and corresponded to hornblende andesites. Weber (1998) establishes that these xenoliths are possibly fragments of the common Tertiary bodies found below Mercaderes.

Apart from the xenoliths of the lower crust, there are also many rock fragments derived from the Upper Crust. For instance, type (C) igneous rock fragment (Fig. 19k), possibly represent a xenolith from the Porphyritic bodies of the Npda unit (Sample B26-1). Likewise, metamorphic rock fragments Type (A) and (B) (Fig. 19l,m,n) are associated to the Buesaco Schists unit (Sample B15-1) and Type (C) and (D) (Fig. 19o,p,q,r) to the Esmita unit (Samples B24-1, B29-1 and B32-1).

Sample B27-1

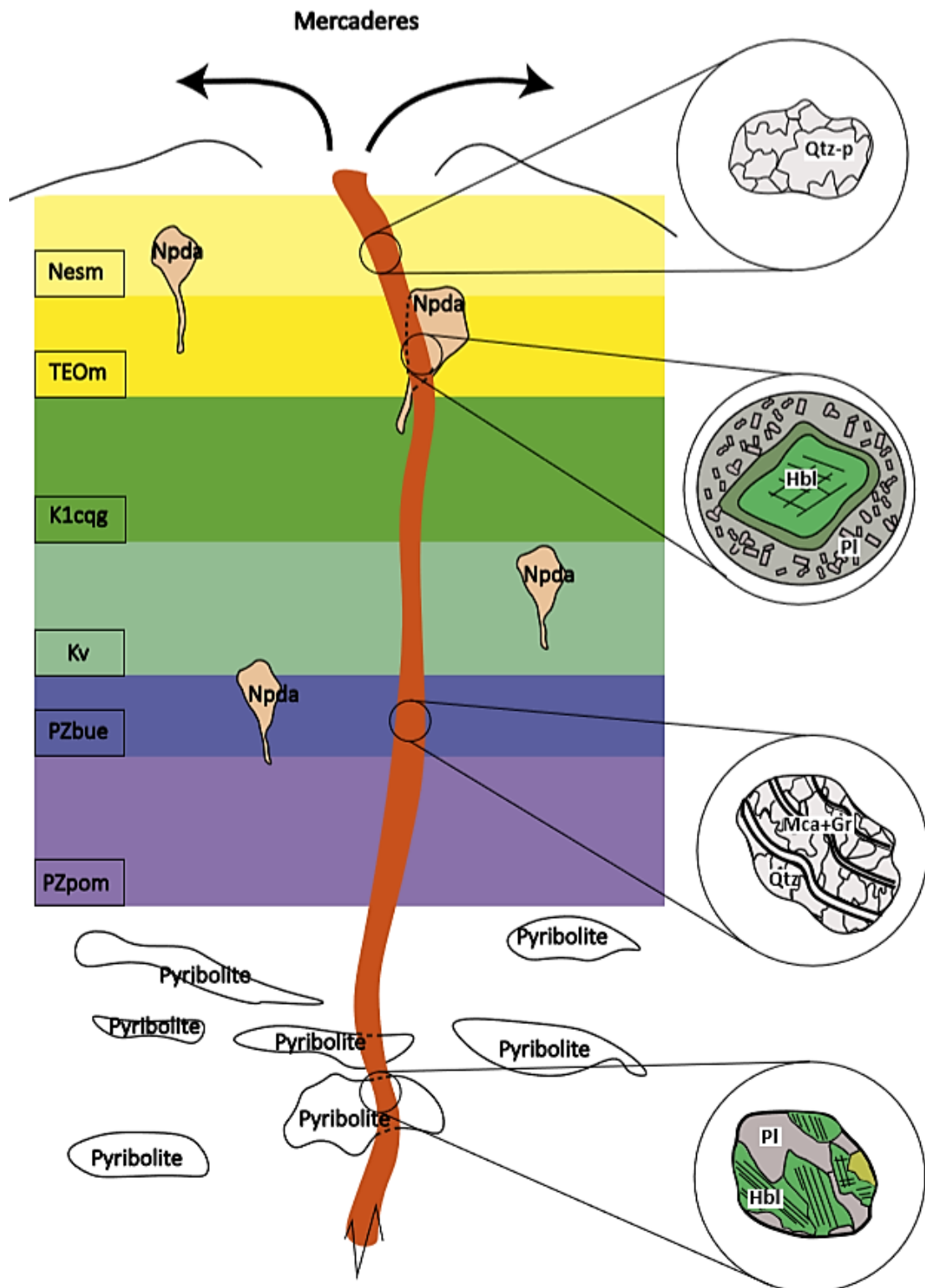


Figure 25: Schematic model Sample B27-1

6.6. Lavas from the Doña Juana Volcanic Complex (DJVC)

6.6.1. Interpretation Sample B22-1

At the first stage (Fig. 26), water-saturated magma could be stored in a deep chamber on a stable magmatic environment. Crystallization of euhedral mesocrystals and larger microcrystals of amphiboles and plagioclase could occur in this stage.

During a second stage, magma could rise to a relatively shallower storage level. Plagioclase stability could have been reduced and underwent dissolution processes (e.g., Blundy and Cashman, 2001). Dissolution is based on the generation of voids in crystals that are filled by the surrounding melt, which later is entrapped inside with the regrowth of that crystals (Renjith, 2014). So, this stage explains the coarse sieve texture that was observed on the core of plagioclase meso and microcrystals (Fig. 21b,c,d). Likewise, amphibole stability could also be reduced, but in this case, crystals started to acquire a skeletal habit and opacitic rims (Fig. 21e,f). The latter can be explained by two possible mechanisms: decreasing water content during decompression or simply the magma rose to a pressure level outside amphibole stability (Rutherford & Hill, 1993).

In the third stage, magma could ascend to a shallower storage level. Similar to sample B26-1, plagioclase crystals started to arrange in aggregates, as a consequence of the dissolution processes they suffered. After crystals were interlocked, they began to behave as a single grain. It is why the aggregates showed continuous oscillatory zoning patterns (Fig. 21b). There have been many proposed explanations to the oscillatory zoning in plagioclases: kinetically or diffusion-controlled growth, decompression, repeated mafic recharge, silicic recharge, and magma convection (Humphreys et al., 2006 and the references there in). However, such interpretations are out of reach of the present study. Additionally, crystallization of euhedral biotite macrocrystals and mesocrystals could occur in this stage following Bowen Series (Fig. I,j,k).

In the fourth stage, magma recharge was inferred. The arrival of a new pulse of magma to the shallow storage level is evidenced by the reaction border of plagioclase aggregates (fine sieve texture) due to their dissolution under higher temperatures (e.g., Renjith, 2014). Although, the reaction border is followed by a rarely euhedral overgrowth rim (Fig. 21b), that may suggest a re-equilibration of plagioclase crystals with the melt. Possibly, the influx of this melt is also the explanation to the observed biotite mesocrystals with amphibole and opaque mineral crowns (Fig. 21k).

Finally, the last stage corresponds to the syn-eruption decompression. An unusual aspect in the sample is the presence of the same huge aggregates of plagioclase with deformation polysynthetic twinning (Fig. 21a) described to the Npda intrusive bodies (B26-1 sample). The difference is that in this sample, the border of the aggregates is locally embayed indicating instability. Additionally, they don't show the same behavior of the aggregates of plagioclase of the third stage with the reaction and overgrowth borders. Then, it can be deduced that these aggregates possibly entered as xenoliths to the magma during the final ascent. In the volcanic conduit, groundmass microlites could crystallize due to related effective cooling and biotite macrocrystals possibly broke apart (Fig. 21h) as a consequence of the expansion of entrapped vesicles in the crystals under decompression (Renjith, 2014).

Sample B22-1

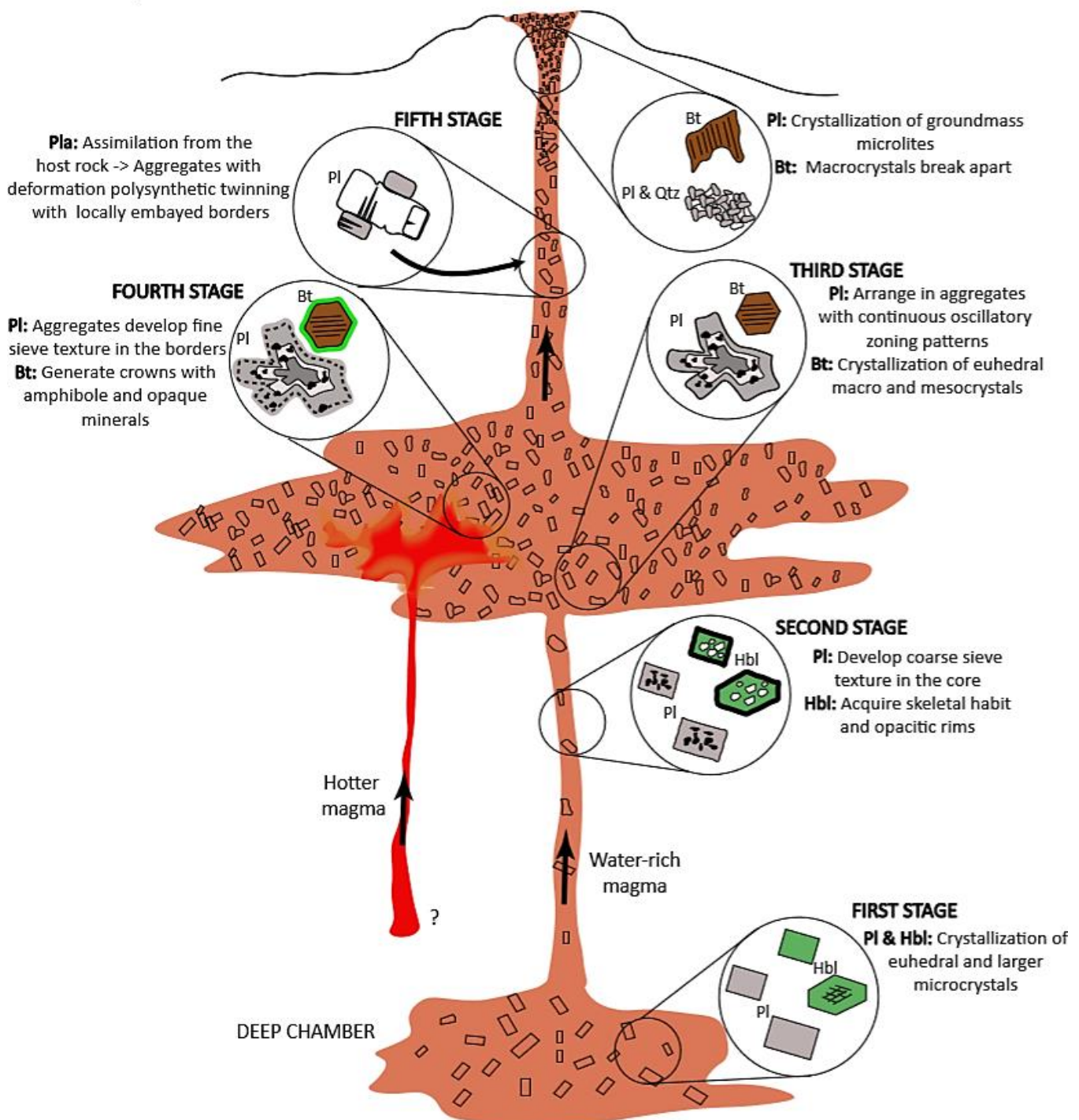


Figure 26: Schematic model Sample B22-1

6.6.2. Interpretation Sample B22-2

The observed textures in the sample B22-2 results to be consistent with the simplified magma plumbing proposed to the sample B22-1: the same stages were recognized. However, there are textural variations in the crystals for each stage (Fig. 27).

At the first stage, there are no changes to which it was mentioned in the sample B22-1.

On the second stage, plagioclase also suffered dissolution processes that explain the coarse sieve texture in macro and microcrystals (Fig. 23f). Additionally, Humphreys et al. (2006) establishes that during water-saturated decompression, plagioclase can develop patchy zoning characterized by an irregular partially resorbed core. Effectively, in the petrographic description this texture was observed in plagioclase crystals (Fig. 23g,h). Likewise, in the sample B22-2, partial resorbing of crystal borders by the melt during the ascent was clearly seen on plagioclase crystals (Fig. 23e). On the other hand, amphibole meso and microcrystals also showed opacitic rims (Fig. 23k) in response to the variations on water content or pressure, as it was mentioned before, but few crystals presented skeletal habit.

In the third stage, not only plagioclase crystals arranged on zoned aggregates (Fig. 23c), but also dissolution processes in amphibole borders facilitated their joint (Fig. 23l). In this sample, biotite crystallization of macro and mesocrystals also occurred in this stage (Fig. m,n).

In the fourth stage, the recharge of hotter magma explains the reaction borders on plagioclase aggregates too and their anhedral shape (Fig. 23c). Likewise, plagioclase free crystals with patchy zoning also developed reaction borders (Fig. 23h). As in sample B22-2, there are plagioclase crystals in which the reaction border is followed by an overgrowth border. However, in this case, this border is predominantly euhedral (Fig. 23h), suggesting that after the recharge, these crystals started to equilibrate with the melt. Again, biotite macro and mesocrystals show amphibole and opaque mineral crowns (Fig. 23m) due to the variations in melt subsequently to the recharge.

Lastly, in the syn-eruptive decompression occurred too with the associated crystallization of microlites. It is important to remark that in the sample B22-2 microlites were tabular with fluidal texture. The latter indicates that they formed under low rate of undercooling (Renjith, 2014). Biotite macrocrystals also broke apart (Fig. 23o). In this sample, the plagioclase aggregates described on of Sample B26-1 also appeared and are interpreted in the same way: a xenolith of the Npda intrusive bodies (Fig. 23a,b).

Sample B22-2

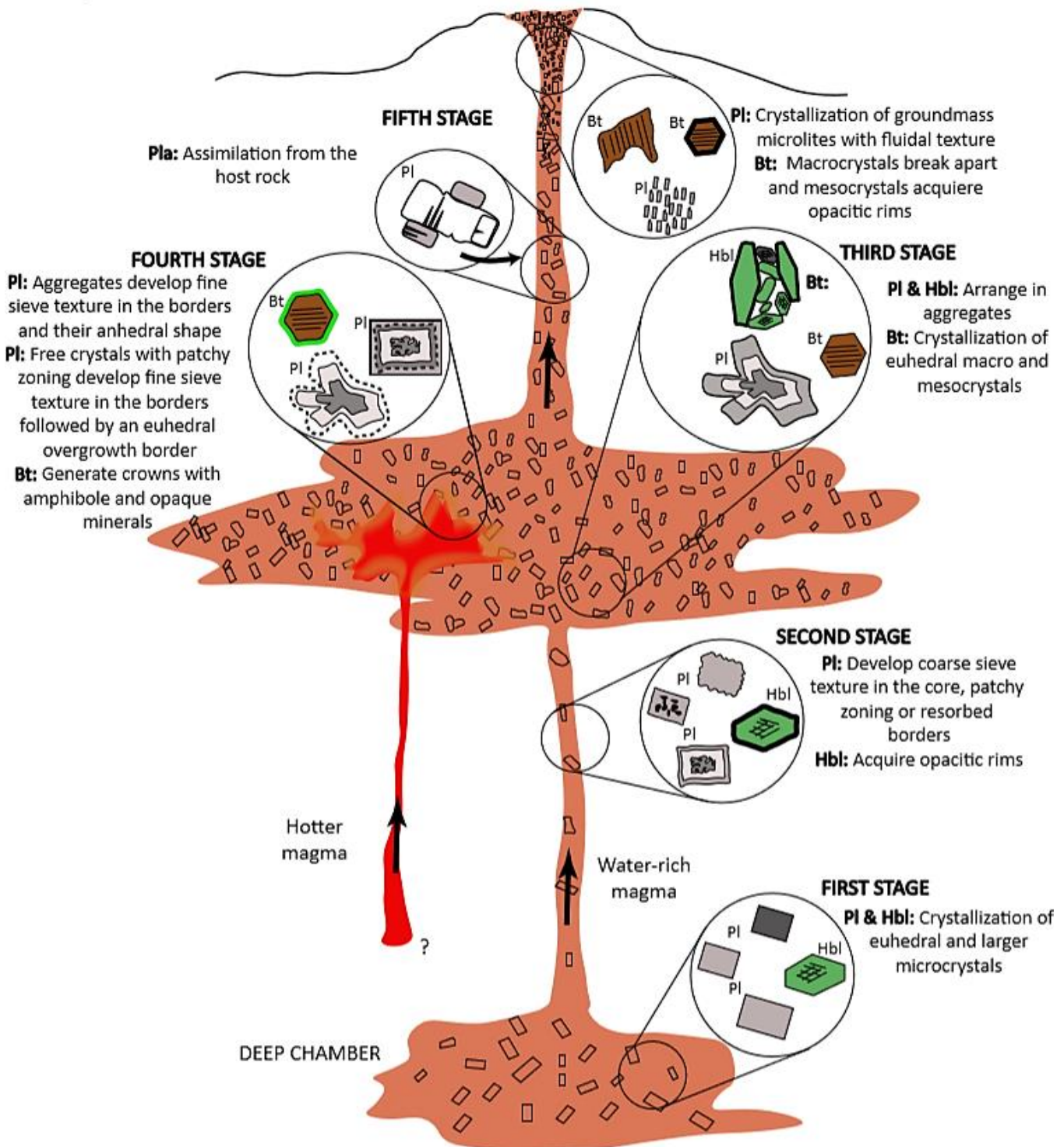


Figure 27: Schematic model Sample B22-2

6.7. General interpretation

When the rock interpretations of each of the sample are tied, it is possible to construct the model showed in Fig. 28

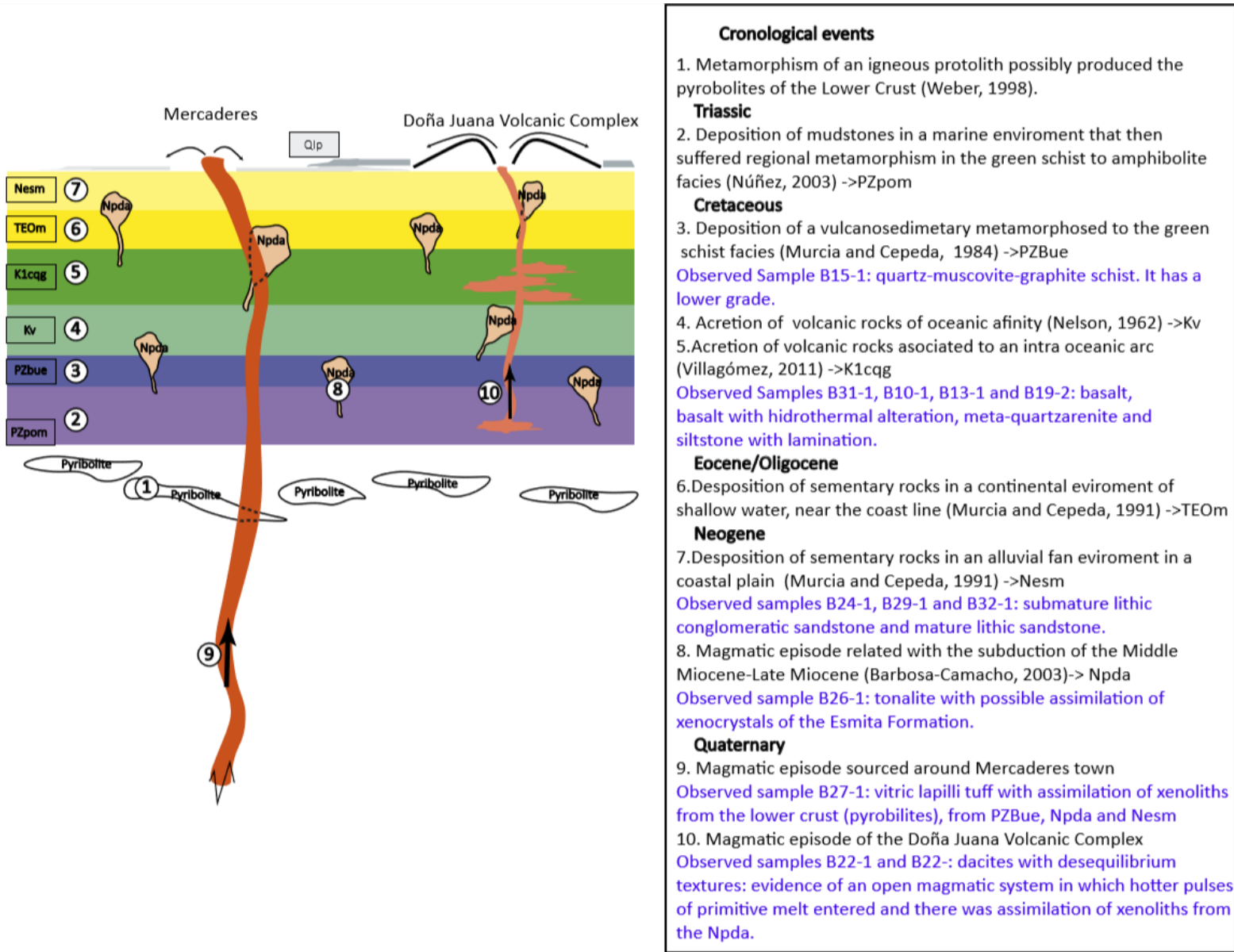


Figure 28: General model

6.8. Implications on the DJVC chemistry

In the Harker diagrams of major elements against silica, it is expected that the FeO and MgO show compatible patterns associated with the fractional crystallization of amphibole in the system. On the other hand, CaO, Na₂O and Al₂O₃ trends are expected to be less clear as a result of the co-existence of several textural and size families of plagioclase with different associated crystallization stories (phenocrystals, microlites and xenocrystals). Likewise, data dispersion is expected in Al₂O₃ and K₂O as a consequence of the crystallization of plagioclase and biotite in an open system.

However, the best way to analyze the influence of contamination processes in a magmatic system is with the evaluation of trace elements levels. Specifically, incompatible elements concentrations are very sensitive to the AFC processes (Rollinson, 1993). In bivariate plots of two highly incompatible elements with similar bulk partition coefficients, like Cs-Rb-Ba, U-Nb-Ta-K, Ce-Pb, P-N, etc., its ratio will not vary to magmatic systems in which only fractional crystallization occurred (Rollinson, 1993). In contrast, any fluctuation in the ratio reflects heterogeneity of the source associated with mixing or contamination (Bougault et al., 1980). Likewise, in systems with heterogeneous source, the trend lines of the data usually do not intercept the origin of the bivariate plot (López-Ruiz & Cebriá Gómez, 1990). So, considering the evidences gave of the open-system magmatic character of the DJVC, it can be expected that effectively in the plots of two incompatible elements the ratio change and that by extending the trend line of data to the origin, they do not intercept. Moreover, another kind of useful diagrams to evaluate open systems are the bivariate plots of an incompatible element in the melt vs. the proportion of this element with a similar incompatible element (Rollinson, 1993). For example, Rb vs. Rb/Ba, Nb vs. Nb/Ba or Th vs. Th/ZR (Pardo, 2018). It is expected high dispersion of data and decoupling patterns in open magmatic system as the DJVC.

7. Conclusions

It was possible to proposed a simplified magma plumbing model for the rocks of the DJVC, based on the different textures identified in the mineral assemblage of two (2) dacitic effusive rocks of the complex, nine (9) samples of the lithological units of the basement and one (1) sample of the Granatífera Tuff, in which there were identified xenoliths from the lower and upper continental crust. Specifically, the model consists of five stages that explains the different process associated to the ascent of the magma from a deep lower chamber to the surface: (1) Water-saturated magma was located in a deep chamber where euhedral mesocrystals and larger microcrystals of amphiboles and plagioclase crystallized. (2) Magma ascended to a shallower storage level. It reduced the minerals stability and caused dissolution processes observed in sieve textures, irregular patchy reabsorbed core and resorbing borders in meso and microcrystals of plagioclase, and in the skeletal habit and opacitic rims of amphibole meso and microcrystals. (3) Magma arrived to a shallower storage level. Plagioclase and amphibole crystals started to arrange in aggregates, as a consequence of the dissolution processes they suffered and began to behave as a single grain. Crystallization of euhedral biotite macrocrystals and mesocrystals could occur in this stage following the Bowen series. (4) There was a magma recharged evidenced in the anhedral shape and reaction border (fine sieve texture) of plagioclase aggregates and of the free crystals

with patchy zoning. In addition, biotite macro and mesocrystals showed amphibole and opaque mineral crowns. (5) Syn-eruption decompression occurred. In this stage aggregates of plagioclase with deformation polysynthetic twinning entered to the magma as xenoliths from the Neogene intrusive bodies. Furthermore, in the volcanic conduit, groundmass microlites could crystallize as a result of related effective cooling and biotite macrocrystals broke apart due to the expansion of entrapped vesicles in the crystals under decompression.

This possible model reflects the open-system magmatic behavior of the DJVC with important consequences in the analysis of the dacitic rocks chemistry. It is probable that Harker diagrams of FeO and MgO against silica exhibit clear compatible patterns related with the fractional crystallization of amphibole in the system. In contrast, it is expected that CaO, Na₂O and Al₂O₃ diagrams show less clear trends given the numerous identified families of plagioclase with different origin. Moreover, in Al₂O₃ and K₂O Harker diagrams high data dispersion is likely as a result of the crystallization of plagioclase and biotite in an open magmatic system. Nevertheless, bivariable plots of incompatible elements concentrations result to be more sensitive to contaminant processes. It is expected that in bivariable plots of two incompatible elements with similar bulk partition coefficients, its ratio will vary and the trend lines of the data may not intercept the origin of the plot. Similarly, in bivariable plots of an incompatible element in the melt vs. the proportion of this element with a similar incompatible element, it is expected a high dispersion of data and decoupling patterns.

References

- Adams, A. E., Mackenzie, W. S., & Guilford, C. (1984). *Atlas of sedimentary rocks under the microscope*. Routledge.
- Allen, R. (1996). *Atlas of alteration: A field and petrographic guide to hydrothermal alteration minerals* (Vol. 6). Geological Assn of Canada.
- Álvarez, J., Orrego, A., Botero, G., & Linares, E. (1978). DETERMINACIÓN DE EDAD K/Ar DEL STOCK DE SUAREZ-CAUCA. *Pub. Geol. Esp. No. II. Fac. de Ciencias, Medellfn*.
- Álvarez, A., & Linares, E. (1979). Edades K Ar del Batolito de Piedrancha y Stock de Arboledas, Departamento de Nariño. *Publicación especial de Geología*, (22).
- Álvarez, J., Marulanda, N., Botero, G. & Linares, E. (1979). Edad K/Ar del stock de San Cristóbal, Nariño. *Publicación especial de Geología*, (18).
- Barbosa-Camacho, G. (2003). Memoria explicativa Mapa Geológico del Departamento del Cauca. Informe Interno Ingeominas, Cali, Colombia.
- Best, M. G. (2003). *Igneous and metamorphic petrology*. Blackwell Science Ltd.
- Blundy, J., & Cashman, K. (2001). Ascent-driven crystallization of dacite magmas at Mount St Helens, 1980–1986. *Contributions to Mineralogy and Petrology*, 140(6), 631-650.
- Boggs, S. (2009). *Petrology of sedimentary rocks*. Cambridge University Press.
- Bougault, H., Joron, J. L., & Treuil, M. (1980). The primordial chondritic nature and large-scale heterogeneities in the mantle: evidence from high and low partition coefficient elements in oceanic basalts. *Phil. Trans. R. Soc. Lond. A*, 297(1431), 203-213.
- Botero, G. (1963). Contribución al conocimiento de la geología de la parte central de Antioquia. Anal. Fac. Minas, 57:101p. Medellín.
- Cashman, K. V., & Scheu, B. (2015). Magmatic fragmentation. In *The Encyclopedia of Volcanoes (Second Edition)* (pp. 459-471).
- Castro, A. (2015). *Petrografía de rocas ígneas y metamórficas*. Ediciones Paraninfo, SA.
- Cediel, F., Shaw, R. P., & Cceres, C. (2003). Tectonic Assembly of the Northern Andean block. *The Circum-Gulf of Mexico and the Caribbean: Hydrocarbon Habitats, Basin Formation and Plate Tectonics*.
- DePaolo, D. J. (1981). Trace element and isotopic effects of combined wallrock assimilation and fractional crystallization. *Earth and planetary science letters*, 53(2), 189-202.
- Fettes, D. J., Desmons, J., & Árkai, P. (2007). *Metamorphic rocks: a classification and glossary of terms: recommendations of the International Union of Geological Sciences Subcommission on the Systematics of Metamorphic Rocks*. Cambridge Univ Pr.
- Folk, R. L. (1951). Stages of textural maturity in sedimentary rocks. *Journal of Sedimentary Research*, 21(3).

- Grosse, E. (1935). Acerca de la geología del sur de Colombia, Patía y Nariño. In: Compilación de los estudios geológicos oficiales en Colombia – 1917 a 1933. Imprenta Nacional, Bogotá.
- Harmon, R. S., Barreiro, B. A., Moorbat, S., Hoefs, J., Francis, P. W., Thorpe, R. S., Déruelle, B., McHugh, J., & Viglino, J. A. (1984). Regional O-, Sr-, and Pb-isotope relationships in late Cenozoic calc-alkaline lavas of the Andean Cordillera. *Journal of the Geological Society*, 141(5), 803-822.
- Hildreth, W., & Moorbat, S. (1988). Crustal contributions to arc magmatism in the Andes of central Chile. *Contributions to mineralogy and petrology*, 98(4), 455-489.
- Humphreys, M. C., Blundy, J. D., & Sparks, R. S. J. (2006). Magma evolution and open-system processes at Shiveluch Volcano: Insights from phenocryst zoning. *Journal of Petrology*, 47(12), 2303-2334.
- Ingeominas & Geoestudios (1998). Mapa geológico de Colombia: Plancha 430 Mocoa. Escala 1:100.000. INGEOMINAS, Informe interno. Bogotá.
- International Subcommission on Stratigraphic Classification (1994). *International Stratigraphic Guide: a guide to stratigraphic classification, terminology, and procedure* (2). Amos Salvador (ed.).
- Jerram, D. A., & Davidson, J. P. (2007). Frontiers in textural and microgeochemical analysis. *Elements*, 3(4), 235-238.
- Jerram, D. A., & Martin, V. M. (2008). Understanding crystal populations and their significance through the magma plumbing system. *Geological Society, London, Special Publications*, 304(1), 133-148.
- LaFemina, P. C. (2015). Melting of the mantle. In: *Encyclopedia of Volcanoes* (eds. H. Sigurdsson, B. Houghton, S. R. McNutt, H. Rymer, and S. Stix). Academic Press, San Diego. pp. 65–92.
- León, L.A., Padilla, L.E., Marulanda, N. (1973). Geología, recursos minerales y geoquímica de la parte noreste del cuadrángulo 05, El Bordo, departamento del Cauca, informe 1652. INGEOMINAS. Popayán
- López Ruiz, J., & Cebriá Gómez, J. M. (1990). *Geoquímica de los procesos magmáticos* (No. 550.42 LOP).
- McKenzie, W. S., Donaldson, C. H., & Guilford, C. (1982). Atlas of igneous rocks and their textures. *Harlow Longman Grain UK Ltd, London*.
- Marín-Cerón, M. I. (2007). *Major, trace element and multi-isotopic systematics of SW Colombian volcanic arc, northern Andes: Implication for the stability of carbonate-rich sediment at subduction zone and the genesis of andesite magma* (Doctoral thesis). Okayama University, Japón.
- McBirney, A. R. (1979). Effects of assimilation. In: *The Evolution of the Igneous Rocks. Fiftieth Anniversary Perspectives* (ed. H. S. Yoder). Princeton University Press. Princeton, NJ.

- Maya, M. & González, H. (1995). Unidades litodémicas en la Cordillera Central de Colombia. INGEOMINAS, *Boletín Geológico*, 35(2-3), 43-57.
- Mindat (2006). Andesite. Retrieved from <https://www.mindat.org/min-48484.html>
- Murcia, A. (1982). El vulcanismo plio-cuarternario de Colombia: depositos piroclasticos asociados y mediciones isotopicas de $^{87}\text{Sr}/^{86}\text{Sr}$, $^{143}\text{Nd}/^{144}\text{Nd}$ y sigma 18-O en lavas de los volcanes Galeras, Purace y Nevado del Ruiz. *Publicaciones Especiales del INGEOMINAS*, 10, 1-17
- Murcia, L. A. & Cepeda, H. (1991). Mapa Geológico de Colombia, Plancha 410 La Unión, Memoria Explicativa. INGEOMINAS. Bogotá.
- Murcia, L. A. & Cepeda, H. (1984). Memoria geológica de la Plancha 429 Pasto. INGEOMINAS, Informe interno. 193 p. Popayán.
- Nelson, S.A. (2018). *Sediment and Sedimentary rocks*. Tulane University. Retrieved from: <https://www.tulane.edu/~sanelson/eens1110/sedrx.htm>
- Nelson, W., 1962. Contribution to the geology of the Central and Western Cordillera of Colombia in the sector between Ibagué and Cali, Boletín Geológico. Vol X No 1-3.
- Nivia, A., Marriner, G. F., Kerr, A. C., & Tarney, J. (2006). The Quebradagrande Complex: A Lower Cretaceous ensialic marginal basin in the Central Cordillera of the Colombian Andes. *Journal of South American Earth Sciences*, 21(4), 423-436.
- Núñez, A. (1990). Análisis de la nomenclatura estratigráfica del Complejo Arquía y unidades correlacionables (Cordillera Central y Valle del río Cauca, Colombia). Informe inédito. INGEOMINAS, Ibagué.
- Núñez, A. (2003). Reconocimiento geológico regional de las planchas 411 La Cruz, 412 San Juan de Villalobos, 430 Mocoa, 431 Piamonte, 448 Monopamba, 449 Fiorito y 465 Churuyaco. *Memoria explicativa, escala 1(100.000)*.
- Pardo, N., Pulgarín, B. & Betancourt, V. (2016). Avances en el conocimiento sobre el Complejo Volcánico Doña Juana: integración del análisis de litofacies, estratigrafía, geocronología y petrología. Informe interno Servicio Geológico Colombiano, Bogotá.
- Pardo, N., Pulgarín, B., Betancourt, V., Lucchi, F., & Valencia, L. J. (2018). Facing geological mapping at low-latitude volcanoes: The Doña Juana Volcanic Complex study-case, SW-Colombia. *Journal of Volcanology and Geothermal Research*.
- Passchier, C. W., & Trouw, R. A. (2005). *Microtectonics* (Vol. 1). Springer Science & Business Media.
- Patchett, P. J. (1980). Thermal effects of basalt on continental crust and crustal contamination of magmas. *Nature*, 283(5747), 559-561.
- Renjith, M. L. (2014). Micro-textures in plagioclase from 1994–1995 eruption, Barren Island Volcano: evidence of dynamic magma plumbing system in the Andaman subduction zone. *Geoscience Frontiers*, 5(1), 113-126.

- Rollinson, H.R. (1993). Using Geochemical Data: Evaluation, Presentation, Interpretation (Longman Geochemistry Series), 352p., Taylor & Francis Ed., EE.UU.
- Ruiz, S.S. (2002}. Geología de la plancha 386 "Mercaderes". Memoria explicativa, Informe interno INGEOMINAS, Bogotá.
- Rutherford, M. J., & Hill, P. M. (1993). Magma ascent rates from amphibole breakdown: an experimental study applied to the 1980–1986 Mount St. Helens eruptions. *Journal of Geophysical Research: Solid Earth*, 98(B11), 19667-19685.
- Stefan, A., Szakács, A. & Seghedi, I. (1996). Dacite from the type locality: Genealogy and Description. *Geological survey of Romania*.
- Villagómez, D., Spikings, R., Magna, T., Kammer, A., Winkler, W., & Beltrán, A. (2011). Geochronology, geochemistry and tectonic evolution of the Western and Central cordilleras of Colombia. *Lithos*, 125(3), 875-896.
- Watson, E. B. (1982). Basalt contamination by continental crust: some experiments and models. *Contributions to Mineralogy and Petrology*, 80(1), 73-87.
- Weber, M. B. (1998). *The Mercaderes-Rio Mayo xenoliths, Colombia: Their bearing on mantle and crustal processes in the Northern Andes* (Doctoral dissertation). University of Leicester.
- Weber, M. B., Tarney, J., Kempton, P. D., & Kent, R. W. (2002). Crustal make-up of the northern Andes: evidence based on deep crustal xenolith suites, Mercaderes, SW Colombia. *Tectonophysics*, 345(1), 49-82.
- Winter, J. D. (2014). *Principles of igneous and metamorphic petrology* (2). Pearson Education Limited.